[American Journal of Science, Vol. 317, March, 2017, P. 251-337, DOI 10.2475/03.2017.01]

American Journal of Science

MARCH 2017

PETROLOGY AND GEOCHRONOLOGY OF MESOPROTEROZOIC BASEMENT OF THE MOUNT ROGERS AREA OF SOUTHWESTERN VIRGINIA AND NORTHWESTERN NORTH CAROLINA: IMPLICATIONS FOR THE PRECAMBRIAN TECTONIC EVOLUTION OF THE SOUTHERN BLUE RIDGE PROVINCE

RICHARD P. TOLLO*,†, JOHN N. ALEINIKOFF**, ALAN P. DICKIN ***, MOLLY S. RADWANY*,§, C. SCOTT SOUTHWORTH§§, and C. MARK FANNING§§§

ABSTRACT. Results from new geologic mapping, SHRIMP U-Pb geochronology, and petrologic studies indicate that Mesoproterozoic basement in the northern French Broad massif near Mount Rogers consists of multiple, mostly granitic plutons, map- and outcrop-scale xenoliths of pre-existing crustal rocks, and remnants of formerly overlying meta-sedimentary lithologies. Zircon and titanite ages demonstrate that these rocks collectively record nearly 350 m.y. of tectonic evolution including periods of igneous intrusion at *ca.* 1190 to 1130 Ma (Early Magmatic Suite) and *ca.* 1075 to 1030 Ma (Late Magmatic Suite) and three episodes of regional metamorphism at *ca.* 1170 to 1140, 1070 to 1020, and 1000 to 970 Ma. The existence of *ca.* 1.3 Ga age crust is indicated by (1) orthogranofels of *ca.* 1.32 Ga age in a map-scale xenolith, (2) inherited zircons of *ca.* 1.33 to 1.29 Ga age in Early Magmatic Suite plutons, and (3) *ca.* 1.36 to 1.30 Ga age detrital zircons in meta-sedimentary lithologies. Mineral assemblages developed in amphibolites and granofelses indicate that metamorphism during both Mesoproterozoic episodes occurred at upper amphibolite- to lower granulite-facies conditions. Syn-orogenic Early Magmatic Suite plutons emplaced at *ca.* 1190 to 1145 Ma are characterized by high-K, variably magnesian, dominantly calc-alkalic compositions, and have trace-element characteristics indicative of continental-arc magmatic origin involving melting of thick continental crust. In contrast, *ca.* 1140 Ma age quartz syenite displays A-type features indicating derivation from depleted crustal sources with increased mantle input during waning stages of regional contraction. Plutons of the compositionally bimodal Late Magmatic Suite include (1) *ca.* 1060 Ma meta-granite with geochemical characteristics transitional between silicic rocks of arc systems and post-collisional granites of A-type lineage, and (2) *ca.* 1055 Ma monzodioritic rocks with A-type compositional characteristics that likely reflect derivation from fertile, mafic sources in the lower crust. Collectively, these data suggest that Mesoproterozoic rocks of the study area preserve evidence of multiple orogenic episodes that likely involved continental-arc development and deformation at *ca.* 1150 Ma followed by crustal thickening at *ca.* 1060 Ma. Field relations and geochronologic data indicate that regional uplift and sedimentation occurred at *ca.* 1100 Ma between the two episodes of overlapping magmatism and orogenesis. The nature and timing of Mesoproterozoic events recorded in basement rocks of the study area illustrate significant differences in

* Geological Sciences Program, George Washington University, Washington, DC 20052, USA
** U.S. Geological Survey, Denver, Colorado, 80225, USA
*** School of Geography and Geology, McMaster University, Hamilton, Ontario, L8S 4M1, Canada
§ Present address: Department of Earth Science, University of Minnesota, Minneapolis, Minnesota 55455, USA
§§ U.S. Geological Survey, Reston, Virginia, 20192, USA
§§§ Research School of Earth Sciences, Australian National University, Mills Road, Canberra, ACT 0200, Australia
† Corresponding author. Fax: +1-202-994-6100; rtollo@gwu.edu (R. P. Tollo).

the lithologic assemblages and geologic history preserved by Mesoproterozoic basement of the adjacent Shenandoah and French Broad massifs, suggesting that the Blue Ridge massifs occupied different locations within the regional Grenville-age orogen until about 1070 Ma when the effects of Ottawan-age tectonics began to affect both areas. The near ubiquity of Ottawan-age orogenic activity recorded in Mesoproterozoic rocks of the Blue Ridge, other Appalachian inliers such as the New Jersey Highlands, and the Grenville province of Canada, including the Adirondacks, suggests that these formerly disparate terranes were amalgamated to form a common, regional orogen by this time.

Keywords: A-type, granite, SHRIMP, Grenville, Blue Ridge, Nd isotopes

INTRODUCTION

The lithologic and structural complexity of deformed, moderate- to high-grade metamorphic terranes presents challenges to geologic investigations ranging from field mapping to application of micro-analytical techniques. Nevertheless, studies have demonstrated the efficacy of an integrated research approach involving combined field- and laboratory-based analysis to provide data necessary to develop a comprehensive understanding of the geology of such areas (for example Frost and others, 2000; Slagstad and others, 2004). This study presents findings of a multidisciplinary investigation of Mesoproterozoic basement rocks located in the Blue Ridge province of southwestern Virginia and northwestern North Carolina. Previous geologic studies in this area (Rankin and others, 1972; Bartholomew and Lewis, 1984) proposed gross distinctions between lithologies but did not involve detailed field mapping supported by analytical information.

We present results of detailed field mapping, petrologic and geochemical studies, and U-Pb geochronologic analyses of the heretofore largely undivided basement located near Mount Rogers, Virginia. Research goals include (1) definition of map-scale lithologic units, (2) documentation of field relations, (3) characterization of petrologic and geochemical features bearing on petrogenesis, and (4) delineation of the timing of major igneous and metamorphic events. Geological relationships characterizing Mesoproterozoic basement in the area are important to studies of regional geology because these rocks occur at the northern termination of the southernmost of two massifs constituting the Blue Ridge province (Rankin and others, 1989) (fig. 1A), and thus provide a basis for lithologic comparison. Moreover, the new data offer a framework for evaluating global-scale models for the provenance and tectonic evolution of Mesoproterozoic terranes in the southern Appalachians and elsewhere.

Field mapping was completed at 1:24,000 scale using available maps (Rankin, unpublished) as initial guides. Lithologic units were initially defined through field and petrographic analysis. Whole-rock major- and trace-element data, were used, where appropriate, to further characterize lithologic units and to investigate petrogenetic relationships. Detailed U-Pb geochronologic analysis of zircon from all lithologic units was performed using secondary ion mass spectrometry (SIMS) techniques to further refine relationships identified through field studies and determine the age of regional igneous and metamorphic activity.

This investigation was undertaken in part to address the need for detailed geologic field studies of Mesoproterozoic rocks in the southern Appalachian Blue Ridge. The study, which was part of a regional initiative by the U.S. Geological Survey (USGS), was designed from the outset to contribute an improved understanding of the Mesoproterozoic basement and to decipher evidence for Precambrian geologic events typically overprinted by the effects of Paleozoic metamorphism and deformation.

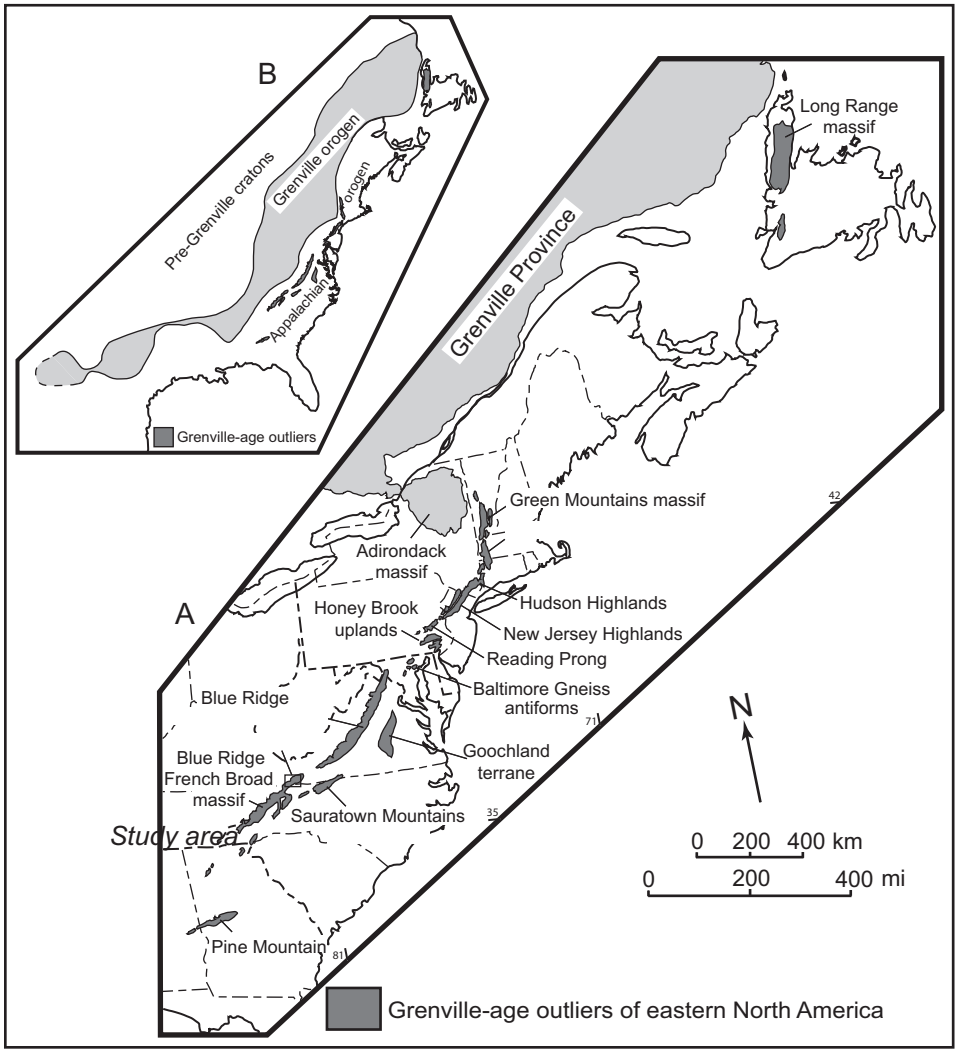

Fig. 1. (A) Generalized map showing distribution of Mesoproterozoic inliers within the Appalachian orogenic belt. Detailed geology of study area located at northern end of the French Broad massif is shown in figure 3. Map modified from Rankin and others (1989). (B) Generalized map showing relationship of Grenville-age inliers of the Appalachians to the Grenville orogen in eastern North America. Map modified from Hoffman (1989).

PRECAMBRIAN GEOLOGY OF THE BLUE RIDGE PROVINCE

The Blue Ridge province of the southern Appalachians is the largest outlier of Mesoproterozoic crust east of the Grenville orogen (fig. 1) (Rankin and others, 1989). The province includes the separate Shenandoah (north) and French Broad (south) massifs (fig. 1A) (Rankin and others, 1989). Both massifs are structural anticlinoria cored by Mesoproterozoic basement; each is fault bounded and allochthonous, having been transported northwestward during regional late Paleozoic Alleghenian orogenesis (Hatcher, 2010). Despite constituting largely intact thrust sheets, each massif is transected internally by sinuous zones of ductile deformation of mostly late Paleozoic

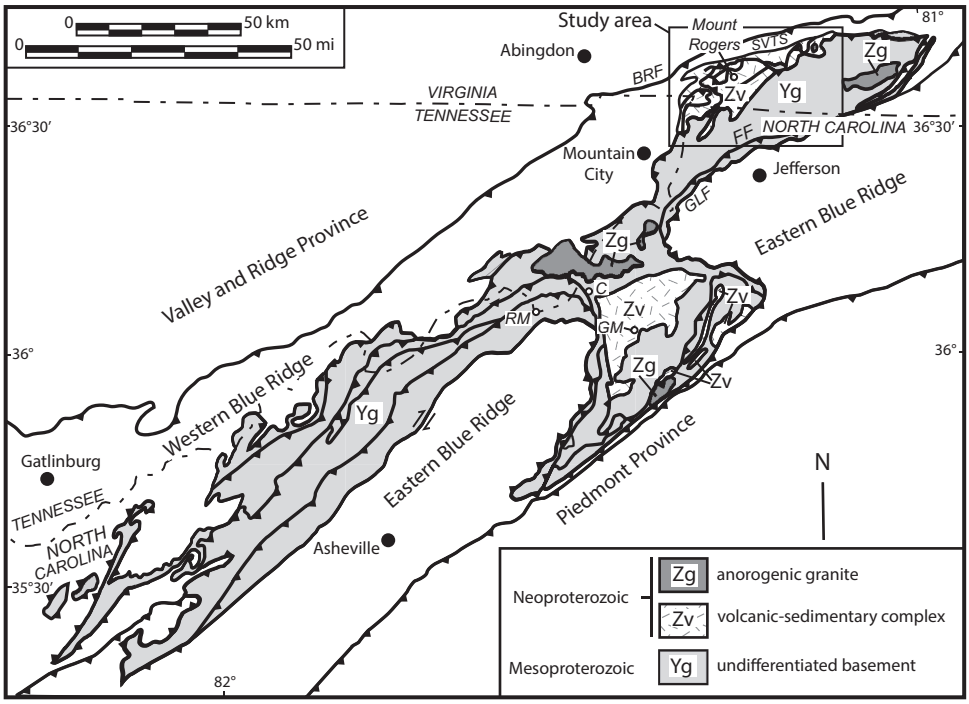

Fig. 2. Generalized geologic map showing major lithotectonic units of the French Broad massif. *C*, Cranberry, North Carolina; *RM*, Roan Mountain; *GM*, Grandfather Mountain; *GLF*, Gossan Lead fault; *FF*, Fries fault; *BRF*, Blue Ridge fault; *SVTS*, Shady Valley thrust sheet. Map modified after Hibbard and others (2006) and Rankin and others (1989).

age that transpose local geology (Bailey and Simpson, 1993; Trupe and others 2004) (fig. 2).

Initial geochronologic studies established the overall *ca.* 1.1 to 1.0 Ga age of basement in both massifs (Tilton and others, 1960; Davis and others, 1962). Early mapping-based investigations documented the near ubiquity of igneous and metamorphic lithologies in the structural core of each region (for example Bryant and Reed, 1970; Gathright, 1976). Subsequent studies, including new geologic mapping, petrologic and geochemical investigations, and application of U-Pb geochronology by sensitive high resolution ion microprobe (SHRIMP), have confirmed the overall Mesoproterozoic age but revealed geologic differences between the massifs (table 1).

The two Blue Ridge massifs are part of a series of *ca.* 1.2 to 1.0 Ga age crustal blocks occurring within the Appalachian orogen (Rankin, 1976). The broad extent of these rocks in eastern North America (fig. 1A) and overlap in age with major orogenic activity in the Canadian Grenville province (Rivers, 1997) led to proposals that Mesoproterozoic basement of the southern Appalachians preserves evidence of comparable events of Laurentian affinity (Herz and Force, 1984; Tollo and others, 2004a). In the Blue Ridge massifs, documentation of episodes of overlapping igneous and metamorphic activity at *ca.* 1190 to 1140 Ma and 1075 to 1020 Ma constituted the basis for correlation to the Shawinigan and Ottawan orogenic intervals, respectively, in Canada (Tollo and others, 2004b). Despite these similarities, regional isotopic investigations indicate significant differences between the Mesoproterozoic massifs of the

TABLE 1

Geologic and temporal characteristics of Blue Ridge massifs in the southern Appalachians

	Shenandoah massif	French Broad massif
Dominant lithologies	charnockites meta-granitoids meta-leucogranites gneisses [1, 6, 7,9]	migmatites meta-granites gneisses amphibolites meta-sedimentary lithologies (including granofels) [1, 2, 3, 4, 5, 8, 10]
Prevailing Mesoproterozoic metamorphic grade	upper amphibolite to granulite [1, 6, 7, 9]	upper amphibolite to lower granulite [1, 5, 8, 10]
Timing of magmatic activity	*ca*. 1185-1100 Ma *ca*. 1080-1030 Ma [6, 7, 9]	*ca*. 1190-1130 Ma *ca*. 1075-1030 Ma [2, 3, 4, 8, 10]
Dominant magmatic compositions	ferroan (tholeiitic) [6, 7]	magnesian (calc-alkaline) except for late orogenic plutons [10]
Timing of metamorphic activity	*ca*. 1080-980 Ma [6, 7, 9]	*ca*. 1170-1140 Ma *ca*. 1070-1020 Ma *ca*. 1000-970 Ma [2, 3, 8, 10]
Presence of anorthosite	yes [1]	no [1, 2, 3, 4, 5, 8, 10]
Evidence for uplift and erosion during transition from Geon 11 to 10	absent [1, 6, 7, 9]	present [10]
Presence of ca. 1.3 Ga and other pre-1.2 Ga crust	no [6, 7, 9]	yes [10]

Sources of information include Bartholomew and Lewis (1984) [1]; Carrigan and others, 2003 [2]; Ownby and others, 2004 [3]; Berquist and others, 2005 [4]; Hatcher and others, 2005 [5]; Tollo and others, 2004 [6], 2006 [7], 2010 [8]; Southworth and others, 2010 [9]; this study [10].

southern and central Appalachians, and between those areas and more northern Grenville-age terranes, suggesting an Amazonian, not Laurentian, origin for the former (Fisher and others, 2010).

The geology of the Blue Ridge province reflects parts of two Wilson cycles that dominated regional tectonics for nearly 1 b.y. (Hatcher, 2010). Mesoproterozoic basement records tectonic convergence associated with amalgamation of Rodinia at *ca.* 1.2 to 1.0 Ga that involved collision between the Laurentian and Amazonian cratons (McLelland and others, 2010). This convergence involved multiple episodes of local magmatism and metamorphism; however, the ubiquity of *ca.* 1070 to 1020 Ma metamorphic ages suggests that a continuous orogenic belt had formed in eastern Laurentia by late Ottawan time (McLelland and others, 2010).

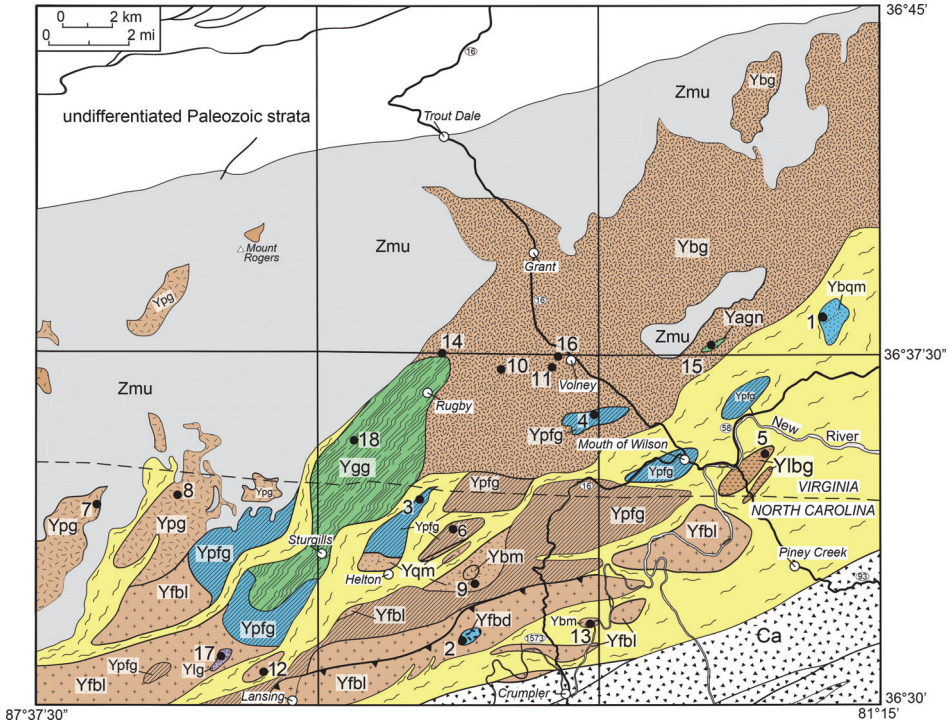

Fig. 3. Generalized geologic map of the Mount Rogers study area showing distribution of Mesoproterozoic rocks and associated high-strain zones. Geology of Neoproterozoic and younger rocks is modified after Rankin and others (1972) and Rankin (1993). Locations for geochronologic samples are indicated by filled circles; numbers refer to tables 5 and 7.

MESOPROTEROZOIC BASEMENT OF THE MOUNT ROGERS AREA

Previous Studies

Rankin and others (1972) mapped rocks across a broad portion of the northern French Broad massif compiled at 1:250,000 scale and correlated all basement rocks with the Cranberry Gneiss for which the type locality is located about 50 km (31 mi) southwest of the study area. Noting that lithologies ranged from diorite to granite, Rankin and others (1973) characterized most of the Mesoproterozoic basement near Mount Rogers as quartz monzonite and quartz monzonite gneiss but distinguished several elongate bodies of augen gneiss that generally correspond to high-strain zones mapped in this study as transecting basement. Subsequent studies include Bartholomew and Lewis (1984) who compiled mapping throughout both Blue Ridge massifs, and mapping for the Geologic Map of Virginia (Virginia Division of Mineral Resources, 1993).

Nomenclature

Rocks were mapped at 1:24,000 scale using textural characteristics, mineralogical composition, and geochemical data as the primary criteria to distinguish lithologic units (fig. 3). Multiple systems of nomenclature were applied based on the degree to which evidence bearing on individual protoliths was discernible. Nomenclature for rocks of demonstrable igneous origin (determination based on relic textures, mineralogy, geochemical composition, and the shape and internal textures of zircon) employs

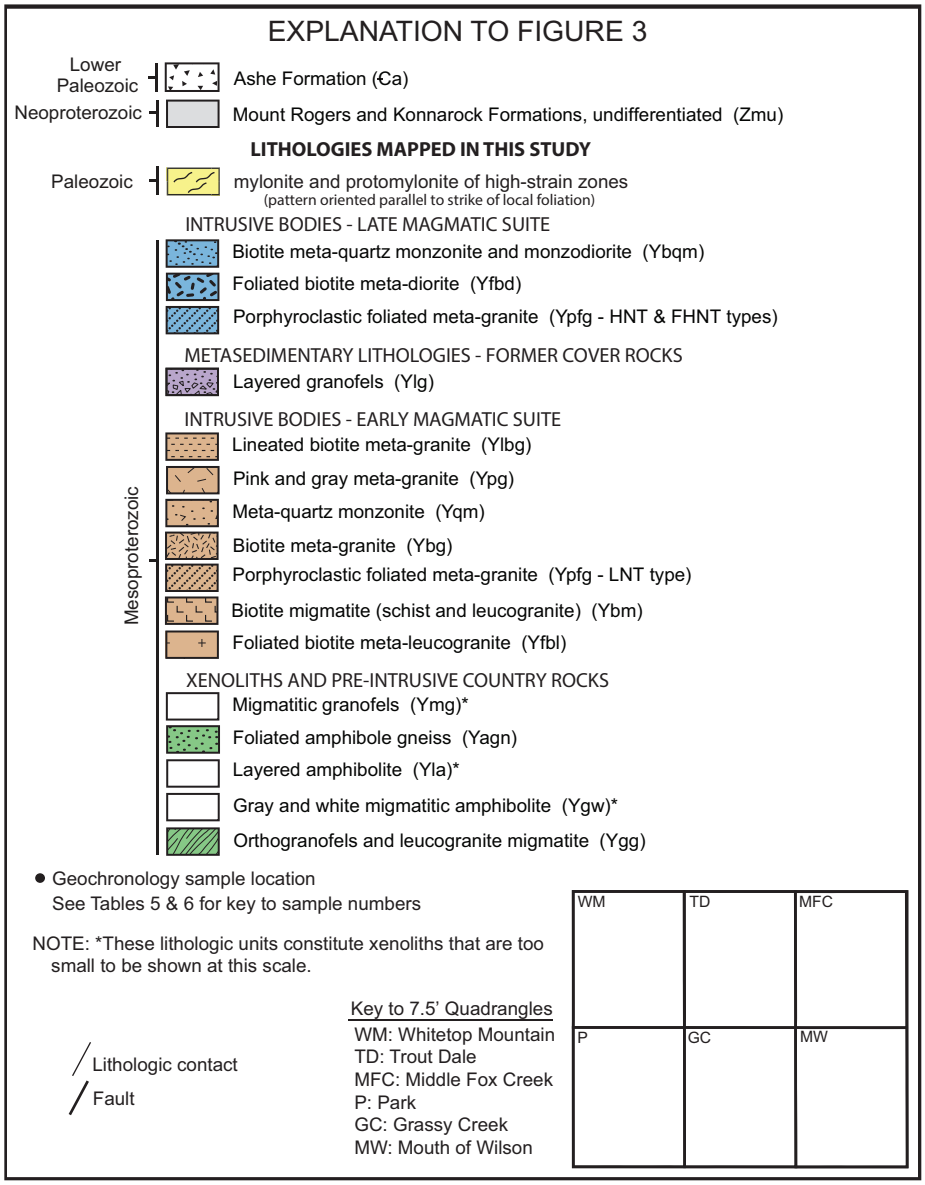

Fig. 3 (continued).

root names derived from Le Maitre and others (2002). In most cases, the major ferromagnesian mineral is used as a modifier along with a textural term for rocks that are pervasively deformed. In contrast, because strongly developed foliation and abundant, coarse-grained phenocrysts and porphyroclasts made modal analysis unreliable for many samples, root names for such rocks were determined using the geochemical approximation (Streckiesen and Le Maitre, 1979) of the standard International Union of Geological Sciences (IUGS) modal quartz-alkali feldspar-plagioclase-feldspathoid (QAPF) diagram (Le Maitre and others, 2002) (fig. 4). Nomenclature

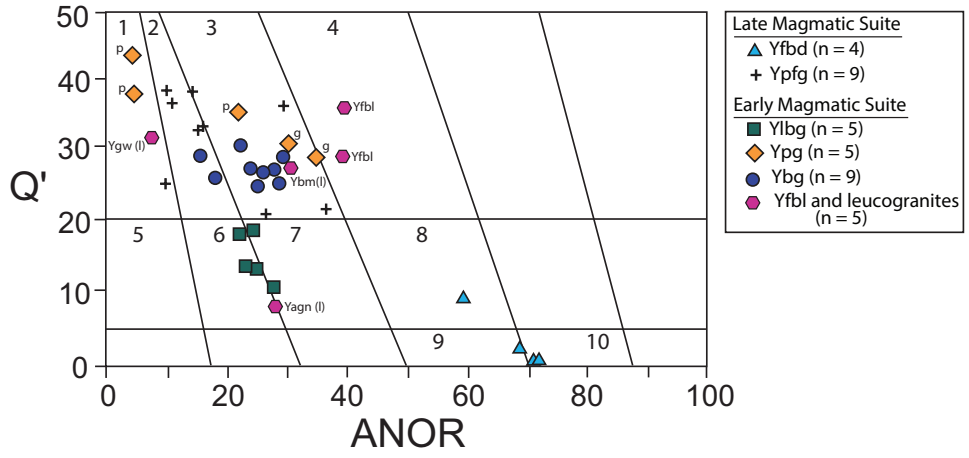

Fig. 4. Plot of ANOR (100 X normative anorthite/(orthoclase + anorthite) vs Q' (normative quartz/(quartz + orthoclase + albite + anorthite) for meta-igneous rocks of the study area. See table 2 for explanation of map unit symbols. Normative compositions were calculated with $Fe^{2+}/Fe_{total} = 0.9$. Field labels include: (1) alkali feldspar granite, (2) syenogranite, (3) monzogranite, (4) granodiorite, (5) quartz alkali feldspar syenite, (6) quartz syenite, (7) quartz monzonite, (8) quartz monzodiorite, (9) monzodiorite, and (10) diorite. Labels "p" and "g" indicate pink (mostly syenogranite) and gray (monzogranite) lithologic components, respectively, of the composite Ypg unit. Data for meta-leucogranites include leucogranitic components of three composite units [indicated by "(l)" labels on diagram] and two samples of the foliated biotite meta-leucogranite (Yfbl) unit. Diagram after Streckeisen and Le Maitre (1979).

applied to recrystallized rocks lacking physical evidence of the protolith is derived from the recommendations of Fettes and Desmons (2007). In some composite lithologies, additional descriptors are included in order to convey characteristic physical features mapped in the field (for example: "gray and white migmatitic amphibolite").

Summary of Geologic Mapping, Field Characteristics, and Mineral Assemblages

Mesoproterozoic basement in the Mount Rogers area includes gneisses, granofels, granites, monzodiorites, amphibolites, and migmatites (table 2). All rocks record moderate-grade metamorphism of Mesoproterozoic age (Tollo and others, 2010, 2012) and Paleozoic low-grade metamorphism (Rankin and others, 1972). Protolith identification is based on (1) map- or outcrop-scale field relations, (2) interpretation of textures, (3) comparison of whole-rock geochemical compositions with unmetamorphosed analogs of known origin, and (4) chemical zoning features in zircon (table 3). Most rocks are igneous in origin; several units define large plutons (for example, biotite meta-granite, Ybg) or lithologically diverse intrusive complexes (for example, lineated biotite meta-granite, Ylbg) (fig. 3). Most rocks display igneous textures variably overprinted by the effects of Paleozoic deformation. Field relationships of igneous origin include dikes, pegmatites, xenoliths, crosscut textures and structures, and multiple lithologic varieties of similar composition occurring within individual plutonic bodies. Rocks of meta-sedimentary origin are much less abundant than meta-igneous types.

Field mapping and geochronologic data indicate that rocks in the study area define (1) a series of intrusive bodies, (2) pre-intrusive country rock and map- and outcrop-scale xenoliths, and (3) meta-sedimentary lithologies that formerly overlay crystalline basement (tables 2–4). Oldest rocks in the study area form map- to outcrop-scale xenoliths or pre-intrusive country rock; all of these rocks are composite

TABLE 2

Characteristics of Mesoproterozoic basement rocks in the study area

Lithologic Nomenclature (map symbol)	Dominant Lithology* Mineral Assemblage	Field Relations
Biotite meta-quartz monzonite and monzodiorite (Ybqm)	quartz monzodiorite/monzodiorite Afs† + Qz + Pl + Bt + *Ep*§ + *Ttn*	Intruded by weakly foliated, medium-grained, biotite granite that truncates foliation in the meta-quartz monzonite
Foliated biotite meta-quartz monzodiorite (Yfbd)	diorite to quartz monzodiorite Pl + Qz + Bt + Mt + Ttn + *Ep* + *Ap*	Occurs as small pluton intrusive into Yfbl meta-leucogranite; intruded by magnetite-rich dikes of likely comagmatic origin
Porphyroclastic foliated meta-granite (Ypfg)	syenogranite to monzogranite Mc + Qz + Pl + Bt + Aln + Mt + *Ep* + *Ms*	Occurs as dismembered map-scale boudins within high-strain zones; locally intrudes Ybg body; encloses decameter-scale xenolith of Yla amphibolite; includes compositional variants of different age
Lineated biotite meta-granite (Ylbg)	quartz syenite Afs + Pl + Qz + Bt + Hbl + Grt + Aln + Mt + Ilm + *Ttn* + *Ep* + *Chl*	Occurs as isolated, elongate bodies within regional high-strain zone
Migmatitic granofels (Ymg)	granofels and leucogranite granofels: Qz + Pl + Bt + *Mus* + *Ep* leucogranite: Qz + Afs + Pl + *Ep*	Occurs as xenolith enclosed within Ylbg meta-granite; layering within migmatite is cut by dikes composed of Ylbg meta-granite
Pink and gray meta-granite (Ypg)	alkali feldspar granite (pink) and monzogranite (gray) pink: Mc + Qz + Pl + *Ep* + *Ms* + *Bt* + *Stp* gray: Mc + Pl + Qz + Aln + *Ep* + *Bt* + *Ms*	Intricate scale of layering and crosscutting relationships indicate origin as magmatic complex; pink component intrudes gray; both are ductilely folded
Meta-quartz monzonite (Yqm)	quartz monzonite Afs + Pl + Qz + Bt + Hbl + *Bt* + *Ep* + *Ttn* + *Mus*	Locally intrudes Yla unit; occurs primarily as map-scale boudins within mylonitic rocks of regional high-strain zones
Biotitic migmatite (Ybm)	leucogranite and schist leucogranite: Afs + Qz + Pl + Bt + *Ep* + *Mus* schist: Pl + Bt + Qz + Ep + Ttn + Mus	Intrusive relations indicate that the lithologic assemblage represents an igneous injection complex; unit occurs only within region of mylonitic rocks

Table 2
(continued)

Lithologic Nomenclature (map symbol)	Dominant Lithology* Mineral Assemblage	Field Relations
Biotite meta-granite (Ybg)	monzogranite Afs + Qz + Pl + Bt + Mt + Chl + Ep	Forms large plutonic body; encloses map-scale xenolith of Yla amphibolite; intruded by Ypfg unit; intruded by pegmatite of likely comagmatic origin; includes (1) medium- to coarse-grained and (2) porphyritic facies
Layered granofels (Ylg)	granofels and leucogranite granofels: Mc + Qz ± Pl +Amph + Grt + Ep + Ttn + Ap leucogranite: Afs + Qz + Plag	Occurs as map-scale inlier within Yfbl unit; age relations suggest that Ylg sedimentary protoliths were deposited unconformably atop Yfbl meta-leucogranite
Foliated biotite meta-leucogranite (Yfbl)	leucogranite Mc + Pl + Qz + Bt +Ap + Ep + Ttn + Ms + Cal	Xenoliths indicate high strain within moderately foliated meta-leucogranite; age relations indicate that Ylbg unit was likely originally overlain unconformably by Ylg meta-sedimentary protoliths
Foliated amphibole gneiss (Yagn)	amphibole gneiss and leucogranite gneiss melanosome: Amph + Cpx + Pl + Qz + Ap + Act + Chl + Ttn granitic leucosome: Afsp + Qz + Pl crosscutting leucogranite: Mc + Qz + Pl + Amph + Aln(?)	Occurs as an elongate xenolith within Ybg metagranite; layering in the gneiss is truncated by nonfoliated meta-leucogranite
Layered amphibolite (Yla)	amphibolite: Pl + Hbl + Qz + Ttn + Act + Ep + Chl granofels: Pl + Hbl + Qz + Ttn + Act + Ep + Chl	Occurs as decameter-scale xenoliths within Ybg and Ypfg plutons; layering is isoclinally folded and crosscut by folded granitoid

Table 2
(continued)

Lithologic Nomenclature (map symbol)	Dominant Lithology* Mineral Assemblage	Field Relations
Gray and white migmatitic amphibolite (Ygw)	amphibolite and leucogranite amphibolite (gray): Hbl + Cpx + Pl + Qz + Act + Chl + Ep leucogranite (white): Pl + Afs + Qz + Ep + Chl	Meta-leucogranite is intrusive into amphibolite; both are ductilely folded
Orthogranofels and meta-leucogranite migmatite (Ygg)	granofels and leucogranite granofels: Pl + Hbl + Qz + Act + Chl + Ep leucogranite: Afs + Qz + Pl + Ep + Chl	Meta-leucogranite is intrusive into granofels; unconformably overlain by Mount Rogers Formation

* Prefix "meta" omitted for clarity; † Mineral abbreviations after Whitney and Evans (2010): Act, actinolite; Afs, alkali feldspar; Aln, allanite; Amph, Amphibole; Ap, apatite; Bt, biotite; Cal, calcite; Chl, chlorite; Cpx, monoclinic pyroxene; Ep, epidote; Grt, garnet; Hbl, hornblende; Mag, magnetite; Mc, microcline; Ms, muscovite; Pl, plagioclase; Qz, quartz; Stp, stilpnomelane; Ttn, titanite; § Retrograde minerals in italics.

TABLE 3

Criteria used in identifying basement rock protoliths

Basement Unit and Protolith	Map Symbol	Field Relations	Rock Texture	Chemical Composition	Zircon Textures*
Igneous Protoliths					
Biotite meta-quartz monzonite	Ybqm	-	-	-	yes
Foliated biotite meta-quartz monzodiorite	Yfbd	yes	-	yes	-
Porphyroclastic foliated meta-granite	Ypfg	yes	yes	yes	yes
Lineated biotite meta-granite	Ylbg	yes	yes	yes	yes
Pink and gray meta-granite (pink)	Ypg	yes	yes	yes	yes
(green)		yes	yes	yes	yes
Meta-quartz monzonite	Yqm	yes	yes	yes	yes
Biotite meta-granite	Ybg	yes	yes	yes	yes
Biotitic migmatite† (meta-leucogranite§)	Ybm	yes	yes	yes	yes
Foliated biotite meta-leucogranite	Yfbl	-	yes	yes	yes
Foliated amphibole gneiss† (amphibole gneiss)	Yagn	-	-	-	yes
(meta-leucogranite)		yes	-	-	yes
Layered amphibolite†	Yla	-	-	yes	-
Gray and white migmatitic amphibolite†	Ygw				
(amphibolite)		-	-	yes	yes
(meta-leucogranite)		yes	yes	yes	yes
Orthogranofels and meta-leucogranite migmatite†	Ygg				
(orthogranofels)		-	-	yes	yes
(meta-leucogranite)		yes	yes	-	-
Sedimentary Protoliths					
Layered granofels†	Ylg	yes	-	-	yes
Migmatitic granofels†	Ymg	-	-	-	yes
Biotitic migmatite† (schist)	Ybm	-	-	-	yes

* Images available in Tollo and others (2010, 2012, this study).
† Composite lithology.
§ Leuocgranite intrudes schist within Ybm intrusive complex.

TABLE 4

Basement rock groups in the study area

Age Group and Lithologic Nomenclature	Map Symbol	Description
Late Magmatic Suite		
Biotite meta-quartz monzonite	Ybqm	occurs as small body within high-strain zone
Foliated biotite meta-quartz monzodiorite	Yfbd	defines small pluton
Porphyroclastic foliated meta-granite (HNT & FHNT*)	Ypfg	occurs as defomed, dismembered bodies
Meta-sedimentary cover rocks		
Layered granofels	Ylg	occurs as isolated body surrounded by older rocks
Biotitic migmatite (schist)	Ybm	occurs only as xenoliths within meta-leucogranite
Early Magmatic Suite		
Lineated biotite meta-granite	Ylbg	occurs as dismembered bodies within high-strain zone
Pink and gray meta-granite	Ypg	occurs as defomed, dismembered pluton
Meta-quartz monzonite	Yqm	poorly exposed; defines small intrusive body
Biotite meta-granite	Ybg	forms large, contiguous pluton
Porphyroclastic foliated meta-granite (LNT*)	Ypfg	occurs as defomed, dismembered bodies
Biotitic migmatite (meta-leucogranite)	Ybm	encloses and intrudes blocks of schist and rare granofels
Foliated biotite meta-leucogranite	Yfbl	poorly exposed, possibly underlies broad area
Xenoliths and pre-intrusive country rock		
Migmatitic granofels§	Ymg	occurs as outcrop-scale xenolith
Foliated amphibole gneiss	Yagn	occurs as outcrop-scale xenolith
Layered amphibolite	Yla	occurs as multiple outcrop-scale xenoliths
Gray and white migmatitic amphibolite	Ygw	defines small map-scale† xenolith
Orthogranofels and meta-leucogranite migmatite	Ygg	constitutes largest map-scale xenolith in study area

* Subdivisions of Ypfg map unit include HNT: high-Nb type; FHNT: fractionated high-Nb type; LNT: low-Nb type.
§ Granofels component is sedimentary in origin.
† Feature can be portrayed on 1:24,000-scale map.

lithologies composed of granofels, gneiss, or amphibolite(s) intruded by leucogranite. Mineralogic assemblages, whole-rock geochemical compositions, and both textural features and geochronologic data from zircon indicate that the non-leucogranitic components in these rocks formed from both igneous and sedimentary protoliths.

The orthogranofels and meta-leucogranite migmatite (Ygg) lithology composes the largest pre-intrusive body, forming a map-scale country-rock block that is locally overlain by stratified rocks of the Neoproterozoic Mount Rogers Formation (fig. 3). All other mapped units that predate the earliest magmatic episode at Mount Rogers, including the migmatitic granofels (Ymg), foliated amphibole gneiss (Yagn), layered amphibolite (Yla), and gray and white migmatitic amphibolite (Ygw) litholgies (tables 3 and 4), occur as small map- (decameter) scale or outcrop- (meter) scale xenoliths. Migmatitic granofels (Ymg) occurs as a xenolith within the *ca.* 1140 Ma lineated biotite meta-granite (Ylbg) pluton; all others constitute xenoliths within the *ca.* 1160 Ma biotite meta-granite (Ybg) pluton (tables 3 and 4; Tollo and others, 2012). All of these lithologic units are composed of a melanocratic component (granofels in Ygg and Ymg, amphibolite in Yla and Ygw, finely layered gneiss in Yagn) intruded by leucogranite (table 2). Protoliths for the melanocratic components in the Ygg and Yagn units are interpreted as igneous based on shape and chemical zoning characteristics of constituent zircons (table 5); igneous protoliths are also inferred for melanocratic components of the Ygw and Yla units on the basis of whole-rock geochemical composition (table 6). However, a sedimentary protolith is indicated for granofels of the Ymg unit by the shape, internal textures, and age range of zircons (tables 5 and 7). U-Pb geochronologic analysis of zircons in meta-leucogranite of the Ygw and Ymg xenoliths, as well as the Ybm (biotite migmatite) intrusive complex (fig. 3), indicates igneous emplacement at *ca.* 1185 to 1170 Ma (tables 5 and 7). Zircons analyzed from the poorly exposed but likely widespread foliated biotite meta-leucogranite (Yfbl) pluton indicate igneous crystallization within this interval, suggesting that leucogranite intrusion was pervasive at this time.

The occurrence of hornblende + clinopyroxene in melanocratic components of the Ygw and Yagn lithologies suggests that peak metamorphism occurred at conditions that were transitional between upper amphibolite and lower granulite facies (Spear, 1993). Ages obtained by U-Pb SHRIMP isotopic analysis of zircons of likely metamorphic origin in melanocratic components of the Ygw, Yagn, and Yla units indicate metamorphism at *ca.* 1170 to 1140 Ma (table 7), a period that, for at least the Ygw unit, coincided with development of hornblende + clinopyroxene (table 2). Geochronologic analysis of zircons in several *ca.* 1180 to 1160 Ma plutons (pink and gray meta-granite (Ypg), biotite meta-granite (Ybg), and foliated biotite meta-leucogranite (Yfbl)) and meta-leucogranite of the composite Ygw lithology indicate similar-age metamorphism. However, U-Pb isotopic data obtained from zircon from numerous plutonic bodies of varying age, as well as the Yagn and Yla xenoliths, indicate that metamorphism also occurred at *ca.* 1070 to 1020 and *ca.* 1000 to 970 Ma, demonstrating that moderate- to high-grade metamorphic conditions were attained during multiple episodes throughout the study area. Application of the Ti-in-zircon geothermometer of Watson and others (2006), as revised by Ferry and Watson (2007), allows further refinement of metamorphic conditions. Concentrations of Ti measured in *ca.* 1050 and *ca.* 1160 Ma zircon overgrowths and discrete metamorphic grains of *ca.* 1050 Ma and *ca.* 1160 Ma age in the porphyroclastic foliated meta-granite (Ypfg, overgrowths only) and Ygw (amphibolite component, both overgrowths and discrete grains) units indicate that metamorphic temperatures reached *ca.* 740 °C during both regional episodes (Tollo and others, 2010), consistent with temperatures that likely characterized the transition from amphibolite- to lower granulite-facies conditions, which resulted in coexistence of hornblende and clinopyroxene in rocks of appropri-

TABLE 5

Lithologic units, locations, and descriptions of zircon and titanite geochronology samples, Mount Rogers area, Virginia

Sample number	Location on Fig. 3	Lithologic unit and rock type[1]	Location Easting	Location Northing	Mineral[2]	Figure number	Description[3]	l/w[4]
Late Magmatic Suite								
MR-10-132	1	Ybqm biotite meta-quartz monzonite	475336	4054336	Zrn	5A	co-lb, eu	2-4
					Ttn	5A	co-db	1-2
MR-09-117	2	Yfbd foliated biotite meta-monzodiorite	460956	4041485	Zrn	5A	co,eu	3-5
MR-06-17	3	Ypfg porphyroclastic meta-syenogranite[5] HNT			Zrn			
MR-08-76	4	Ypfg porphyroclastic meta-syenogranite HNT	466425	4050699	Zrn	5B	lb,eu	3-4
Early Magmatic Suite								
MR-11-193	5	Ylbg lineated biotite meta-granite	472624	4048678	Zrn	5B	lb-mb, eu	2-4
MR-06-19	7	Ypg biotite meta-granite (alkali feldspar granite)	446200	4047320	Zrn	5B	mb, eu	2-4
MR-06-1	8	Ypg biotite meta-granite (alkali feldspar granite)[5]			Zrn			
MR-06-22	8	Ypg meta-granite (monzogranite)[5]			Zrn			
MR-08-79	6	Ypfg porphyroclastic meta-syenogranite LNT	460449	4046050	Zrn	5D	lb-mb, eu	2-5
MR-08-88	9	Yqm meta-quartz monzonite	461358	4043748	Zrn	5C	mb, su-eu	2-4
MR-08-66	10	Ybg biotite meta-granite (med- to crs-grained)	462483	4052445	Zrn	5C	db, eu	1-4
					Ttn	5C	lb-mb, pg, an	1-2
MR-08-71	11	Ybg biotite meta-granite (porphyritic)	464813	4052509	Zrn	5D	db, eu	2-5
MR-09-100	12	Yfbl biotite meta-leucogranite	452051	4040285	Zrn	5D	db, eu	3-5
Leucocratic components of composite units								
MR-08-84	13	Ybm meta-alkali feldspar granite	465933	4042152	Zrn	5E	lb-mb, eu	3-5
MR-08-65	14	Ygw meta-leucogranite[5]			Zrn			
MR-10-124	15	Yagn amphibole meta-leucogranite	471184	4053763	Zrn	5E	mb, eu	2-5

Table 5
(continued)

Sample number	Location on Fig. 3	Lithologic unit and rock type[1]	Location Easting	Location Northing	Mineral[2]	Figure number	Description[3]	l/w[4]
Xenoliths								
MR-10-123	15	Yagn amphibole gneiss	471184	405373	Zrn	5F	dk, eu	2-4
					Ttn	5F	co-mb	1-2
MR-08-70	16	Yla layered amphibolite	464857	405282	Zrn	5G	mb, eu	3-5
					Ttn	5G	co-mb	1-2
MR-06-4	14	Ygw medium-grained amphibolite (gray)[5]			Zrn			
MR-06-7	18	Ygg amphibole granofels[5]			Zrn			
Meta-sedimentary rocks								
MR-12-223	5	Ymg migmatitic granofels	472528	404860	Zrn	5H	DZ	
MR-09-104	17	Ylg amphibole + biotite layered granofels	451392	404075	Zrn	5I	DZ	
MR-08-83B	13	Ybm biotite schist	465933	404212	Zrn	5J	co, su-eu	1-2

[1] Abbreviations: HNT (high-Nb type), LNT (low-Nb type).
[2] Abbreviations: Zrn(zircon), Ttn (titanite).
[3] Abbreviations: eu (euhedral, prismatic), co (colorless), lb (light brown), mb (medium brown), db (dark brown), pg (pale green), su (subhedral), an (anhedral), DZ (detrital zircon).
[4] l/w (length-to-width ratio).
[5] Data in Tollo and others (2010).

TABLE 6

Geochemical compositions of representative samples of Mesoproterozoic basement units

	Sample number and map unit					
Map location	1*	2*	3*	4*	5A*	5B*
Map Unit	Ybqm	Yfbd	Ypfg	Ypfg	Ylbg	Ylbg
Lithology	quartz monzonite	quartz monzodiorite	syenogranite	alkali fsp granite	granodiorite	quartz syenite
Sample	MR-10-132	MR-09-117	MR-06-17	MR-08-76	MR-11-167	MR-11-193
SiO_2	62.54	54.10	71.61	69.43	70.26	64.71
TiO_2	1.33	2.29	0.67	0.60	0.37	0.65
Al_2O_3	14.91	15.25	13.54	14.96	15.05	16.11
Fe_2O_3†	6.74	11.70	3.25	3.28	3.01	5.55
MnO	0.10	0.20	0.05	0.05	0.05	0.13
MgO	1.51	2.61	0.69	0.74	1.11	0.59
CaO	3.28	6.79	1.52	1.06	1.76	2.6
Na_2O	4.27	3.18	2.51	3.44	6.11	4.18
K_2O	4.27	2.32	5.65	5.75	1.90	5.09
P_2O_5	0.64	1.03	0.20	0.23	0.14	0.15
Total	99.58	99.47	99.69	99.54	99.76	99.76
Rb	82.7	51.9	138.3	153.7	37.7	95.2
Ba	3022	3358	1330	1115	850	1618
Sr	310	1051	301	321	259	234
Pb	15	23	19	21	7	14
Th	3.97	5.77	36.3	35.0	10.20	2.57
U	0.81	1.2	1.9	2.7	0.36	0.79
Zr	563	1132	392	402	169	629
Hf	14.1	33.9	13.5	11.8	5.0	19.5
Nb	25.1	34.8	31.9	33.8	4.3	23.7
Ta	1.22	1.47	3.67	3.08	0.20	1.22
Ni	8	2	4	4	5	3
Zn	125	311	57	74	36	118
Cr	37	9	19	49	20	27
Ga	21	27	19	22	15	21
V	78	96	29	32	30	14
La	72	162	136	124	45	44
Ce	225.0	348.0	346.0	357.0	113.0	102.0
Nd	105	178.0	116.0	119.0	40.0	56.2
Sm	17.7	30.20	18.40	17.40	5.57	11.40
Eu	4.08	6.70	2.77	2.70	1.34	3.29
Gd	15.2	21.10	12.60	10.80	3.49	10.90
Tb	1.69	2.78	1.80	1.53	0.45	1.54
Ho	1.77	2.71	2.02	1.78	0.50	1.74
Tm	0.62	0.91	0.79	0.66	0.19	n.d.
Yb	3.65	5.13	4.86	4.03	1.07	4.43
Lu	0.54	0.7	0.7	0.6	0.17	0.65
Y	41.5	67.0	47.6	31.6	11.4	43.1
Sc	13.10	23.40	2.87	3.58	6.53	13.20
Group§	LMS	LMS	LMS#	LMS#	EMS	EMS

NOTE: Major elements expressed in weight percent; trace elements in ppm. Elements in italics anayzed by neutron activation; others by X-ray fluorescence.

* U/Pb dating locality; † total iron expressed as Fe_2O_3 ; n.d., not detected.

§ Groups: EMS, Early Magmatic Suite; LMS Late Magmatic Suite; XEN, map-scale xenolith; SED, meta-sedimentary; # High-Nb type of Ypfg lithologic unit.

TABLE 6
(continued)

	Sample number and map unit					
Map location	6*	7*	7*	8*	9*	9*
Map Unit	Ymg	Ypg	Ypg	Ybm	Ybg	Ybg
Lithology	granofels	syenogranite (pink)	monzogranite (gray)	leucogranite	monzogranite	monzogranite
Sample	MR-12-223 A	MR-06-1	MR-06-22	MR-08-84	MR-08-66	MR-08-71
SiO_2	74.84	76.48	71.73	69.86	70.54	71.03
TiO_2	0.36	0.09	0.43	0.43	0.38	0.38
Al_2O_3	12.08	13.54	13.96	15.16	15.05	14.88
Fe_2O_3†	4.54	1.09	3.12	3.21	3.07	3.07
MnO	0.07	0.02	0.04	0.05	0.06	0.06
MgO	1.36	0.17	0.89	1.32	0.74	0.80
CaO	1.04	0.33	1.92	1.80	1.88	1.49
Na_2O	2.30	3.18	4.07	4.53	4.56	3.95
K_2O	3.03	5.18	3.32	3.05	3.63	3.76
P_2O_5	0.08	0.02	0.13	0.12	0.13	0.13
Total	99.70	100.10	99.61	99.53	100.04	99.55
Rb	79.1	113.4	78.3	37.9	103.2	111.6
Ba	656	371	1070	1524	1179	1142
Sr	104	98	306	662	400	329
Pb	21	18	6	23	11	14
Th	8.63	18.1	11.4	8.2	11.6	9.7
U	1.07	4.2	4.5	0.4	1.7	3.4
Zr	152	88	273	145	183	186
Hf	4.53	3.8	7.2	4.3	4.7	5.1
Nb	7.2	8.6	10.4	5.3	9.2	8.5
Ta	0.29	0.43	0.61	0.17	0.70	0.86
Ni	9	2	4	5	4	4
Zn	108	111	38	60	46	59
Cr	32	16	19	37	24	25
Ga	12	14	15	17	17	16
V	54	3	29	44	26	22
La	17	18	38	37	26	36
Ce	54.7	42.8	99.5	76.7	78.0	72.3
Nd	26.7	17.3	40.2	27.9	32.2	29.3
Sm	6.06	4.24	6.69	4.32	5.53	5.20
Eu	0.96	0.43	1.14	1.31	1.09	1.03
Gd	6.39	4.36	5.09	2.98	4.64	3.97
Tb	0.92	0.80	0.74	0.35	0.61	0.61
Ho	1.21	1.25	0.92	0.34	0.77	0.83
Tm	0.51	0.60	0.34	0.09	0.31	0.30
Yb	3.39	3.78	2.15	0.49	1.88	1.80
Lu	0.53	0.6	0.3	0.1	0.3	0.3
Y	31.1	32.5	21.4	7.2	17.6	19.0
Sc	9.10	2.18	4.24	4.11	4.66	4.56
Group§	XEN	EMS	EMS	EMS	EMS	EMS

NOTE: Major elements expressed in weight percent; trace elements in ppm. Elements in italics anayzed by neutron activation; others by X-ray fluorescence.

* U/Pb dating locality; † total iron expressed as Fe_2O_3 ; n.d., not detected.

§ Groups: EMS, Early Magmatic Suite; LMS, Late Magmatic Suite; XEN, map-scale xenolith; SED, meta-sedimentary.

TABLE 6
(continued)

	Sample number and map unit					
Map location	10*	11*	13*	12*	13*	14*
Map Unit	Ylg	Yfbl	Ygw	Yla	Ygw	Ygg
Lithology	granofels	leucogranite	leucogranite	amphibolite	amphibolite	granofels
Sample	MR-09-104	MR-09-100	MR-08-65	MR-08-70	MR-06-4	MR-06-7
SiO_2	67.57	73.95	75.62	56.31	53.39	62.30
TiO_2	0.91	0.28	0.04	1.08	1.23	0.61
Al_2O_3	11.18	14.34	13.24	18.13	17.12	17.23
Fe_2O_3†	5.38	2.10	0.32	8.24	9.17	5.70
MnO	0.11	0.05	0.01	0.16	0.22	0.10
MgO	1.27	0.53	0.01	3.42	4.60	2.90
CaO	7.13	1. 6	0.91	6.11	7.93	4.00
Na_2O	0.69	4.99	2.14	2.88	3.40	3.35
K_2O	5.45	1.72	7.70	3.18	2.39	2.97
P_2O_5	0.24	0.08	0.01	0.31	0.61	0.35
Total	99.91	99.50	100.00	99.82	100.06	99.51
Rb	96.2	40.8	164.1	95.8	93.6	105.2
Ba	1278	1096	1667	1141	918	1602
Sr	173	136	195	637	564	497
Pb	18	3	22	7	32	12
Th	12.2	29.2	1.2	3.9	8.6	7.7
U	3.0	2.6	0.09	2.4	2.5	0.5
Zr	238	162	23	175	223	127
Hf	6.4	5.8	0.62	4.2	5.8	3.7
Nb	14.4	4.9	0.3	9.0	13.2	10
Ta	1.06	0.13	0.01	0.49	0.78	0.63
Ni	23	5	2	9	44	25
Zn	77	23	5	100	161	79
Cr	134	28	19	36	89	47
Ga	11	15	10	20	20	19
V	76	24	1	139	139	90
La	28	27	11	18	54	43
Ce	69.9	65.4	17.1	69.3	135.0	101.0
Nd	34.1	21.0	4.32	34.7	67.8	41.6
Sm	6.28	2.96	0.56	7.05	13.40	7.06
Eu	1.47	0.99	0.89	2.01	3.13	1.57
Gd	5.99	2.80	0.54	5.42	10.50	5.13
Tb	0.81	0.22	0.03	0.93	1.40	0.64
Ho	1.11	0.25	0.04	1.20	1.66	0.84
Tm	0.44	0.08	0.05	0.50	0.67	0.30
Yb	2.75	0.46	0.06	2.99	4.01	1.81
Lu	0.4	0.1	0.01	0.4	0.6	0.3
Y	22.8	3.9	0.4	25.1	39.4	18.3
Sc	10.30	2.99	0.14	17.90	19.10	11.60
Group§	SED	EMS	EMS	XEN	XEN	XEN

NOTE: Major elements expressed in weight percent; trace elements in ppm. Elements in italics anayzed by neutron activation; others by X-ray fluorescence; * U/Pb dating locality; † total iron expressed as Fe_2O_3; n.d., not detected.

§ Groups: EMS, Early Magmatic Suite; LMS, Late Magmatic Suite; XEN, map-scale xenolith; SED, meta-sedimentary.

TABLE 6
(continued)

Standard	Sample number and map unit: USGS G-2 mean values	USGS G-2 stnd dev	BHVO-2 mean values	BHVO-2 stnd dev	Reference[#] mean values
SiO_2	69.35	0.288			**69.14**
TiO_2	0.48	0.008			**0.48**
Al_2O_3	15.39	0.128			**15.39**
Fe_2O_3[†]	2.66	0.013			**2.66**[†]
MnO	0.05	0.007			**0.03**
MgO	0.72	0.044			**0.75**
CaO	2.04	0.046			**1.96**
Na_2O	4.19	0.223			**4.08**
K_2O	4.49	0.031			**4.48**
P_2O_5	0.14	0.003			**0.14**
Total	99.49				-
Rb	166.4	0.963			**170**
Ba	1873.5	19.9			**1880**
Sr	480.1	2.26			**478**
Pb	30.3	0.478			**30**
Th			*1.21*	0.047	*1.22*
U			*0.45*	0.033	*0.403*
Zr	320.2	3.51			**309**
Hf			*4.33*	0.085	*4.36*
Nb	12.0	0.137			**12**
Ta			*1.22*	0.032	*1.14*
Ni	3.1	0.229			
Zn	91.8	0.713			**86**
Cr	8.2	2.15			
Ga	21.7	0.733			**23**
V	32.0	1.00			**36**
La	98.5	3.78			**89**
Ce			*38.02*	0.613	*37.5*
Nd			*24.81*	0.811	*24.5*
Sm			*6.20*	0.187	*6.07*
Eu			*2.07*	0.028	*2.07*
Gd			*6.30*	0.132	*6.24*
Tb			*0.95*	0.027	*0.92*
Ho			*1.06*	0.046	*0.98*
Tm			*0.35*	0.014	*0.33*
Yb			*2.04*	0.035	*2*
Lu			*0.29*	0.006	*0.274*
Y	9.1	0.491			**11**
Sc			*31.52*	0.422	*32*
no of analyses	80 (majors) 19 (traces)		12 (traces)		

NOTE: Major elements expressed in weight percent; trace elements in ppm. Elements in italics anayzed by neutron activation; others by X-ray fluorescence; * U/Pb dating locality; [†] total iron expressed as Fe_2O_3; n.d., not detected; [§] Groups: EMS, Early Magmatic Suite; LMS, Late Magmatic Suite; XEN, map-scale xenolith; SED, meta-sedimentary.

[#] USGS standard G-2 was run with XRF analyses; BHVO-2 was run with INA analyses. Values in bold from U.S. Geological Survey (http://crustal.usgs.gov/geochemical_reference_standards/granite.html); values in italics from GeoReM (http://georem.mpch-mainz.gwdg.de/sample_query_pref.asp).

TABLE 7

Summary of U-Pb geochronology, Mount Rogers area, Virginia

Sample number	Location on Fig. 3	Lithologic unit and rock type	Calculation method[1]	Igneous age (Ma)[3]	Metamorphic age (Ma)[3]	Inheritance age (s) (Ga)[4]
Late Magmatic Suite						
MR-10-132	1	Ybqm biotite meta-quartz monzonite	CA	1046 ± 14	1055 ± 11	
			TW3d		995 ± 22 (Ttn)	
			TW3d		906 ± 46 (Ttn)	
MR-09-117	2	Yfbd foliated biotite meta-monzodiorite	$^{206}Pb/^{238}U$	1055 ± 16	~ 990	
MR-06-17	3	Ypfg porphyroclastic meta-syenogranite[5] HNT	CA	1061 ± 5	1053 ± 5	
MR-08-76	4	Ypfg porphyroclastic meta-syenogranite HNT	$^{207}Pb/^{206}Pb$	1065 ± 9	1061 ± 7	
Early Magmatic Suite						
MR-11-193	5	Ylbg lineated biotite meta-granite	$^{207}Pb/^{206}Pb$	1140 ± 9	1049 ± 8	
					984 ± 17	
MR-06-19	7	Ypg biotite meta-granite (alkali feldspar granite)	$^{207}Pb/^{206}Pb$	1153 ± 8	discordant	
MR-08-88	9	Yqm meta-quartz monzonite	$^{207}Pb/^{206}Pb$	1155 ± 12	~1050-1000	1.31-1.22
MR-08-66	10	Ybg biotite meta-granite (med- to crs-grained)	CA	1157 ± 9	~1050-900	1.28-1.20
			TWa		1028 ± 30 (Ttn)	
MR-08-79	6	Ypfg porphyroclastic meta-syenogranite LNT	CA	1160 ± 7	~1050	
MR-06-22	8	Ypg meta-granite (monzogranite)[5]	$^{207}Pb/^{206}Pb$	1161 ± 7	1156 ± 10	1.33-1.29
					1117 ± 6	
					1047 ± 11	
					989 ± 9	
MR-06-1	8	Ypg biotite meta-granite (alkali feldspar granite)[5]	$^{207}Pb/^{206}Pb$	1162 ± 4	1157 ± 6	
					~1050	
MR-08-71	11	Ybg biotite meta-granite (porphyritic)	CA	1164 ± 10		
MR-09-100	12	Yfbl biotite meta-leucogranite	$^{207}Pb/^{206}Pb$	1181 ± 10	1163 ± 6	
Leucocratic components of composite units						
MR-08-84	13	Ybm meta-alkali feldspar granite	$^{207}Pb/^{206}Pb$	1166 ± 9	~1100	1.32-1.27
MR-08-65	14	Ygw meta-leucogranite[5]	$^{207}Pb/^{206}Pb$	1174 ± 6	1158 ± 7	
					1031 ± 12	
MR-10-124	15	Yagn amphibole meta-leucogranite	$^{207}Pb/^{206}Pb$	1183 ± 17	~1100-1050	

TABLE 7
(continued)

Sample number	Location on Fig. 3	Lithologic unit and rock type	Calculation method[1]	Igneous age (Ma)[3]	Metamorphic age (Ma)[3]	Inheritance age (s) (Ga)[4]
Xenoliths						
MR-10-132	1	Ybqm biotite meta-quartz monzonite	CA	1046 ± 14	1055 ± 11	
MR-10-123	15	Yagn amphibole gneiss	$^{207}Pb/^{206}Pb$	1177 ± 15	1168 ± 18	1.37-1.24
			$^{207}Pb/^{206}Pb$		1033 ± 11 (Ttn)	
			$^{207}Pb/^{206}Pb$		996 ± 11 (Ttn)	
MR-08-70	16	Yla layered amphibolite	$^{207}Pb/^{206}Pb$		1145 ± 5	
					~950	
			TWa		974 ± 45 (Ttn)	
MR-06-4	14	Ygw medium-grained amphibolite (gray)[5]	$^{207}Pb/^{206}Pb$		1164 ± 6	
					1148 ± 8	
					~1130	
					~1040	
MR-06-7	18	Ygg amphibole granofels[5]	CA	1327 ± 7	~1140-1060	
Meta-sedimentary rocks						
MR-12-233	5	Ymg migmatitic granofels			1049 ± 10	~1320-1150
MR-09-104	17	Ylg amphibole + biotite layered granofels			~1050-990	~1760-1120
MR-08-83B	13	Ybm biotite schist			1059 ± 9	

[1] Abbreviations: CA (Concordia Age), $^{206}Pb/^{238}U$ (weighted average of $^{206}Pb/^{238}U$ ages), $^{207}Pb/^{206}Pb$ (weighted average of $^{207}Pb/^{206}Pb$ ages), TW3d (Terra-Wasserburg 3-dimensional linear regression), Twa (Terra-Wasserburg, anchored at initial Pb).
[2] 2-sigma uncertainties.
[3] All ages are for zircon, unless indicated by (Ttn) = titanite.
[4] For meta-sedimentary rocks, the listed age range is for detrital zircon grains.
[5] Data in Tollo and others (2010).

ate composition (Spear, 1993) (table 2). In contrast, aggregates of fine-grained actinolite + chlorite + epidote in all amphibolites, low-silica granofels, and melanocratic components of composite gneissic units, indicate recrystallization at middle to upper greenschist-facies conditions (Spear, 1993). In such rocks, actinolite is locally intergrown with, or forms rims enveloping, prograde hornblende, a texture that suggests hornblende breakdown during retrograde metamorphism of likely Paleozoic age (Rankin and others, 1989).

Intrusive rocks typically define relatively large, mostly continuous bodies or smaller, discontinuous fragments of formerly larger plutons that were dismembered by faulting associated with Paleozoic high-strain zones (fig. 3). All plutons display high Afsp/plag ratios and are biotite bearing (table 2); primary hornblende occurs only in the meta-quartz monzonite (Yqm) and lineated biotite meta-granite (Ylbg) plutons. Magnetite, which is minor to absent in most plutons, occurs locally in the porphyroclastic foliated meta-granite (Ypfg) and is especially abundant in the foliated biotite meta-quartz monzodiorite (Yfbd) body. All plutons display coarse hypidiomorphic and interlocking crystalline textures indicative of probable magmatic origin. Nevertheless, all intrusive rocks are variably foliated with the extent of foliation related to biotite content. As a result, some relatively biotite-poor, older rocks such as the biotite meta-granite pluton (Ybg) appear to be less deformed than younger biotite-rich lithologies (for example, foliated biotite meta-quartz monzodiorite, Yfbd). Some intrusive rocks [for example, lineated biotite meta-granite (Ylbg) and pink and gray meta-granite (Ypg)] exhibit isoclinal folds that likely formed during Mesoproterozoic orogenesis (Tollo and others, 2012). Mineral assemblages indicative of high-grade metamorphism are lacking in all of the plutonic rocks; however, most plutonic rocks exhibit replacement of plagioclase by clinozoisite and primary ferromagnesian silicates by epidote + chlorite, preserving evidence of retrograde reactions that likely resulted from Paleozoic greenschist-facies metamorphism (Rankin and others, 1989).

The biotite meta-granite (Ybg) pluton, which is overlain by Neoproterozoic rocks along its northern border (fig. 3), composes the largest contiguous intrusive body in the study area and locally includes scattered xenoliths of older, migmatitic and amphibolitic rocks (for example, Yagn, Yla, and Ygw lithologies). The Ybg body includes porphyritic and medium- to coarse-grained varieties of otherwise mineralogically similar lithologies, as well as locally crosscutting, biotite-bearing pegmatite dikes of probable co-magmatic origin (table 2). The similarly inhomogeneous pink and gray meta-granite body (Ypg) contains approximately equal proportions of meta-alkali feldspar granite (pink) and meta-monzogranite (gray) that locally define centimeter- to decameter-scale layers. Crosscutting dikes indicate that alkali feldspar granite intruded monzogranite. Most other plutons are composed of a single, dominant lithology but contain internal features such as mineralogically similar dikes and pegmatitic segregations.

U-Pb geochronologic analysis indicates that intrusive activity occurred at *ca.* 1190 to 1130 Ma (herein called the Early Magmatic Suite) and *ca.* 1075 to 1030 Ma (herein called the Late Magmatic Suite) (tables 4 and 7). Crosscutting field relationships and map patterns among the plutonic rocks are consistent with an extended magmatic history (table 2, fig. 3). For example, the xenolith-bearing, biotite meta-granite pluton (Ybg) is locally intruded by meta-syenogranite of the porphyroclastic foliated meta-granite (Ypfg) lithology, whereas the latter is intruded by the small foliated biotite meta-quartz-monzodiorite (Yfbd) pluton. Evidence of extended magmatic processes is preserved by small xenoliths of layered amphibolite (Yla) that are included within *ca.* 1160 Ma biotite meta-granite (Ybg) and *ca.* 1060 Ma meta-syenogranite of the porphyroclastic foliated meta-granite (Ypfg) plutons, suggesting that some of the oldest

country rock in the area was repeatedly intruded during episodic pulses of plutonism (table 2).

Rocks constituting nearly all plutons are mutually distinguishable in the field based on differences in characteristic texture and mineral assemblage (table 2). However, results from detailed geochemical and geochronologic analysis indicate that one of the ten bodies composed of porphyroclastic foliated meta-granite (Ypfg) is compositionally and temporally distinct from the others (tables 6–8). Consequently, and because this distinction cannot be reliably observed in this strongly deformed lithology in the field, the original map unit is retained with the compositional variants defined as LNT (low-Nb type, *ca.* 1160 ± 7 Ma) and HNT (high-Nb type, *ca.* 1065 Ma). The latter includes the FNHT (fractionated, high-Nb type) derivative of presumed similar age.

Age sequences, areal extent of individual plutons, and mutual contact relations are locally obscured by numerous, generally NE-striking, high-strain zones that traverse the study area (fig. 3). The generally sinuous and anastomozing high-strain zones are mapped wherever mylonite and/or protomylonite constitute the prevailing rock type and have undergone sufficient recrystallization to preclude determination of protolith (Tollo and others, 2012). Wherever small strands or boudins of less deformed plutonic rock are present or identification of protolith is reliably accomplished by other means [for example, through comparison of trace-element concentrations (Radwany, unpublished BS thesis, George Washington University)], the pre-mylonitic protolith is mapped. In all cases, the orientation of high-strain zones is mapped as parallel to local mylonitic foliation. The existence of multiple strands of anastomozing high-strain zones is not reflected in previous reconnaissance-scale, geologic maps of the area in which researchers generally portrayed single, thoroughgoing faults of regional extent (for example, the Fries fault zone of Rankin and others, 1972).

Rocks that originally constituted sedimentary cover include the granofels component of the composite layered granofels (Ylg) and migmatitic granofels (Ymg) map units, and the schist component of the composite biotitic migmatite (Ybm) (table 4) (see photographs in Tollo and others, 2012). The sedimentary nature of protoliths is deduced primarily on the basis of (1) geochemical composition (table 6), (2) mineralogic assemblages (table 2), and, especially, (3) the presence and shape of constituent zircons (table 5). Originally psammitic units contain detrital zircon whereas originally finer-grained rocks contain only zircon produced by *in situ* metamorphic crystallization. Layered granofels (Ylg) occurs as an isolated body surrounded by *ca.* 1180 Ma foliated biotite meta-leucogranite (Yfbl) (fig. 3) but contains zircons of detrital origin that are younger than the igneous crystallization age of the meta-leucogranite (table 7). As a result, the layered granofels is interpreted as unconformably overlying the meta-leucogranite. Meta-leucogranite occurring within the Ylg unit correspondingly must be younger than leucogranitic components in other, lithologically composite units (Ygw, Ymg, and Ybm). The migmatitic granofels lithologic unit (Ymg) likewise occurs as an isolated block surrounded by lineated biotite meta-granite (Ylbg) (fig. 3). However, the migmatitic granofels, which contains detrital zircons as young as *ca.* 1159 Ma, is intruded by the *ca.* 1140 ± 9 Ma meta-granite, indicating that sedimentation occurred 10 to 20 m.y. prior to granite emplacement. Biotite schist of the lithologically composite biotitic migmatite (Ybm) unit is intruded by *ca.* 1166 ± 9 Ma meta-leucogranite but, likely because of the fine-grained nature of sedimentary protolith, lacks detrital zircon that might define a possible interval for sedimentation.

U-Pb Geochronology

Methods.—Zircon and titanite were extracted from *ca.* 5 kg samples collected at outcrops. Standard mineral separation procedures, carried out at USGS-Denver laboratories, involved crushing and pulverizing, followed by processing using a Wilfley table,

TABLE 8

Compositions of representative samples of geochemical types of the Ypfg lithologic unit

	Sample number and map unit					
Map Unit	Ypfg	Ypfg	Ypfg	Ypfg	Ypfg	Ypfg
Type*	LNT	LNT	LNT	HNT	FHNT	FHNT
Lithology	monzogranite	monzogranite	monzogranite	monzogranite	syenogranite	syenogranite
Sample	MR-08-79†	MR-09-87	MR-09-111	MR-09-93	MR-09-112	MR-09-114
SiO_2	72.72	67.06	72.22	73.87	76.13	75.62
TiO_2	0.36	0.56	0.38	0.42	0.10	0.08
Al_2O_3	13.31	15.65	14.09	13.15	12.46	12.73
Fe_2O_3§	3.11	3.78	2.71	2.53	2.31	2.12
MnO	0.06	0.08	0.07	0.05	0.06	0.05
MgO	0.36	1.38	0.91	0.40	0.00	0.00
CaO	1.37	3.19	2.24	1.24	0.72	0.75
Na_2O	2.82	3.71	2.74	2.40	2.84	3.06
K_2O	5.32	4.04	4.11	5.26	5.20	5.18
P_2O_5	0.09	0.19	0.12	0.13	n.d.	n.d.
Total	99.52	99.64	99.59	99.45	99.82	99.59
Rb	77.0	75.3	76.9	153.0	142.4	173.1
Ba	925	1384	1024	1046	11	2
Sr	275	594	428	413	16	7
Pb	11	17	15	25	23	30
Th	8.3	5.9	6.9	41.6	17.7	18.7
U	0.8	0.3	0.4	2.8	1.8	2.3
Zr	266	168	131	306	196	147
Hf	7.8	5.5	4.0	10.6	11.0	10.4
Nb	9.2	8.8	6.2	27.7	72.0	73.8
Ta	0.48	0.52	0.37	2.28	3.73	4.18
Ni	2	8	7	2	3	3
Zn	40	60	47	45	93	121
Cr	36	40	21	16	9	12
Ga	16	16	14	20	26	28
V	13	53	31	15	n.d.	n.d.
La	57	37	33	122	48	32
Ce	111.0	89.9	82.7	282.0	137.0	112.0
Nd	52.5	40.8	33.2	83.1	90.2	73.6
Sm	8.42	7.19	5.37	11.80	27.70	24.50
Eu	1.66	1.63	1.27	1.88	0.40	0.28
Gd	7.30	5.64	4.16	8.02	29.00	28.60
Tb	0.97	0.86	0.58	1.02	5.21	4.97
Ho	1.16	1.00	0.69	1.19	6.42	6.54
Tm	0.43	0.39	0.22	0.46	2.34	2.47
Yb	2.42	2.42	1.37	2.81	13.00	13.90
Lu	0.4	0.3	0.2	0.4	1.8	2.0
Y	24.9	25.2	15.3	23.8	142.0	135.9
Sc	6.46	7.81	4.54	1.69	0.48	0.28

Major elements expressed in weight percent; trace elements in ppm. Elements in italics anayzed by neutron activation; others by X-ray fluorescence.

* Geochemical types include: LNT, low-Nb type; HNT, high-Nb type; and FHNT, fractionated high-Nb type.

† U/Pb dating locality § total iron expressed as Fe_2O_3 n.d., not detected.

magnetic separator, and heavy liquids to obtain heavy-mineral concentrates that contain zircon ± titanite. Titanite and zircon were separated by operating the magnetic separator at full current (~1.8A) and decreasing the side tilt (between about 5 and 10°) such that most zircon remained in the non-magnetic split, whereas titanite was concentrated in the magnetic split. The least damaged zircon and titanite grains from meta-igneous rocks were hand picked and placed onto double-sided tape; detrital zircon from meta-sedimentary rocks was sprinkled to minimize sampling bias. Zircon and titanite were mounted in epoxy, ground to about half thickness, and sequentially polished using 6 μm and 1 μm diamond suspensions. All polished grains were imaged in reflected and transmitted light using a petrographic microscope. Using the USGS-Denver JEOL5800LV scanning electron microscope (SEM), zircon was imaged in cathodoluminescence (CL), whereas titanite was imaged by backscattered electrons (BSE). Many samples contain multiple morphologies of zircon and titanite; representatives of all morphologies were selected for analysis.

Zircon and titanite were dated by the U-Pb method using SHRIMP techniques following methods described in Williams (1998). Specifically, 14 (of 15) zircon samples from meta-igneous rocks were analyzed on a SHRIMP II, either at the Research School of Earth Sciences (RSES), Australian National University, Canberra or at the Geological Survey of Canada (GSC), Ottawa. One igneous zircon sample (MR-08-79z) and two (of three) detrital zircon samples were analyzed on the USGS/Stanford SHRIMP-RG (sensitive high resolution ion microprobe-reverse geometry); one detrital sample (MR-12-233z) was analyzed on the RSES SHRIMP II. Titanite samples were analyzed on the GSC SHRIMP II or USGS/Stanford SHRIMP-RG. For all analyses, the primary beam was adjusted to a diameter of about 20 to 25 μm. For igneous or metamorphic zircon and titanite, the magnet was cycled through the appropriate mass stations five or six times, whereas for detrital zircon the magnet was cycled four times to maximize the number of grains analyzed. Measured $^{206}Pb/^{238}U$ ratios for zircon and titanite analyses were normalized to values for standards R33 (419 Ma; Black and others, 2004) and BLR-1 (1047 Ma; Aleinikoff and others, 2007), respectively.

SHRIMP age data for zircon and titanite are reduced using Squid 1 or Squid 2 (Ludwig, 2001, 2009) and plotted using Isoplot 3 (Ludwig, 2003). All data are plotted as 2-sigma error ellipses or error bars, and all calculated ages are reported with 2-sigma uncertainties. Concentrations of U and Th are believed to be accurate to about ± 20 percent, (Ireland and others, 1999) and are only used for comparative purposes. U-Pb age data for zircon from Mesoproterozoic intrusive rocks are shown on conventional concordia plots. Emplacement ages are calculated using either the weighted average of selected $^{207}Pb/^{206}Pb$ or $^{206}Pb/^{238}U$ ages or, if there are a sufficient number of concordant analyses, as a Concordia Age (Ludwig, 2003). U-Pb data for Paleozoic titanite are shown on Tera-Wasserburg plots. Due to high common Pb and low U concentrations, ages are calculated using either the three-dimensional linear fit algorithm in Isoplot 3 if there is sufficient spread in the data or by anchoring the regression to a common Pb value for $^{207}Pb/^{206}Pb$ and determining the lower intercept age. U-Pb data for detrital zircon are screened to exclude ages that are discordant by more than 10 percent as indicated by Relative Probability plots of age distributions.

Results.—U-Pb geochronologic data for samples from the study area are discussed below in order of increasing age within five groupings: (1) Late Magmatic Suite, (2) Early Magmatic Suite, (3) leucocratic components of composite units, (4) xenoliths, and (5) meta-sedimentary rocks. For all samples, we include CL images of representative grains, a concordia plot of U-Pb data, and, in many cases, a weighted average plot showing the number of analyses used to calculate the age. For samples that yielded concordant data, the Concordia Age is given. Sample numbers, rock type, locations of dated samples, and zircon (and titanite if present) morphologies are summarized in

table 5. A summary of U-Pb results for dated basement rocks of the Mt. Rogers area (both new and previously published in Tollo and others, 2010) is presented in table 7.

Late Magmatic Suite

MR-10-132 (Ybqm biotite meta-quartz monzonite).—Zircon from MR-10-132 is colorless to light brown, euhedral and prismatic, and has length-to-width ratios (l/w) of about 2 to 4 (table 5). All grains contain oscillatory-zoned cores and most grains have discontinuous, narrow, faintly oscillatory-zoned rims (fig. 5Aa). Cores and rims are geochemically distinct; cores have relatively low U (~24–120 ppm) and high Th/U (0.7–1.3), whereas rims have higher U (~180–350 ppm) and lower Th/U (0.4–0.7) (Appendix A). Both cores and rims yield similar concordant data, resulting in Concordia Ages of 1046 ± 14 Ma (n=13) and 1055 ± 11 Ma (n=9), respectively (fig. 5Ab). These data suggest that the igneous protolith was metamorphosed shortly after it was emplaced, both at about 1050 Ma. Alternatively, considering the indistinguishable (within error) ages of the cores and rims, and the moderately high Th/U of the rims, it is possible that the darker outer areas of the grains reflect the latest crystallization of igneous zircon.

Two populations of titanite from MR-10-132 were analyzed: (1) dark brown, anhedral, with U contents of 34 to 255 ppm, and (2) colorless, anhedral, with U contents of 5 to 17 ppm (Appendix B). Dark brown grains frequently have colorless rims (fig. 5Ac, right). As shown in BSE imagery, pale gray cores are overgrown by dark gray rims, reflecting the relatively higher U in the cores (fig. 5Ac, left). A three-dimensional linear regression through data from 13 brown grains and 3 colorless grains yields an intercept age of 995 ± 22 Ma. Analyses of four other grains (3 colorless grains and 1 pale brown grain; fig 5Ad) yield an imprecise younger intercept age of 906 ± 46 Ma.

MR-09-117 (Yfdb foliated biotite meta-monzodiorite).—Zircon from MR-09-117 is colorless, euhedral and prismatic, and has l/w of about 3 to 5 (table 5). All grains have oscillatory-zoned, partially resorbed cores that are overgrown by one or more rims. The rims are light-gray and broad, or black, narrow, and discontinuous in CL (fig. 5Ae). Cores and rims are geochemically distinct; cores have relatively low U (~20–152 ppm) and high Th/U (0.7–1.3), whereas rims have higher U (~165–282 ppm) and lower Th/U (0.5–0.7) (Appendix A). The weighted average of 13 (of 14) $^{206}Pb/^{238}U$ ages for cores is 1055 ± 16 Ma (fig. 5Af), which is interpreted as the age of crystallization of the igneous protolith. Four rims yield ages of about 990 Ma.

MR-08-76 (Ypfg porphyroclastic meta-syenogranite-HNT).—Zircon from MR-08-76 is light brown, euhedral, and prismatic (l/w of about 3–4; table 5). All grains are extensively cracked, making it difficult to locate pristine areas for SHRIMP analysis. All grains include oscillatory-zoned, partially resorbed cores that are overgrown and locally invaded by black rims (fig. 5Ba). Cores and rims are geochemically distinct; cores have relatively low to moderate U (~45–332 ppm) and moderate to high Th/U (0.4–2.5), whereas rims have higher U (~269–814 ppm) and much lower Th/U (0.1–0.5). Although the ages for cores and rims are very similar, we calculate separate ages for each because of the marked textural distinctions. The weighted average of nineteen $^{207}Pb/^{206}Pb$ ages for cores is 1065 ± 9 Ma, which is interpreted as the emplacement age of the igneous protolith. The weighted average of twelve $^{207}Pb/^{206}Pb$ ages for rims is 1061 ± 7 Ma. (fig. 5Bb). We interpret these results to indicate that crystallization of igneous protolith was followed closely by metamorphic crystallization that formed the invasive overgrowths.

Early Magmatic Suite

MR-11-193 (Ylbg lineated biotite meta-granite).—Zircon from sample MR-11-193 is light to medium brown, euhedral, and prismatic (l/w of 2–4; table 5); many of the

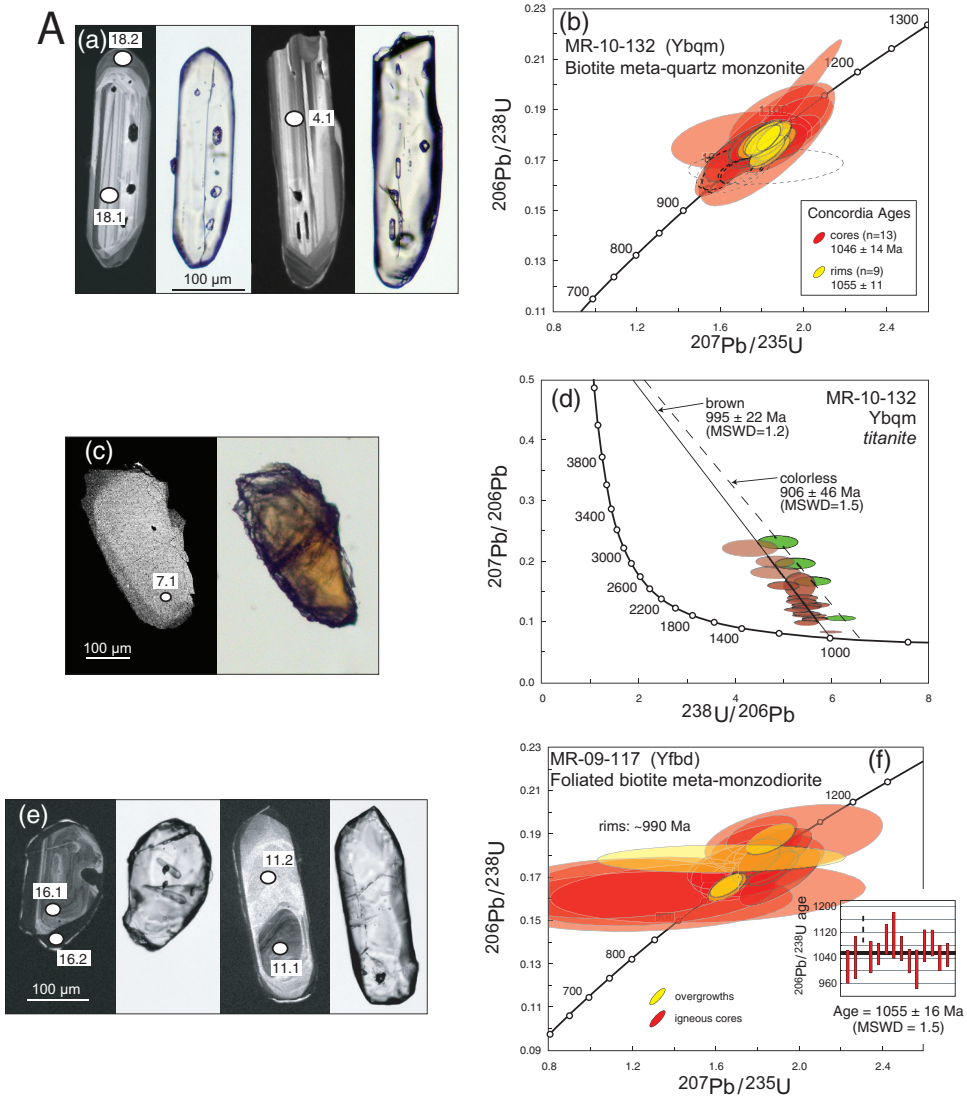

Fig. 5. Imagery of representative grains and plots of isotopic data for analyzed samples. In all geochronologic plots, data used to calculate ages are shown as colored error ellipses: red for zircon cores, yellow for zircon rims, and tan for inherited material; brown and green for titanite. In all figures, cathodoluminescence (CL) (left) and transmitted light (right) image pairs for representative zircon or back-scattered electrons (BSE) (left) and transmitted light (right) image pairs for representative titanite are shown. Also shown are conventional Concordia plots (for zircon) and Tera-Wasserburg Concordia plots (for titanite) of SHRIMP data. Where data are concordant, a Concordia Age (Ludwig, 1980, 2003) is calculated. For slightly discordant data, a weighted average of selected $^{207}Pb/^{206}Pb$ ages is calculated. See text for further discussion. MSWD—mean square of weighted deviates. Locations of SHRIMP analytical spots are indicated by white ovals. (A). a—Prismatic and stubby zircon, showing oscillatory-zoned igneous cores and faintly-zoned (or unzoned) dark rims; from Ybqm sample MR-10-132. b—Both cores and rims yield concordant data from which Concordia ages are calculated. c—Faintly zoned, anhedral titanite from sample MR-10-132. The transmitted light image shows a thin rim of colorless material (dark gray in BSE) partly surrounding a brown core (light gray in BSE). d—three-dimensional linear regressions through isotopic data for brown and colorless titanite. e—stubby and prismatic zircon showing oscillatory-zoned igneous cores and light and dark rims; from Yfbd sample MR-09-117. f—Concordia plot for cores and rims, weighted average plot for cores only. Due to the limited number of analyses, the rim age is approximated.

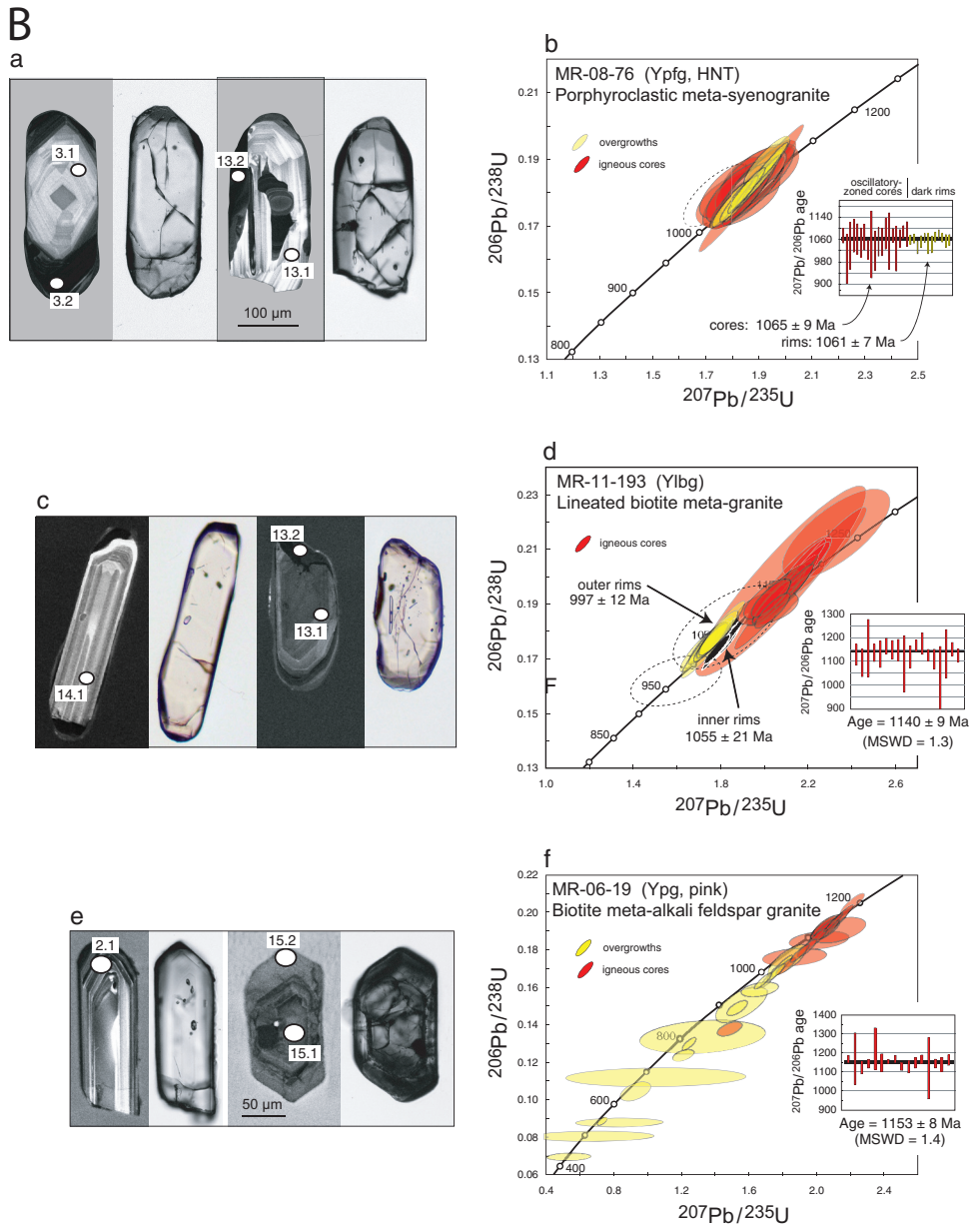

Fig. 5B. a—Prismatic zircon showing dark rims surrounding and invading oscillatory-zoned cores; from Ypfg (HNT type) sample MR-08-76. b—Concordia plot showing overlapping analyses of cores and rims; ages of cores and rims are calculated separately. Error bars for rims are smaller than for cores due to higher U content of rims. c—Prismatic and stubby zircon, showing oscillatory-zoned igneous cores overgrown by two generations of medium to dark gray unzoned rims; from Ylbg sample MR-11-193. d—Concordia plot of analyses of cores, plus inner and outer rims. Weighted average plot for cores only. e—Two populations of zircon (light and dark in CL and transmitted light); from meta-alkali feldspar granite component of the Ypg lithologic unit, sample MR-06-19. f—Concordia plot for cores also showing extreme discordance of isotopic data from rims. Weighted average plot for cores only.

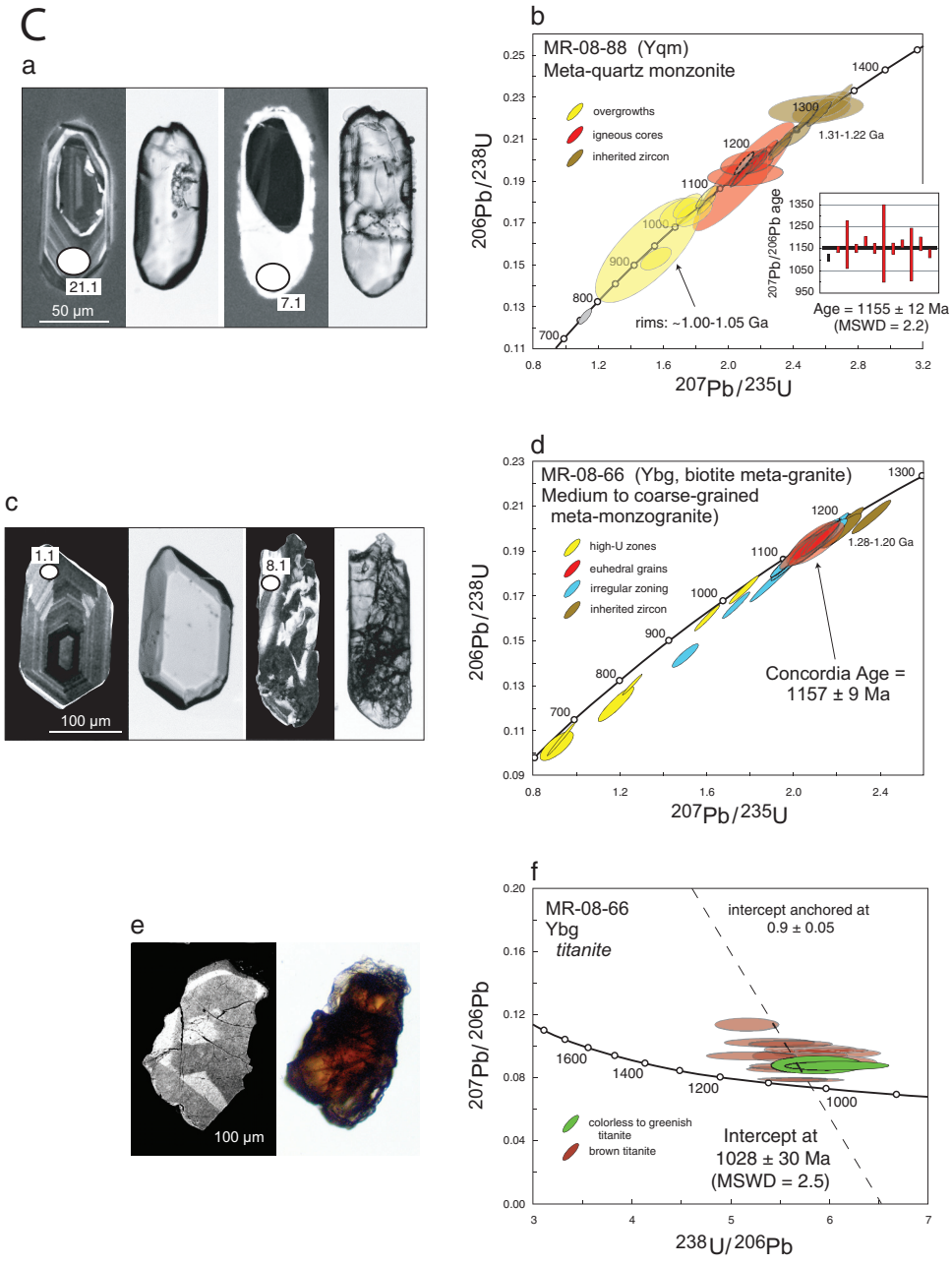

Fig. 5C. a—Prismatic zircon showing CL zoning of cores, and light and dark rims; from Yqm sample MR-08-88. b—Concordia plot showing analyses of inherited, igneous core, and rim components. Weighted average plot for igneous cores only. c—Stubby (pristine) and prismatic (fractured) morphologies of zircon showing two types of CL zoning; from Ybg (medium- to coarse-grained facies) sample MR-08-66. d—Concordia plot distinguishing isotopic data for inherited cores, euhedral (pristine) cores (with Concordia Age calculated), irregularly zoned cores, and high-U rims. e—Zoned, anhedral titanite from sample MR-08-66. The transmitted light image shows a thin rim of colorless material (dark gray in BSE) overgrown on a brown core (light gray and white in BSE). f—Linear regression (anchored) through analyses for brown variety of titanite.

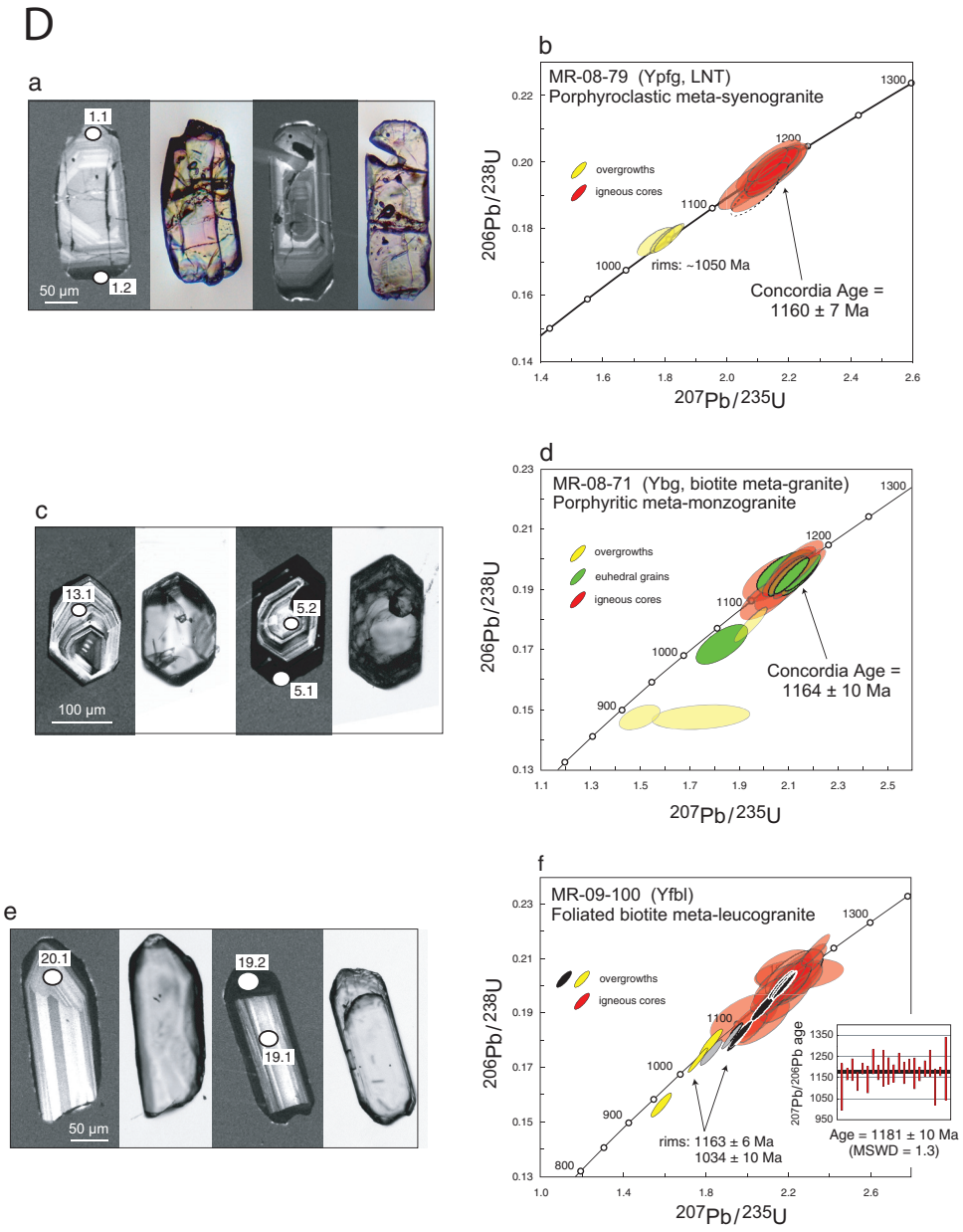

Fig. 5D. a—Prismatic zircon showing oscillatory-zoned cores and dark, unzoned rims; from Ypfg sample MR-08-79. Note extensive fracturing of grains. b—Concordia plot showing concordant analyses of cores and approximate age of rims. c—Stubby zircon showing oscillatory-zoned cores and thin to thick (and invasive) dark, unzoned rims; from Ybg (porphyritic facies) sample MR-08-71. d—Concordia plot for analyses from two morphologies of cores, plus rims. Concordia Age calculated using both types of cores. e—Prismatic zircon showing oscillatory-zoned cores and dark, unzoned rims; from Yfbl sample MR-09-100. f—Concordia plot showing isotopic data for cores and two types of rims. Weighted average plot for cores only. Data shown by gray ellipses are excluded from rim age calculation.

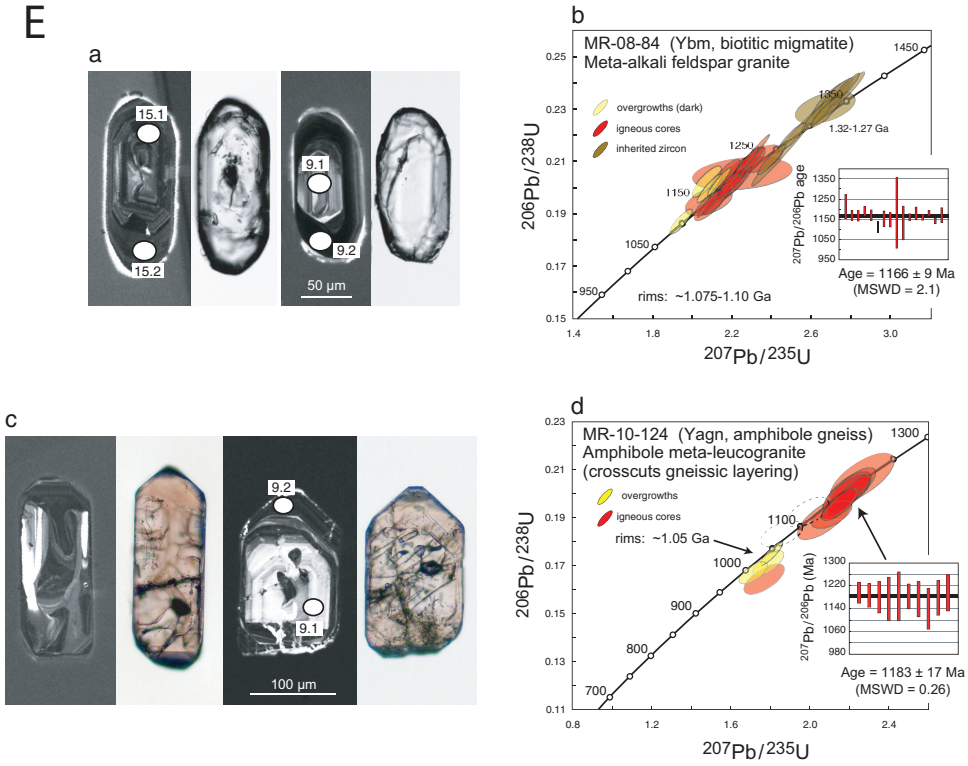

Fig. 5E. a—Prismatic zircon displaying inherited cores, igneous cores, and faintly zoned to dark, unzoned rims; from meta-alkali feldspar granite (meta-leucogranite component) of the Ybm composite lithologic unit, sample MR-08-84. b—Concordia plot showing isotopic analyses for inherited cores, igneous cores, and rims. Weighted average plot for igneous cores only. c—Prismatic and stubby zircon showing extensive fracturing and dark, faintly zoned invasive rims; from amphibole meta-leucogranite that crosscuts compositional layering in the Yagn composite lithologic unit, sample MR-10-124. d—Concordia plot showing isotopic data for cores and rims. Weighted average plot for cores only.

grains contain cracks and inclusions. Zircon grains are composed of oscillatory-zoned cores and two distinct types of overgrowths: (1) dark gray to black (in CL), low Th/U inner rims, and (2) light to medium gray (in CL), high Th/U outer rims (fig. 5Bc). Eighteen analyses of cores yield a weighted average of $^{207}Pb/^{206}Pb$ ages of 1140 ± 9 Ma (fig. 5Bd), which is interpreted as the time of igneous crystallization. Inner rims have a weighted average of $^{207}Pb/^{206}Pb$ ages of 1055 ± 21 Ma (n = 4), whereas outer rims have a weighted average of $^{207}Pb/^{206}Pb$ ages of 997 ± 12 Ma (n = 9).

MR-06-19 (Ypg biotite meta-alkali feldspar granite).—Zircon having two morphologies were extracted from sample MR-06-19: (1) colorless to light brown, euhedral, and prismatic (l/w of 3-4), and (2) medium to dark brown, euhedral, prismatic (l/w of 2–3), and extensively cracked (table 5). In CL, Type 1 grains are composed of oscillatory-zoned cores and thin, dark, discontinuous rims, whereas Type 2 grains are dark, oscillatory-zoned, and have broad, dark, unzoned rims (fig. 5Be). Cores in Type 1 grains have relatively low U (mostly between about 250 and 1200 ppm) and modest Th/U (0.26–0.69), whereas Type 2 grains (cores and rims) have higher U (about 630–3800 ppm) and similar Th/U (mostly 0.24–0.64). Sixteen oscillatory-zoned cores from Type 1 grains yield a weighted average of $^{207}Pb/^{206}Pb$ ages of 1153 ± 8 Ma (fig. 5Bf) that is interpreted as the igneous crystallization age. Analyses of Type 2 dark cores

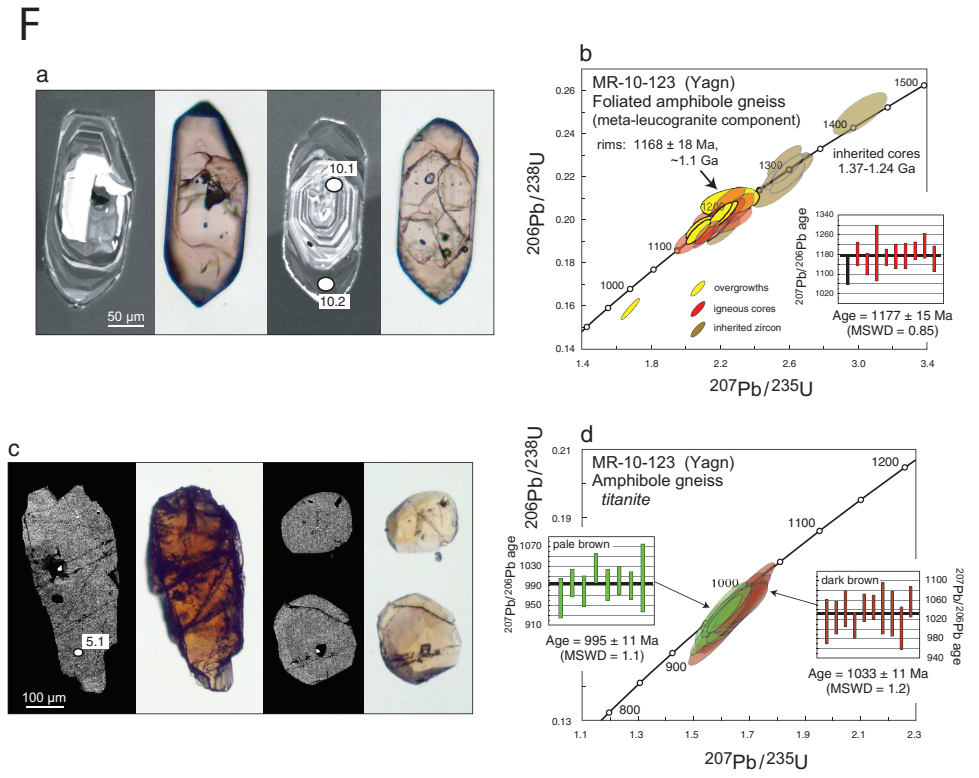

Fig. 5F. a—Prismatic zircon showing oscillatory-zoned cores and medium-gray, faintly zoned rims; from meta-leucogranite component of the Yagn composite lithologic unit, sample MR-10-123. b—Concordia plot showing isotopic data for inherited cores, igneous cores, and two episodes of rims. Weighted average is for cores only. c—Two morphologies of titanite: (1) brown, anhedral and (2) light tan, euhedral from sample MR-10-123. d—Concordia plot of isotopic data for two morphologies of titanite. Ages calculated separately using the weighted average of $^{207}Pb/^{206}Pb$ ages.

and rims result in a discordant array, which suggests original formation at about 1.04 Ga and episodes of Pb-loss and possibly new zircon growth during the mid-Paleozoic.

MR-08-88 (Yqm meta-quartz monzonite).—Zircon from sample MR-08-88 is medium brown, subhedral to euhedral, and has l/w of 2 to 4 (table 5). Most grains contain inclusion-rich cores and are extensively fractured. CL imagery reveals (in order, from interior to exterior of grains): (1) a heterogeneous population of partially resorbed cores with truncated oscillatory zoning, (2) concentric, oscillatory-zoned cores and mantles, locally overgrown on resorbed cores (#1, above), (3) faintly zoned, light to medium gray mantles, and (4) white material that ranges in size from very thin enclosing rinds to thick mantles around a small relict core (fig. 5Ca).

Nine partially resorbed cores (Type 1) have $^{207}Pb/^{206}Pb$ ages that range from 1.31 to 1.22 Ga; these cores are interpreted as inherited. Eleven (of 12) concentrically-zoned cores (Type 2) yield a weighted average of $^{207}Pb/^{206}Pb$ ages of 1155 ± 12 Ma, which is interpreted as the time of igneous crystallization (fig. 5Cb). However, the data from these cores can be subdivided into two groups on the basis of Th/U: (a) low Th/U (0.02–0.04; n=3) and (b) high and variable Th/U (0.2–0.9; n=9). Low Th/U is usually characteristic of metamorphic zircon, whereas higher values are typical of igneous origin (Rubatto, 2002). A syn-tectonic origin for this rock is suggested by the similarity of ages determined for the compositionally distinct Type 2.

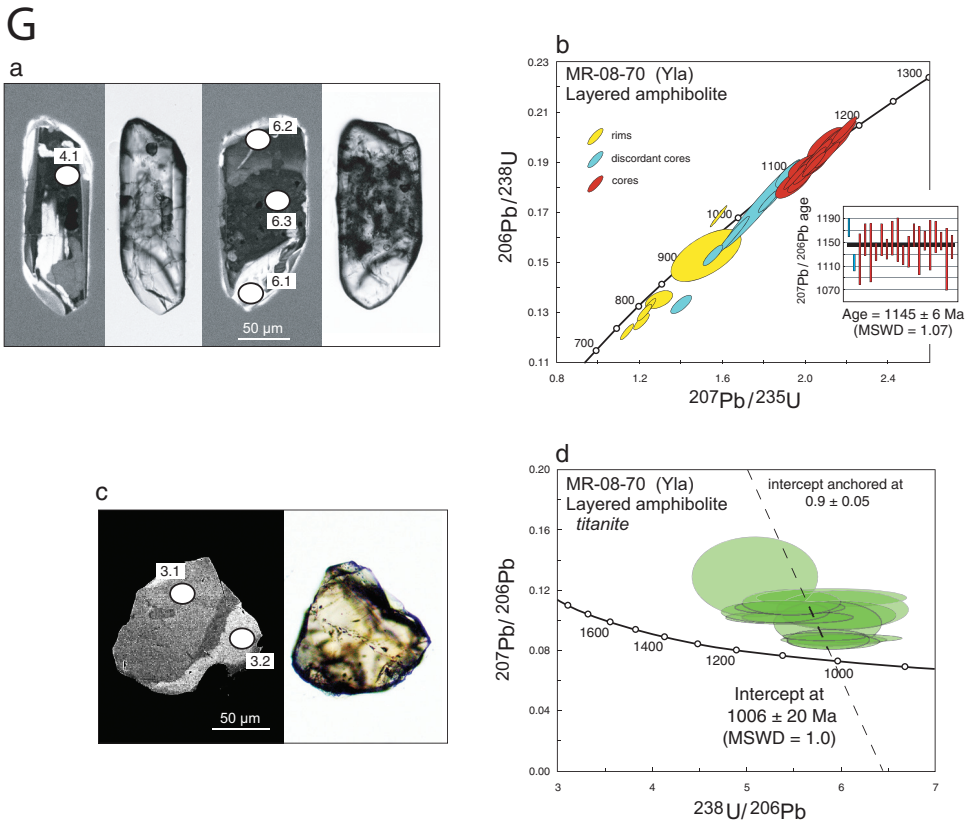

Fig. 5G. a—Prismatic zircon showing unusual, irregular CL zoning and mottled appearance in transmitted light; from amphibolite of the Yla composite lithologic unit, sample MR-08-70. b—Concordia plot showing two episodes of metamorphic zircon growth. Weighted average is for concordant and nearly concordant data (red ellipses) only. c—Faintly zoned anhedral titanite from sample MR-08-70. d—Linear regression (anchored) for titanite.

Type 3 and Type 4 overgrowths formed between about 1.00 and 1.05 Ga, respectively. Three analyses of the white outer rims are notable because they indicate unusually high (2.4–3.0) Th/U, due to relatively low U concentrations (as indicated by white CL shading). In addition, one platy, sector-zoned grain yielded an age of 767 ± 9 Ma. This grain may have formed as a result of heating associated with emplacement of a nearby mafic dike of the regional Bakersville swarm (Tollo and others, 2012).

MR-08-66 (Ybg biotite meta-monzogranite).—Sample MR-08-66 contains two morphologically distinct types of zircon: (1) stubby (l/w = 2–3), euhedral, pristine grains with fine-scale, concentric oscillatory zoning, and (2) prismatic (l/w = 4–6), extensively fractured grains with irregular zoning (table 5; fig. 5Cc). The latter zoning appears to be caused by replacement of white (in CL), low-U material by dark (in CL) speckled high-U zircon. Type 1 grains and white material in Type 2 grains have U contents of about 56 to 568 ppm, whereas Type 2, dark replacement zircon contains 1000 to 3100 ppm U. Three cores with ages of 1.20 to 1.28 Ga are interpreted as xenocrystic. Fifteen analyses (from 7 cores of Type 1 grains and 8 white areas of Type 2 grains) yield a Concordia Age of 1157 ± 9 Ma (fig. 5Cd). High-U replacement zircon yields discordant data with ages between about 1050 and 700 Ma (fig. 5Cd).

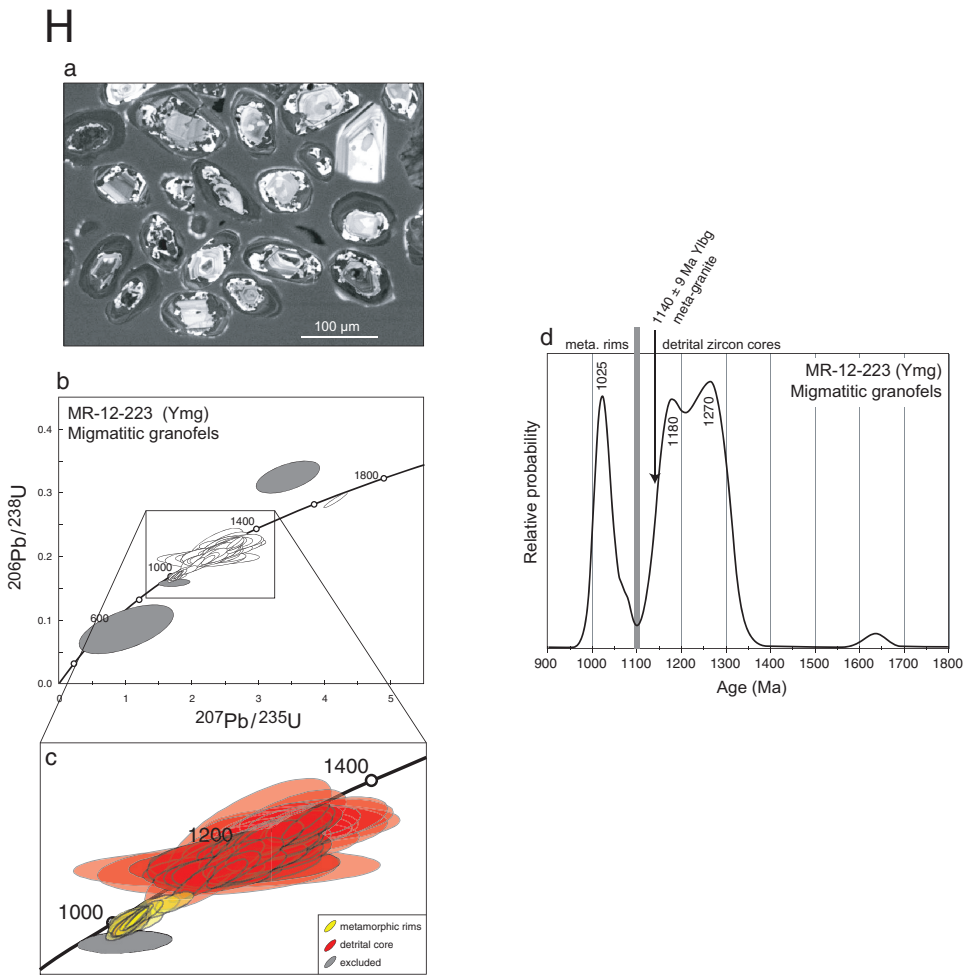

Fig. 5H. a—CL image of detrital zircon (many displaying oscillatory-zoned cores and dark, unzoned rims); from micaceous granofels of the Ymg composite lithologic unit, sample MR-12-223. b—Concordia plot of data from sample MR-12-223. Gray ellipses represent discordant data excluded from calculation of Relative Probability curve. c—inset of figure 5Hb distinguishing isotopic data for cores and rims. d—Relative Probability plot for ages of detrital zircon from sample MR-12-223, with ages for major peaks (in Ma).

Two populations of titanite occur in sample MR-08-66. Type T1 grains (n = 17) are light to medium brown, anhedral, and contain 63 to 356 ppm U. Type T2 grains (n = 2) are pale greenish to colorless, anhedral, and contain 48 to 84 ppm U. High-contrast BSE imagery reveals weak zoning in some Type T1 grains. Some Type T1 grains have narrow Type T2 overgrowths (fig. 5Ce). As is typical of metamorphic titanite, most grains contain significant common Pb (about 1–5 % common ^{206}Pb). We assume an initial ^{207}Pb/^{206}Pb of 0.9 ± 0.05 because the initial common Pb composition for this titanite is unknown. A best-fit line anchored at this value and regressed through data for Type T1 analyses has a lower intercept age of 1028 ± 30 Ma (fig. 5Cf), which is interpreted to record growth during metamorphism. Two analyses of Type T2 grains suggest a younger age of 976 ± 40 Ma, although the reliability of a 3-point isochron is uncertain.

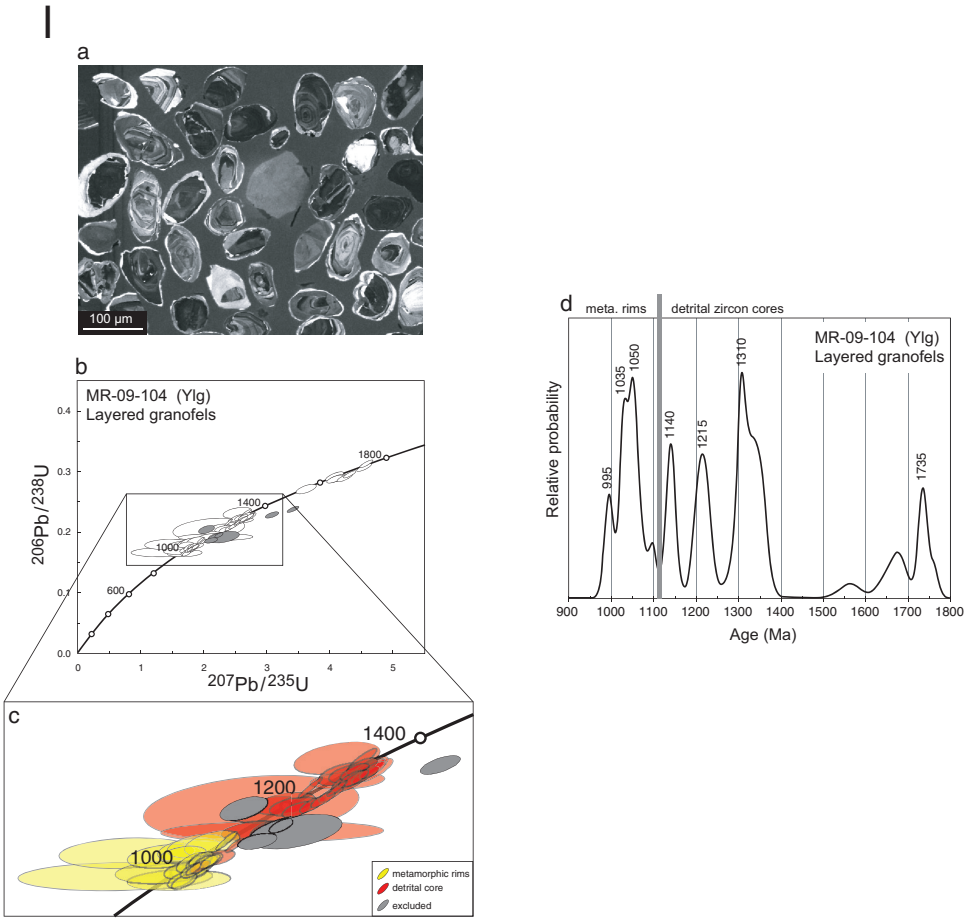

Fig. 5I. a—CL image of detrital zircon (many displaying oscillatory-zoned cores and white, unzoned rims); from amphibole + garnet-bearing granofels of the Ylg composite lithologic unit, sample MR-09-104. b—Concordia plot of all data from sample MR-09-104. Gray ellipses represent discordant data excluded from calculation of Relative Probability curve. c—inset of figure 5Ib distinguishing isotopic data for cores and rims. d—Relative Probability plot for ages of detrital zircon from sample MR-09-104, with ages for major peaks (in Ma).

MR-08-79 (Ypfg porphyroblastic meta-syenogranite-LNT).—Zircon from sample MR-08-79 is light to medium brown, euhedral, and prismatic (l/w of 2–5; table 5). CL imagery shows that zircon grains are composed of oscillatory-zoned cores and dark gray to black, unzoned rims (fig. 5Da). Cores contain modest U concentrations (109–325 ppm) and Th/U is 0.37 to 0.42. In contrast, rims contain greater U (681–791) and have lower Th/U (0.12–0.14). Eleven (of 12) analyses of cores yield concordant data that produce a Concordia Age of 1160 ± 7 Ma (fig. 5Db), which is interpreted as the time of igneous crystallization. Three analyses of rims indicate younger ages of about 1050 Ma that is interpreted as a time of metamorphism.

MR-08-71 (Ybg biotite meta-monzogranite).—Zircon in sample MR-08-66 forms both pristine euhedral grains (Type 1) and dark fractured grains (Type 2) (table 5), as is also characteristic of sample MR-08-66 (above). In CL, Type 1 grains display fine concentric oscillatory zoning and dark, narrow, discontinuous rims, whereas Type 2

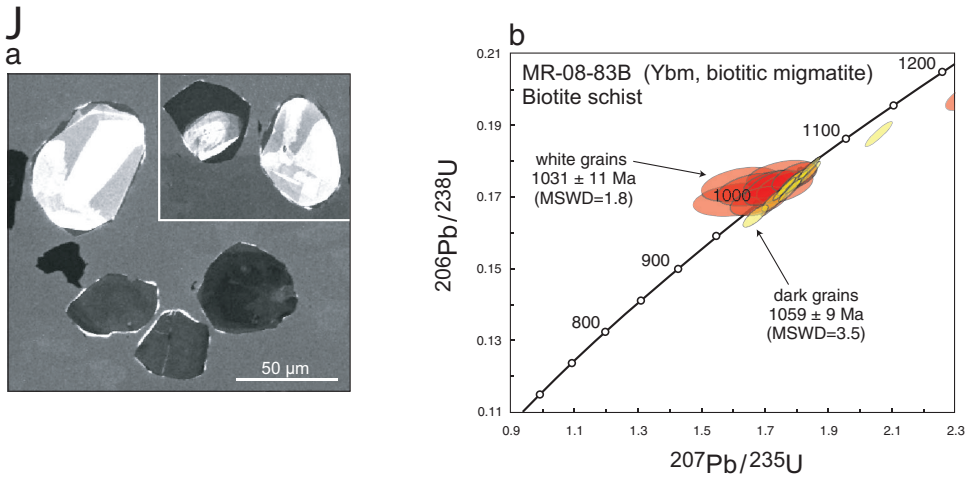

Fig. 5J. a—Two types of CL zoning (light, sector-zoned; dark, very faintly sector-zoned) in zircon; from meta-leucogranite that intrudes biotite schist of the Ybm composite lithologic unit, sample MR-08-83B. b—Concordia plot suggesting that the dark grains are slightly older than the white grains.

grains have partially resorbed oscillatory-zoned cores and thick dark rims (fig. 5Dc). Eighteen analyses of cores (twelve Type 1 grains and six Type 2 grains) yield a Concordia Age of 1164 ± 10 Ma (fig. 5Dd). Analyses of three dark rims yield discordant data and are not considered further.

MR-09-100 (Yfbl biotite meta-leucogranite).—Zircon from sample MR-09-100 is dark brown, euhedral, and has l/w of 3 to 5 (table 5). In CL, the grains are composed of oscillatory-zoned cores and dark, unzoned rims (fig. 5De). Cores contain relatively low U (70–746 ppm) and have high Th/U (0.32–1.32), whereas rims contain 852 to 2709 ppm U and most have Th/U of 0.05 to 0.35. Twenty-one analyses of cores result in a weighted average of $^{207}Pb/^{206}Pb$ ages of 1181 ± 10 Ma (fig. 5Df), which is interpreted as the time of igneous crystallization. Analyses of rims yield two ages of metamorphic growth: 1163 ± 6 Ma (n = 6) and 1034 ± 10 Ma (n = 4).

Leucocratic components of composite units

MR-08-84 (Ybm meta-alkali feldspar granite).—Zircon from sample MR-08-84 is light to medium brown, euhedral, and has l/w of 3 to 5 (table 5). In CL, the grains are composed of oscillatory-zoned cores, oscillatory-zoned mantles, and dark, unzoned rims (fig. 5Ea). U-Pb ages of cores define two age groups: (1) 1.32 to 1.27 Ga, and (2) 1.21 to 1.13 Ga. Cores in Group 1 tend to be overgrown by oscillatory-zoned mantles, whereas cores in Group 2 are overgrown by dark, unzoned rims. We interpret the textural and age data to indicate that Group 1 domains are xenocrystic. Th/U data for fifteen analyses from Group 2 oscillatory-zoned cores can be subdivided into two populations: (1) Th/U of 0.04 to 0.19 (n=5), and (2) Th/U of 0.50 to 1.64 (n=10). Averaged separately, the resulting ages are 1170 ± 17 Ma (low Th/U) and 1162 ± 13 (high Th/U). The 1166 ± 9 Ma weighted average of all fifteen $^{207}Pb/^{206}Pb$ ages is interpreted as the time of igneous crystallization (fig. 5Eb) because the origin of these geochemically different, but probably contemporaneous, zones remains obscure. This interpretation is supported by the occurrence of *ca.* 1190 to 1170 Ma meta-leucogranites of similar composition and age in the study area, where rocks of this type form both leucocratic components of migmatitic lithologies (Ygw and Yagn units) and

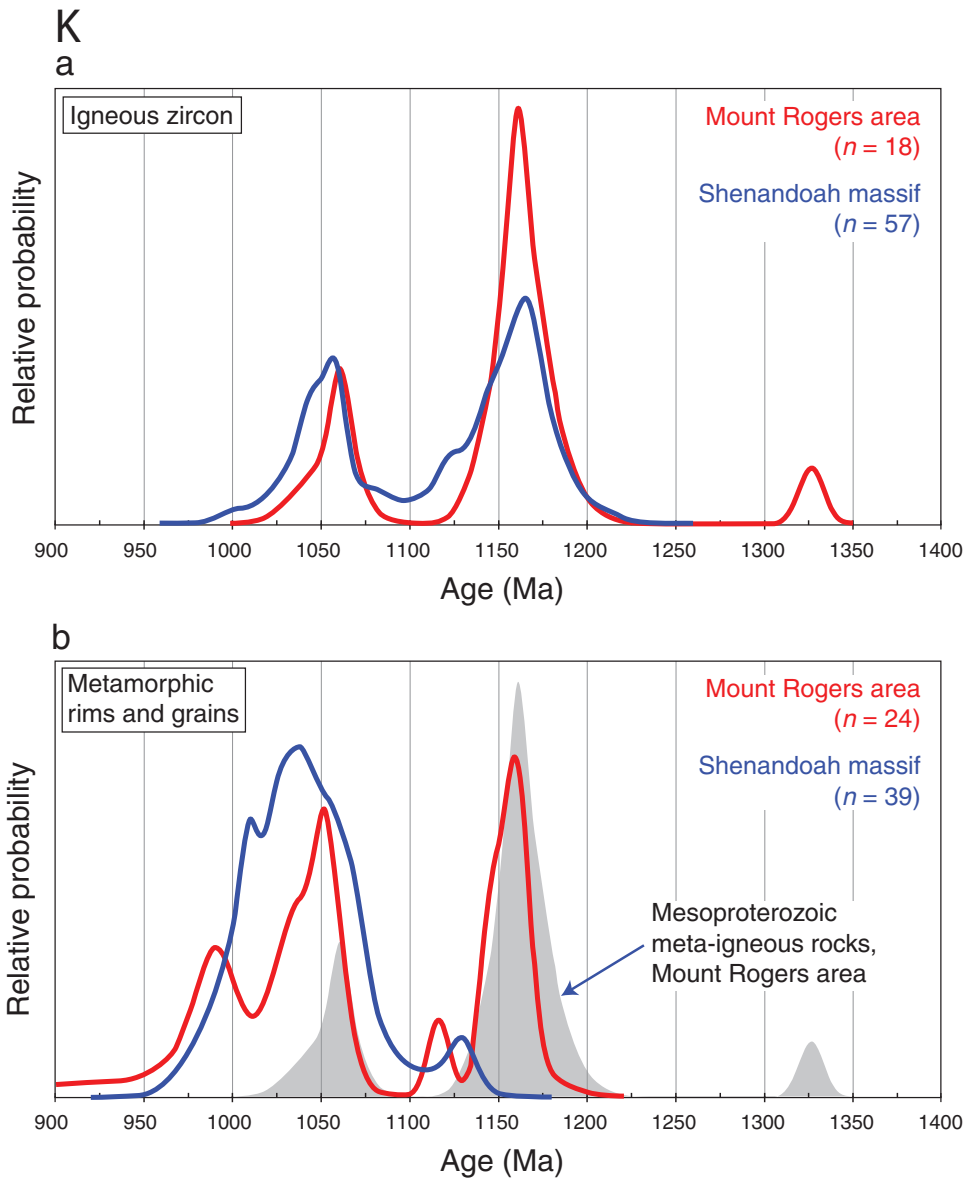

Fig. 5K. Relative probability plots comparing age data for rocks of the Mount Rogers area (red curves) with other samples of Mesoproterozoic basement in Virginia (Shenandoah massif; blue curves). a—Age distributions for igneous zircon. b—Age distributions for zircon of metamorphic origin (both rims and whole grains). Age distribution defined by igneous ages from the study area are shown by the shaded gray area in B to facilitate comparison. Sources of data: Carter and others, 2012; Southworth and others, 2010; Tollo and others, 2004a, 2010; Aleinikoff (unpublished data).

map-scale plutons (Yflb) (tables 2 and 7). Four analyses of rims are slightly to substantially reversely discordant and suggest an age of about 1100 to 1075 Ma.

MR-10-124 (Yagn amphibole meta-leucogranite).—Zircon from sample MR-10-124 is medium brown, euhedral, and has l/w of 2-5 (table 5). In CL, the grains are composed of oscillatory-zoned cores and dark, unzoned to faintly oscillatory-zoned rims

(fig. 5Ec). Most grains are significantly fractured. Ten analyses of cores indicate moderate U contents (105–536 ppm) and relatively high Th/U (0.37–1.31); three analyses of rims have higher U contents (733–1410 ppm) and relatively low Th/U (0.13–0.22). The weighted average of $^{207}Pb/^{206}Pb$ ages from cores is 1183 ± 17 Ma (fig. 5Ed), which is interpreted as the time of igneous crystallization. $^{207}Pb/^{206}Pb$ ages of rims suggest formation at about 1.05 Ga.

Xenoliths

MR-10-123 (Yagn amphibole gneiss).—Zircon from sample MR-10-123 is dark brown, euhedral, and has l/w of 1 to 3 (table 5). Most grains are extensively fractured. CL imagery reveals concentric oscillatory-zoned cores that are overgrown by dark, unzoned rims (fig. 5Fa). As in sample MR-08-84, oscillatory-zoned cores can be subdivided into two groups: (1) 1.37 to 1.24 Ga, and (2) 1.22 to 1.11 Ga. Group 1 cores contain 156 to 611 ppm U, and have Th/U of 0.49 to 1.44, whereas Group 2 cores contain 233 to 564 ppm U and have Th/U of 0.97 to 1.77. Rims have higher U (563–2547 ppm) and lower Th/U (0.02– 0.14). We interpret Group 1 cores as representing older inherited material. Nine analyses of Group 2 cores yields a weighted average of $^{207}Pb/^{206}Pb$ ages of 1177 ± 15 Ma (fig. 5Fb), which is interpreted as the time of igneous crystallization. The weighted average of six analyses of rims is 1168 ± 18 Ma, whereas two other rims are about 1.1 Ga.

Two types of titanite occur in sample MR-10-123: (1) dark brown, anhedral, and extensively fractured, and (2) very pale brown to colorless, equant, subhedral to euhedral, and fairly pristine (table 5; fig. 5Fc). Both morphologies have similar, unusually high U contents (Type 1: 260–634 ppm; Type 2: 421–665 ppm) and low common Pb (<0.5% common ^{206}Pb for both types). $^{206}Pb/^{238}U$ ages for Type 1 and Type 2 grains are slightly discordant and have weighted averages of $^{207}Pb/^{206}Pb$ ages of 1033 ± 11 (n=10) and 996 ± 11 Ma (n=8), respectively (fig. 5Fd).

MR-08-70 (Yla layered amphibolite).—Amphibolite sample MR-08-70 was collected to provide additional evidence bearing on the timing of metamorphic events in the region. Geochemical data from a sample of the dominant amphibolite type in the Yla lithologic unit (table 6) indicates a major-element composition corresponding to basaltic andesite to basaltic trachyandesite (Le Maitre and others, 2002). Nevertheless, the uniformly fine-grained, black appearance of the amphibolite collected for analysis suggests a more mafic protolith that might not have contained zircon of igneous origin (Hoskin and Schaltegger, 2003). Instead, lacking conclusive textural evidence for zircon growth in an igneous environment, we propose that zircon crystallized in this rock during high-grade metamorphism during which reaction of igneous pyroxene to metamorphic amphibole released Zr that subsequently formed zircon, an interpretation that is consistent with observed textures (fig. 5Ga). Consequently, the age of zircon from this sample likely records the time of prograde high-grade metamorphism.

Zircon from sample MR-08-70 is medium brown, subhedral to euhedral, and has l/w of 1 to 3 (table 5). Many grains appear to be partially or completely "speckled" due to large to tiny (40–5 microns) inclusions (fig. 5Ga). CL imagery reveals cores composed of irregular bands of white, light gray, and dark gray zoning, that are overgrown and invaded by dark, mottled material. Cores have a wide range of U concentrations (157–1355 ppm) and Th/U (0.10–1.45). Mottled rims have higher U (1209–2455 ppm) and a broader range of Th/U (0.25–5.4). Eighteen (of 20) analyses of cores result in a weighted average of $^{207}Pb/^{206}Pb$ ages of 1145 ± 6 Ma (fig. 5Gb), which is interpreted as representing growth during an initial episode of high-grade metamorphism that likely occurred shortly after or during emplacement of the enclosing *ca.* 1160 Ma Ybg pluton. Six analyses of mottled overgrowths yield discordant and reversely discordant ages suggesting an additional metamorphic event at about 950 to 1000 Ma. However, the isotopic systematics are complicated by seven additional

analyses of cores that yield a discordant data array with intercept ages of 1117 ± 29 and 478 ± 160 Ma. It is possible that these younger ages represent domains that underwent Pb loss because the CL zoning patterns of these cores are very similar to CL patterns in the 1145 Ma cores. The apparent coherence of the analyses may be fortuitous and the upper intercept age may not represent an actual geologic event.

Titanite from sample MR-08-70 is pale to medium brown, anhedral, and has l/w of 1 to 2 (table 5). BSE imagery reveals broad zoning (fig. 5Gc). These grains contain low U (7–144 ppm) and high common Pb (1.7–18.8% common ^{206}Pb); consequently, isotopic analyses have large uncertainties. The regression was anchored at an initial ^{207}Pb/^{206}Pb of 0.9 ± 0.05 because of very limited spread in isotopic ratios that results in a lower intercept age of 1006 ± 20 Ma (fig. 5Gd), in reasonable agreement with the age of zircon overgrowths (above).

Meta-sedimentary Rocks.—Samples of three meta-sedimentary rocks were collected for dating detrital zircon in order to determine the maximum age of deposition (youngest detrital zircon population), timing of metamorphism(s) (age(s) of overgrowths), and ages of sediment sources. Two of these samples (MR-12-223 and MR-09-104) contain detrital zircon, whereas zircon from sample MR-08-83B was determined to be metamorphic in origin.

MR-12-223 (Ymg fine- to medium-grained micaeous granofels).—Sample MR-12-223 is a micaeous granofels that forms a large xenolith (*ca.* 100 X 40 m) within meta-granite of the fault-bounded Ylbg pluton. Samples of both the xenolith and enclosing meta-granite (sample MR-11-193, tables 5 and 7) were collected in close proximity within the Mountain Materials quarry near Mouth of Wilson, Virginia (location 5, fig. 3). The shape (spherical to oblong to elongate) and color (light brown to dark brown) of zircon from MR-12-233 vary considerably (table 5). In CL, most grains display partially resorbed, oscillatory-zoned cores and dark, faintly zoned rims (fig. 5Ha). The cores are interpreted as detrital in origin, whereas the rims formed during subsequent metamorphism. A total of 69 zircon grains were analyzed, including 54 cores and 15 overgrowths (fig. 5Hb, c). Three analyses of cores are excluded from further consideration due to excessive (>10%) discordance. Age data from cores define two major populations: (1) *ca.* 1180 and (2) 1270 Ma (fig. 5Hd). The age of deposition is constrained to be between the youngest age group of detrital cores (1159 ± 15 Ma; n=7) and 1140 ± 9 Ma, the igneous crystallization age of the Ylbg meta-granite that intrudes the granofels xenolith.

Fifteen dark (in CL) overgrowths have high U concentrations (753–1771) and low Th/U (0.01–0.08), typical of metamorphic zircon. Fourteen analyses yield a weighted average of ^{207}Pb/^{206}Pb ages of 1027 ± 10 Ma. One dated rim on zircon from the enclosing meta-granite (sample MR-11-193) yielded a similar age of 1031 ± 13 (Appendix A). One rim on zircon from the granofels yielded an older age of 1157 ± 31 Ma.

MR-09-104 (Ylg layered granofels).—Interlayered orthogranofels and meta-leucogranite of the Ylg composite lithologic unit define a small body surrounded, without discernible contacts or evidence of faults, by a large expanse of foliated biotite meta-leucogranite of the Yfbl pluton (fig. 3). The combination of lithologic characteristics and field relations suggest that the layered granofels either forms a xenolith within Yfbl leucogranite or unconformably overlies the leucogranite. Zircons from the orthogranofels were analyzed in order to better define these relations and provide additional evidence bearing on the sedimentary history of the area.

The shape (oblong to elongate) and color (light brown to dark brown) of zircon from sample MR-09-104 vary considerably (table 5). In CL, most grains display rounded oscillatory-zoned cores and narrow, light gray rims (fig. 5Ia). Some grains are entirely dark gray and sector zoned. Seventy-one analyses of these grains included: (1) forty-six detrital oscillatory-zoned cores (of which 5 were >10 percent discordant

and excluded for further consideration), (2) twenty rims, and (3) five dark gray grains (fig. 5Ib, c). Collectively, the isotopic data define a range of more than 300 m.y. (fig. 5Ib, c). Detrital cores have major age populations at about 1735, 1310, 1215, and 1140 Ma; major age populations of rims and dark grains occur at about 1050, 1035, and 995 Ma (fig. 5Id). The age of deposition of the sedimentary protolith of the layered granofels is constrained to be between the youngest age population of cores (1140 ± 9 Ma; $n = 6$) and the oldest age population of rims (1107 ± 13 Ma; $n=5$). The geochronologic data indicate that the maximum depositional age of Ylg sediments is resolvably younger than the minimum igneous crystallization age of the surrounding Yfbl pluton, which indicates that Ylg sedimentary protoliths were deposited unconformably atop exhumed Yfbl granite.

MR-08-83B (Ybm biotite schist).—Sample MR-08-83B was collected from mica-rich meta-pelite with the intention of analyzing the detrital zircon population. However, zircon extracted from the biotite schist do not have morphologic characteristics typical of detrital origin; instead, grains are angular, and clear to pale brown (table 5). As shown by CL imagery (fig. 5Ja), three populations are present: (1) about 95 percent of the analyzed zircon grains are dark gray to black and preserve very faint broad sector zoning; nearly all of these grains have extremely narrow, white overgrowths; (2) about 5 percent of the analyzed grains are white and have broad sector zoning; all of these grains have narrow to broad, discontinuous, dark, unzoned overgrowths; (3) a few oscillatory-zoned, mottled grains (<1% of the zircon population).

Dark and white zircon grains are compositionally distinct. Dark grains have relatively high U (866–3102 ppm) and low Th/U (0.05–0.36), whereas white grains have relatively low U (80–530 ppm) and high Th/U (0.61–1.64). Ten (of 11) dark grains yielded a weighted average of $^{207}Pb/^{206}Pb$ ages of 1059 ± 9 Ma, which is interpreted as a time of metamorphism (fig. 5Jb). One dark grain has an older age of 1186 ± 7 Ma. Ten (of 11) white grains yielded a weighted average of $^{206}Pb/^{238}U$ ages of 1031 ± 11 Ma that may represent a second metamorphic event (fig. 5Jb). One white grain with oscillatory zoning has an older age of 1330 ± 19 Ma. The two older ages suggest that these grains are detrital. The younger metamorphic age of 1031 ± 11 Ma is similar to age peaks derived from analyses of dark metamorphic rims in meta-sedimentary samples MR-12-223 and MR-09-104 (about 1027 and 1035 Ma, respectively).

Summary of geochronologic results.—SHRIMP U-Pb geochronologic data (tables 5 and 7; Appendices A and B) define a series of regional Mesoproterozoic igneous and metamorphic episodes (fig. 5Ka, b). The majority of igneous crystallization ages establish a period of magmatic activity at *ca.* 1190 to1130 Ma during which the Early Magmatic Suite was emplaced (fig. 5Ka). This magmatism involved intrusion of both plutonic bodies and leucogranitic components of composite lithologies (for example Ybm and Ygw migmatites; Yagn gneiss). Following a *ca.* 60 m.y. hiatus, syenogranite and monzodiorite plutons of the bimodal Late Magmatic Suite were emplaced at *ca.* 1075 to 1030 Ma.

Ages of zircon and titanite indicate that three episodes of regional metamorphism at moderate- to high-grade conditions affected rocks of the study area during the late Mesoproterozoic and early Neoproterozoic (fig. 5Kb). Overgrowths on primary igneous zircon and grains of solely metamorphic origin indicate an initial period of regional metamorphism at 1170 to 1140 Ma (table 7), synchronous with emplacement of Early Magmatic Suite plutons (fig. 5Kb). A second episode of metamorphism occurred at 1070 to 1020 Ma (table 7), synchronous with emplacement of Late Magmatic Suite plutons (fig. 5Kb). The third episode of regional metamorphism at 1000 to 970 Ma (fig. 5Kb, table 7) does not correlate with igneous activity. Significantly, zircon in the meta-monzogranite component of the pink and gray meta-granite (Ypg) preserves isotopic and textural evidence of all three episodes of regional heating, underscoring (1) the ability of zircon to resist geochronologic resetting and (2) the

usefulness of high resolution SHRIMP U-Pb zircon geochronology in deciphering the timing of multiple thermal events in polymetamorphosed orogens.

The three metamorphic intervals documented in this study are contemporaneous with orogenic events recognized elsewhere in eastern North America, including the regional Shawinigan (1190–1140 Ma), Ottawan (1090–1020 Ma), and Rigolet (1010–980 Ma) episodes (Rivers, 1997, 2008; McLelland and others, 2010), but these data do not provide direct evidence for regional correlation which is unlikely for the oldest activity because the Blue Ridge rocks were not yet amalgamated to Laurentia (Fisher and others, 2010). Nevertheless, the oldest (1327 ± 7 Ma) lithology in the study area is contemporaneous with rocks in the Green Mountain massif (Ratcliffe and others, 1991; Aleinikoff and others, 2011), Hudson Highlands (Walsh and others, 2004), and New Jersey Highlands (Volkert and others, 2010).

Geochemistry

Methods.—Minimally weathered, 20 to 30 lbs (9–14 kg) samples were collected at representative outcrops, and cleaned, split, pulverized, and powdered using standard laboratory equipment and techniques at George Washington University. For composite units, samples of each lithologic component were collected only where physically separable in the field. Whole-rock major- and trace-element abundances of powdered splits were determined using X-ray fluorescence (XRF) and instrumental neutron activation analysis (INAA) techniques. Concentrations of major elements and Rb, Ba, Sr, Pb, Zr, Nb, Ni, Zn, Cr, Ga, V, La, and Y were determined by XRF at the Ronald B. Gilmore Laboratory, University of Massachusetts in Amherst, employing methods described by Rhodes and Vollinger (2004) and Rhodes (1996). Concentrations of rare-earth elements (REE) and Th, U, Hf, Ta, and Sc were measured by INA techniques at the U.S. Geological Survey (USGS) laboratories in Denver using methods summarized by Budahn and Wandless (2002). Results of replicate analyses of USGS reference standards G-2 and BHVO-2 are included in table 6 with recommended values for oxide and elemental concentrations from the USGS and GeoReM, respectively. Recognizing that original magmatic concentrations of some elements might be variably affected by metamorphism, we use the data qualitatively solely to identify possible magmatic source types, recognize compositionally correlative suites, and evaluate possible petrogenetic lineages.

Normative compositions and major-element characteristics.—Meta-igneous rocks of the study area have normative mineral assemblages indicating dominantly granitic protoliths ranging from alkali feldspar granite to monzogranite (fig. 4). The lineated biotite meta-granite (Ylbg) and foliated biotite meta-quartz monzodiorite (Yfbd) are notable exceptions characterized by less silicic and intermediate compositions, respectively. Internal compositional variability varies among units and likely results from numerous factors. For example, the biotite meta-granite (Ybg) pluton displays a relatively restricted compositional range that we interpret as indicating derivation from a well-mixed magma (Bea, 2010), whereas broader chemical variation characteristic of the pink and gray meta-granite (Ypg) pluton likely results from fractionation that is indicated by highly evolved, silica-rich intrusive facies and local dikes. Among the various plutons, evaluating the petrogenetic evolution of the Ybg, Ypg, Ylbg, Ypfg, and Yfbd units is most tractable because petrographic characteristics indicate that these bodies are least affected by recrystallization associated with high-strain zones (table 2).

Most plutonic rocks have moderate- to high-silica (63–77 wt. %) compositions and low concentrations of crystal-compatible major elements (figs. 6A and 6B). The lineated biotite meta-granite (Ylbg) and foliated biotite meta-quartz monzodiorite (Yfbd), are the youngest and least silicic (containing 63–67 and 48–54 wt. % SiO_2, respectively) rocks within each magmatic suite. Most plutons are subalkaline and marginally to moderately peraluminous (molar $Al_2O_3/(CaO + Na_2O + K_2O =$

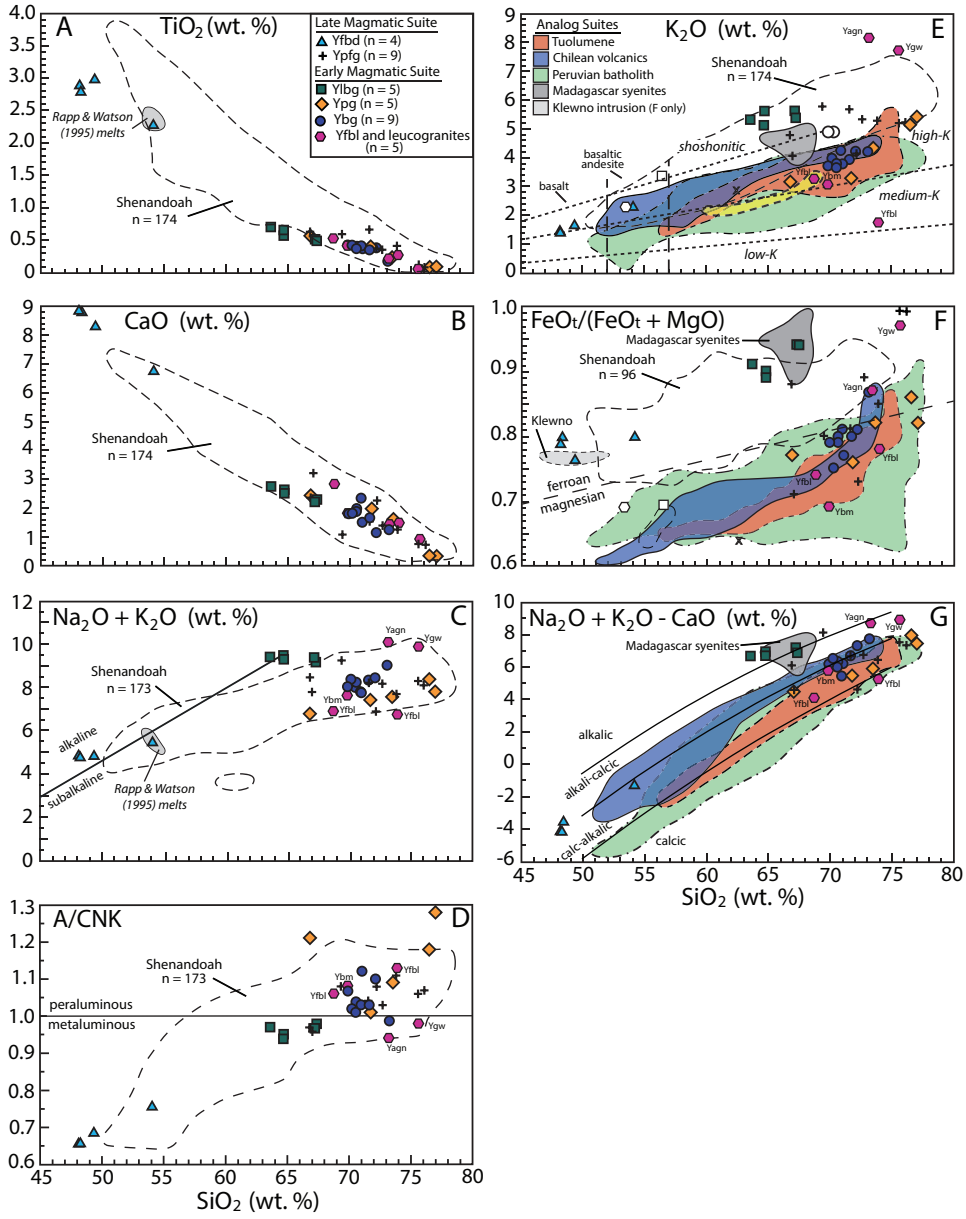

Fig. 6. Plots of (Y + Nb) versus Rb (A) and Yb versus Ta (B) for meta-igneous rocks of the study area. Symbols are the same as in figure 4. Data for the Yfpg pluton is subdivided as (1) low-Nb type (LNT), (2) high-Nb type (HNT), and (3) fractionated high-Nb type (FHNT). Compositional fields of the Nevados de Payachata volcanic region of Chile (blue, n = 27) (Davidson and others, 1990), Tuolumne Intrusive Suite, California (red, n = 22) (Bateman and Chappell, 1979), post-orogenic syenites from Madagascar (gray, n = 5, 7A only) (Nédélec and others, 1995), and Hawkeye granite suite of the Adirondack Highlands (small filled circles, n = 6, 7A only) (McLelland and others, 2001; J. McLelland unpublished data, 2014). All data expressed in parts per million. Diagrams modified after Pearce and others, (1984).

1.0–1.15); however, Ylbg and Yfbd rocks exhibit more alkaline affinity and are metaluminous (figs. 6C and 6D). The compositionally evolved Ybg and Ypg plutons have high-K, variably magnesian, and calc-alkalic to mildly alkali-calcic compositions (figs. 6E–6G). In contrast, the Ylbg and Yfbd plutons are ferroan and more alkalic but also K rich (figs. 6C, 6E, and 6F).

Trace-Element Characteristics and Tectonic Affinities

Early magmatic suite.—Mesoproterozoic plutonic rocks of the study area display contrasting trace-element characteristics that reflect differences in both age and petrologic evolution. The *ca.* 1180 to 1145 Ma biotite meta-granite (Ybg) and pink and gray meta-granite (Ypg) plutons contain lower concentrations of HFSE than the *ca.* 1140 Ma Ylbg rocks that are, in turn, generally less enriched than the *ca.* 1065 to 1050 Ma porphyroclastic foliated meta-granite (Ypfg) and foliated biotite meta-quartz monzodiorite (Yfbd) bodies (figs. 7A and 7B). Normalized multi-element patterns for Ybg and Ypg rocks overlap, are moderately negatively sloped (average Rb_N/Y_N = 38.8 and 30.7, respectively), and are characterized by (1) selective large-ion lithophile element (LILE) enrichment relative to the HFSE and (2) well developed negative Ta-Nb anomalies (fig. 8A). The distinctive trace-element patterns displayed by rocks of the Ybg and Ypg plutons (fig. 8A), similarity to younger rocks associated with active or recently active subduction systems (figs. 6E, 6F, 7A and 7B), and overall geochemical attributes including degree of K enrichment (fig. 6E), calc-alkalic characteristics (fig. 6G), and magnesian affinity (fig. 6F) suggest that protolith magmas were produced in a subduction-related magmatic arc setting (Hildreth and Moorbath, 1988; Davidson and others, 1990).

The *ca.* 1140 Ma lineated biotite meta-granite (Ylbg) pluton, which differs from the older rocks in displaying ferroan and alkalic affinity (figs. 6F and 6G), is enriched, relative to the magnesian Ypg and Ybg granites, in HFSE including Ta, Nb, Zr, Hf, Ti, Y, and Yb (average Rb_N/Y_N = 13.0) (figs. 7A, 7B and 8B). These characteristics, together with very high K enrichment (fig. 6E), collectively suggest that Ylbg magmas were derived from different sources than the earlier Ybg and Ypg plutons, most likely involving greater input of continental crust (Gill, 1981; Coulon and Thorpe, 1981; Clemens and others, 1986; Hildreth and Moorbath, 1988).

Composition and age variation: subdivision of the Ypfg lithologic unit.—Rocks mapped as the porphyroclastic foliated meta-granite unit (Ypfg) consist of variably coarse-grained, alkali-feldspar porphyroclastic, moderate- to high-silica meta-granitoids that form 10 map-scale, dismembered bodies that form large boudins in mylonite and protomylonite associated with regional shear zones (fig. 3). These rocks were originally mapped as a single intrusive unit (Tollo and others, 2010, 2012); however, geochemical data indicate that the Ypfg unit includes three compositionally distinct types (table 8):

(1) Low-Nb type (LNT): moderate to high SiO_2 contents; has negative Ta-Nb anomaly and lower Th, Ta, Nb, and Ce concentrations than other types (fig. 8C).
(2) High-Nb type (HNT): overlaps LNT rocks in the upper range of their SiO_2 contents; has similar Ta-Nb anomaly but higher Th, Ta, Nb, and Ce concentrations (fig. 8C).
(3) Fractionated high-Nb type (FHNT): markedly higher SiO_2 contents than the other types; however, FHNT rocks have compositions that are otherwise similar to the HNT group. Importantly, these rocks have marked, differentiation-related depletions of Sr and Ba (feldspar fractionation), P (apatite fractionation), and Ti (fractionation of Fe-Ti oxide minerals) (fig. 8C). Significantly lower Eu/Eu* relative to HNT rocks further supports a differentiation relationship involving feldspar removal (fig. 9D).

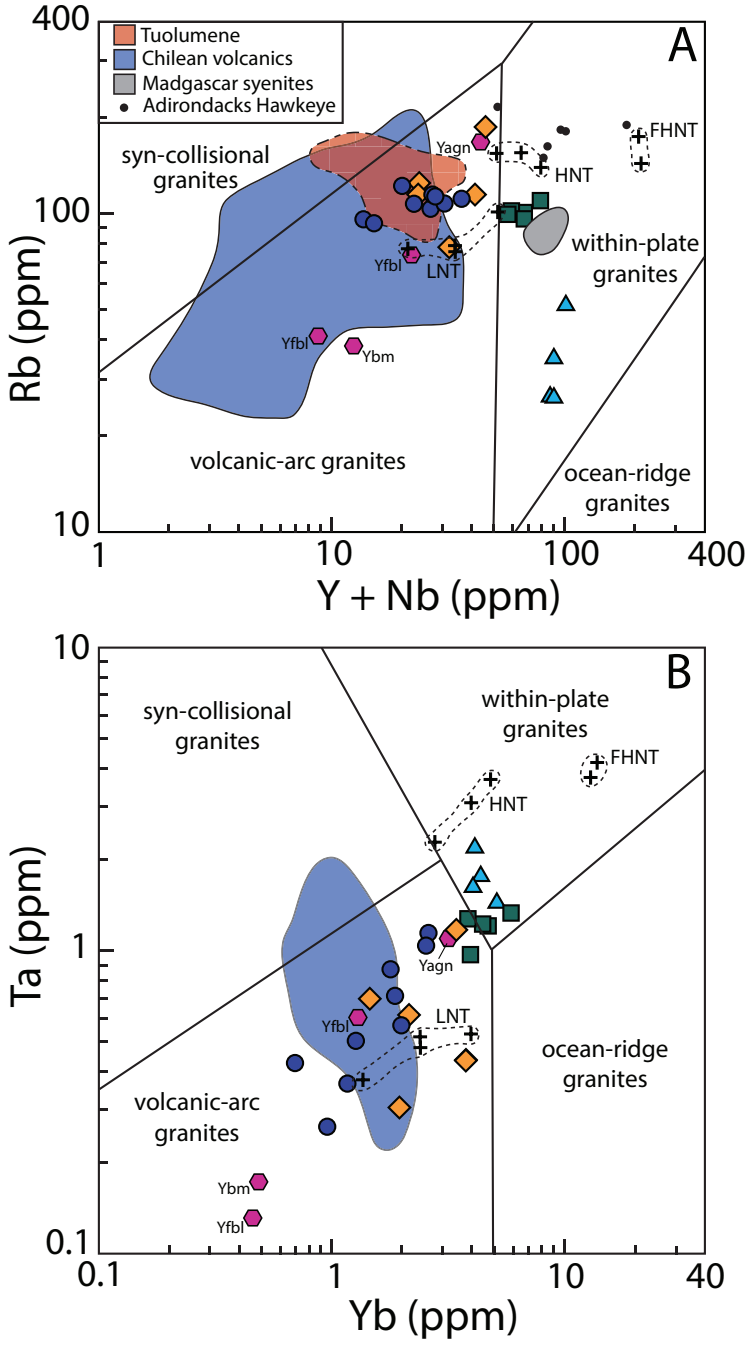

Fig. 7. Plots of SiO_2 versus TiO_2 (A), CaO (B), $Na_2O + K_2O$ (C), aluminum saturation index (A/CNK = molar $Al_2O_3/(CaO + Na_2O + K_2O)$) (D), K_2O (E), $FeO_t/(FeO_t + MgO)$ (F), and $Na_2O + K_2O - CaO$ (modified alkali-line index of Frost and others (2001)) (G) for meta-igneous rocks of the study area. Symbols are the same as in figure 4. Dashed fields in A-F enclose compositions of *ca.* 1180–1020 Ma basement rocks from the Shenandoah massif in northern Virginia (Tollo and others, 2006). Field boundaries are modified after Irvine and Baragar, 1971 (C), Le Maitre and others, 2002 (E), Peccerillo and Taylor, 1976 (E), and Frost and others, 2001 (F and G). All data expressed in weight percent. FeO_t in F refers to total iron

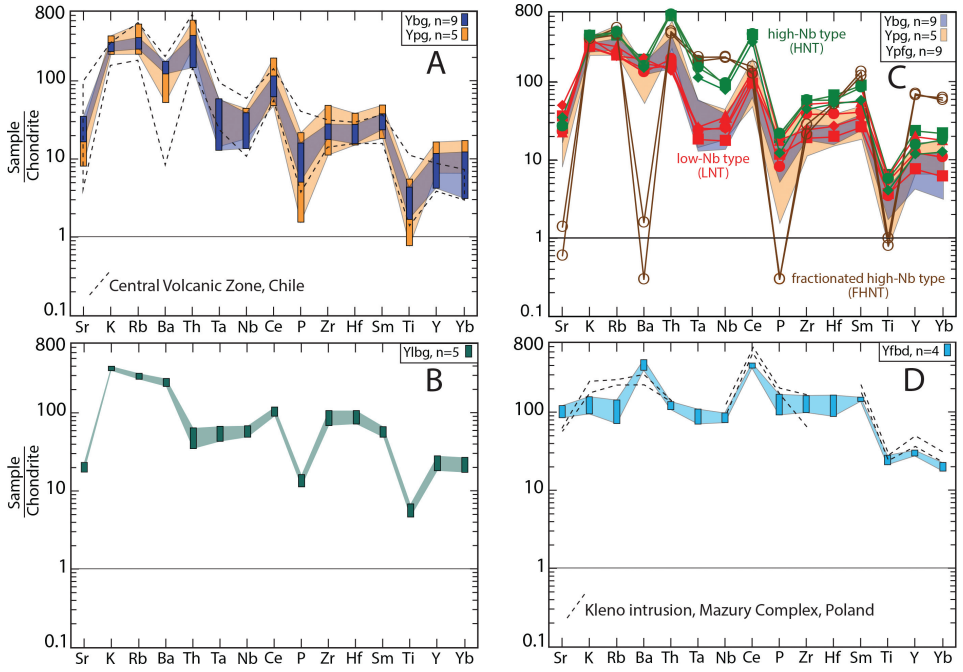

Fig. 8. Plots of selected major and trace elements normalized to chondritic values of Thompson (1982) for rocks of the biotite meta-granite (Ybg) and pink and gray meta-granite (Ypg) (A), lineated biotite meta-granite (Ylbg) (B) porphyroclastic foliated meta-granite (Ypfg) (C), and foliated biotite meta-quartz monzodiorite (Yfbd) (D) plutons in the Mount Rogers study area. Vertical bars show range of data for analyzed samples from each lithologic unit. Elemental sequence is from Pearce (1983). Dashed lines in A define the compositional range of volcanic rocks containing >60 wt. % SiO_2 from the the Nevados de Payachata region of Chile (Davidson and others, 1990). Dashed lines in D indicate the compositional range of the Klewno intrusion of the Mazury Complex in Poland (Duchesne and others, 2010). Diagram C displays color-coded compositions of samples from the diachronous Ypfg pluton including (1) low-Nb type (LNT, red), (2) high-Nb type (HNT, green), and (3) fractionated high-Nb type (FHNT, brown). Compositional ranges of the *ca.* 1160 Ma Ypg and Ybg plutons are shown for comparison.

U-Pb SHRIMP geochronologic analyses of zircon from two Ypfg samples of HNT composition collected from different structural blocks yield igneous crystallization ages of *ca.* 1061 ± 5 and 1065 ± 9 Ma (table 7), indicating that HNT and FHNT rocks belong to the regional Late Magmatic Suite. In contrast, U-Pb isotopic analyses of zircon from a separate LNT body indicate an igneous crystallization age of 1160 ± 7 Ma, demonstrating that this subtype is part of the Early Magmatic Suite. HFSE

Fig. 7 (continued). expressed as FeO. Additional symbols in E and F represent samples of Ygg orthogranofels (X) and amphibolites from the Ygw () and Yla () composite units. Compositional fields defined by samples of the Tuolumne Intrusive Suite (red, n = 22) (Bateman and Chappell, 1979), Nevados de Payachata volcanic region of the Chilean Andes (blue, n = 27) (Davidson and others, 1990), Coastal Batholith of Peru (green, n = 167) (Bussell, 1983; Atherton and Sanderson, 1985; and Boily and others, 1989), and post-orogenic syenites from Madagascar (dark gray, n = 5) (Nédélec and others, 1995) are shown for comparison in E-G. Range of data for the Klewno intrusion (Duchesne and others, 2010) is indicated by the light gray field in (F). Compositions of glasses produced in the melting experiments of Carroll and Wyllie (1990) (yellow, n = 7) and Skjerlie and Johnston (1992) (unfilled circles, n = 2) are shown for comparison in (E). Light gray fields in A and C indicate compositions of melts produced by partial melting of high-Al basalt at 1075–1125 °C and 0.8–2.7 GPa by Rapp and Watson (1995).

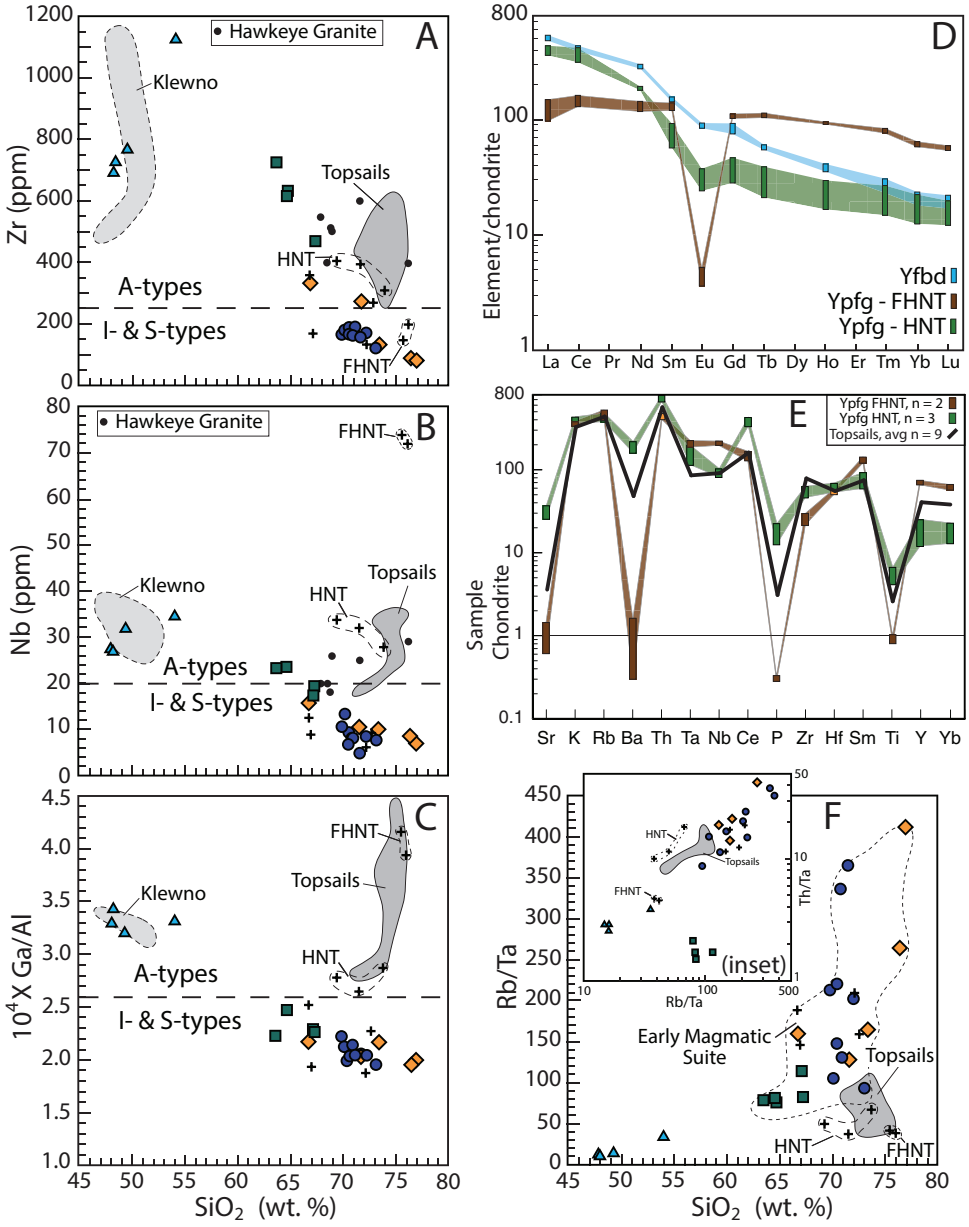

Fig. 9. Plots of SiO_2 vs Zr (A), Nb (B), and 10^4 X Ga/Al (C) for rocks of the study area. Field boundary for A-type granites from Whalen and others (1987). Symbols are the same as in figure 4. (D) Plot of REE concentrations in Ybfd, Ypfg-HNT, and Ypfg-FHNT samples normalized to chondritic values of Nakamura (1974) with additions for Tb, Ho, and Tm from Haskin and others (1968). (E) Plot of selected major and trace elements normalized to chondritic values of Thompson (1982) for rocks the *ca.* 1060 Ma Ypfg HNT (green) and FHNT (brown) subunits. Vertical bars show range of data for samples. Average composition of granitoids from the Topsails igneous suite (Whalen and Currie, 1990) indicated by heavy black line. (F) Plot of SiO_2 vs Rb/Ta for plutonic rocks of the study area. Inset shows plot of SiO_2 vs Th/Ta for the same samples. Range of data for the Topsails suite (Whalen and Currie, 1990) is indicated by the dark gray fields in (A), (B), (C), (F), and (F inset). Range of data for the mafic Klewno intrusion from Poland (Duchesne and others, 2010) is indicated by the light gray fields in (A), (B), and (C). Data for the Hawkeye granite suite of the Adirondack Highlands (filled circles) in (A) and (B) from McLelland and others (2001) and J. McLelland (unpublished data).

concentrations in LNT rocks are comparable to those of the *ca.* 1180 to 1145 Ma Ybg and Ypg plutons and therefore likely reflect generation from similar sources (fig. 7) (Pearce and others, 1984; Förster and others, 1997). In contrast, higher concentrations of Rb, Nb, and Ta, coupled with lack of compositionally transitional varieties, suggest that the younger HNT rocks, which display within-plate source characteristics (fig. 7), were derived through different processes and are unrelated petrologically to LNT types. FHNT rocks, which form a single body, likely developed through fractionation of HNT magma, as indicated by (1) higher SiO_2 and $FeO_t/FeO_t + MgO$), (2) lower Ba, Sr, and Sc, (3) lower Eu/Eu*, (4) very high K/Ba, and (5) significantly higher Ga/Al (tables 6 and 8). Thus, rocks with nearly identical field characteristics have very different chemical compositions and ages, which highlight the need for integrating multiple analytical techniques to decipher the geologic history of similar-appearing rocks.

Late magmatic suite.—Rocks of the silicic porphyroclastic foliated meta-granite (Ypfg; *ca.* 1060 Ma; HNT and FHNT variants only) and mafic foliated biotite meta-quartz monzodiorite (Yfbd; *ca.* 1055 Ma) plutons constitute the Late Magmatic Suite, contrasting with the largely granitic lithologies of the earlier suite (figs. 6A–6F). Yfbd rocks are markedly enriched in HFSE (fig. 8D) relative to magnesian plutons of the Early Magmatic Suite, and, as a result, display within-plate source characteristics (figs. 7A and 7B). Elevated concentrations of Zr, Nb, Ce, and Zn, and high Ga/Al (figs. 9A–9C, table 7) further indicate A-type affinity for these low-silica rocks (cf. Whalen and others, 1987; Eby, 1990). HFSE enrichment characteristic of these rocks reflects derivation from chemically fertile magmatic sources.

The typically K-rich, peraluminous Ypfg rocks of *ca.* 1060 Ma age have exclusively granitic (>69 wt. %) compositions (figs. 6A–6F) and trace-element characteristics, including small Ta-Nb anomalies, that are similar, albeit mostly at higher concentrations, to those of the older magnesian plutons (fig. 8C). These compositional features distinguish Ypfg rocks from the older arc-related lithologies and suggest petrogenesis involving greater input of within-plate type sources (figs. 7A and 7B) (Pearce and others, 1984). Enriched concentrations of Zr, Nb, Hf, and Ce relative to older arc-related lithologies, accompanied by high Ga/Al ratios, indicate an A-type lineage for the Ypfg rocks (figs. 9A–9C, table 8). However, low concentrations of Y and Zn, which are typically enriched in A-type rocks (Eby, 1990), suggest that Ypfg granites represent a hybrid magma type that is compositionally transitional between those of arc systems and those typical of post-collisional, A-type settings.

Nd Isotope Results

Fifteen samples were analyzed for Nd and Sm concentrations and Nd isotopic compositions. Data for representative samples from plutons of each magmatic suite and orthogranofels of the *ca.* 1.32 Ga Ygg xenolith are presented in table 9, and include nine samples for which crystallization ages are reported in table 7.

Analytical methods.—Sm-Nd analysis followed procedures described in Holmden and Dickin (1995). After dissolution using HF and HNO_3, samples were split and one aliquot spiked with a mixed ^{150}Nd-^{149}Sm spike. Standard cation and reverse phase column separation methods were used. Nd isotope analyses were performed on a VG Isomass 354 mass spectrometer at McMaster University using double filaments and a 4 collector peak-switching algorithm, and were normalized to a $^{146}Nd/^{144}Nd$ ratio of 0.7219. An average value of 0.51185 +/−2 (2-sigma) was determined for the La Jolla standard. Analysis by this technique yielded Sm/Nd = 0.2280 +/−2 for U.S. Geological Survey standard BCR-1. Average within-run precision for samples was ± 0.000012 (2 sigma). Reproducibilities of model ages and initial Nd ratios are estimated at +/−20 m.y. and +/−0.4 epsilon units respectively (2 sigma), based on analyses of duplicate dissolutions.

Nd isotope results.—Nd isotope compositions and Sm-Nd concentration data were used to calculate a T_{DM} model age for each sample using the depleted mantle model of DePaolo (1981) (table 9). Model ages for rocks of both magmatic suites and the *ca.* 1327 ± 7 Ma Ygg xenolith range from 1.67 to 1.44 Ga and are significantly older than corresponding igneous crystallization ages obtained through analysis of zircon. Consequently, none of the lithologies are juvenile, indicating instead derivation mostly through melting of older REE-enriched continental crust, which is consistent with the geochemical data. Older crust as a source of magmas is corroborated by inherited, *ca.* 1.37 to 1.22 Ga-age xenocrystic zircon cores in several plutons (table 7).

The 1.67 to 1.44 Ga range of model ages is consistent with the 1.75 to 1.34 Ga age range determined in previous studies of Grenville-age plutonic rocks of the Blue Ridge (Carrigan and others, 2003; Fisher and others, 2010). Consequently, data for the analyzed rocks might reflect mixing between mantle differentiates and crustal melts, a possibility evaluated by considering εNd(1150) values (part per 10,000 deviation from Bulk Earth at 1150 Ma) relative to Nd concentration (fig. 10A). Most of the analyzed samples lie between two mixing lines between Nd-rich mantle differentiates and compositions of Nd-poor crustal melts that might result from variable degrees of melting producing REE-rich residua. Accordingly, mixing is a reasonable explanation for the compositions of the studied Grenville-age plutonic rocks. However, the crustal source would have to have less radiogenic Nd than the plutons themselves.

Evolution of a possible source is represented by the 1.32 Ga orthogranofels xenolith of the Ygg lithologic unit (fig. 10B), as evaluated by comparison of initial Nd isotope ratios for each lithologic unit at the time of igneous crystallization, expressed by εNd(t) (table 9). These data fall well below the depleted mantle evolution growth curve, but somewhat above the possible crustal evolution curve, which is consistent with the proposed mixing model.

Epsilon Nd values for plutons of the *ca.* 1190 to 1130 Ma Early Magmatic Suite are similar to those of contemporaneous rocks in the Shenandoah massif. Fisher and others (2010) reported comparable εNd values and depleted mantle model ages for similar-age basement rocks elsewhere in the southern Appalachians.

DISCUSSION

The geochemistry of Mesoproterozoic basement rocks in the Mount Rogers area provides an effective means for deciphering the likely tectonic setting by comparison with rocks of both similar and significantly younger age in other orogens or in different parts of the North American Grenville orogen.

Comparison with Shenandoah Massif

The predominance of generally granitic, subalkaline, and peraluminous intrusives in the study area is similar to that of comparable-age lithologies constituting Mesoproterozoic basement in the northern Shenandoah massif (Tollo and others, 2006). However, in the latter region, silicic charnockites and meta-leucogranites are most abundant, whereas such rocks are absent to minor in the study area (table 1). The terranes also differ in the widespread emplacement of low-silica charnockite and intermediate biotite-rich meta-granitoid of 1060 to 1020 Ma age in the Shenandoah region, an episode that produced an overall continuum of magmatic compositions that contrasts with the bimodal distribution of rocks in the Mount Rogers area (compare unfilled dashed fields in figs. 6A–6D). Lastly, basement rocks in northern Shenandoah are highly K enriched and are strongly ferroan, compositional characteristics that distinguish the Shenandoah lithologies from all but the lineated biotite meta-granite (Ylbg) and the foliated biotite meta-quartz-monzodiorite (Yfbd) plutons in the Mount Rogers area (figs. 6E and 6F).

TABLE 9

Sm-Nd Isotopic data for samples of Mesoproterozoic rocks of the Mount Rogers area

Sample Number	Unit	Lithology*	Age† (Ma)	Nd (ppm)	Sm (ppm)	$^{147}Sm/^{144}Nd$	$^{143}Nd/^{144}Nd$	εNd	T_{DM} (Ga)
Late Magmatic Suite									
MR 09-117	Yfbd	quartz monzodiorite†	1055 ± 16	180.3	31.00	0.1038	0.511899	-1.9	1.58
MR-13-238	Yfbd	quartz monzodiorite		171.3	28.77	0.1015	0.511912	-1.4	1.54
MR 06-17	Ypfg	syenogranite (HNT)	1061 ± 5	121.8	18.08	0.0897	0.511797	-1.9	1.53
Early Magmatic Suite									
MR-13-241	Ylbg	quartz syenite	(1135 ± 7)§	41.9	9.22	0.1329	0.512175	0.2	1.64
MR-13-242	Ylbg	quartz syenite		44.7	10.36	0.1401	0.512236	0.4	1.67
MR 08-66	Ybg	granite	1168 ± 10	30.5	5.36	0.1062	0.511937	-0.2	1.57
MR 08-71	Ybg	granite	1172 ± 10	42.5	7.10	0.1009	0.511922	0.3	1.51
MR 10-122	Ybg	granite		36.8	6.24	0.1025	0.511987	1.3	1.44
MR10-126	Ybg	granite		28.8	5.24	0.1102	0.511984	0.1	1.56
MR 06-1	Ypg	syenogranite (pink)	1162 ± 4	16.4	3.66	0.1353	0.512181	0.2	1.67
MR 06-22	Ypg	monzogranite (gray)	1161 ± 7	35.2	5.79	0.0996	0.511886	-0.3	1.55
MR 09-100	Yfbl	leucogranite	1177 ± 7	20.8	2.67	0.0778	0.511695	-0.6	1.51
MR-08-65	Yfbl	leucogranite		4.4	0.59	0.0809	0.511727	-0.6	1.51
Xenoliths									
MR 06-7A	Ygg	orthogranofels	1327 ± 7	40.1	6.55	0.0988	0.511802	0.2	1.64
MR06-7B	Ygg	orthogranofels		41.6	6.82	0.0989	0.511790	0.0	1.66

* Prefix "meta" omitted for clarity.
† Igneous crystallization age (U-Pb SHRIMP technique).
§ Ages in parentheses indicate geochronologic analysis obtained from different sample in same lithologic unit.

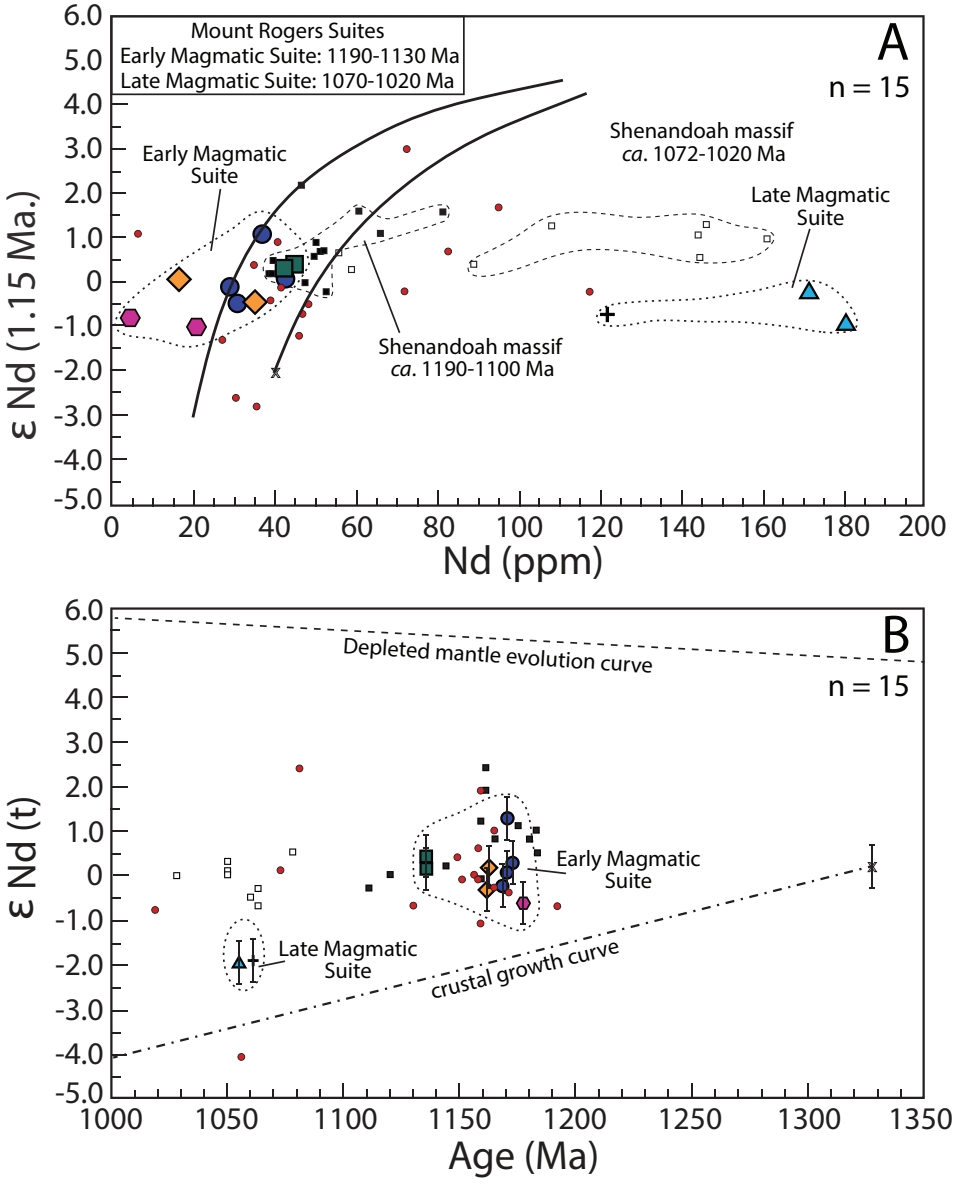

Fig. 10. (A) Plot of Nd concentration versus εNd calculated at 1150 Ma for rocks of the study area. Symbols are the same as figure 4. Possible mixing curves between Nd-rich mantle differentiates and Nd-poor continental melts are indicated by solid lines. Data for Shenandoah massif includes meta-igneous rocks of *ca.* 1070–1020 Ma (unfilled squares) and *ca.* 1190–1100 Ma (filled squares) age (Tollo and others, 2006). Data from previous studies of Grenville-age crust of the Blue Ridge (red circles) from Carrigan and others (2003) and Fisher and others (2010). (B) Plot of Nd isotope evolution vs age for rocks of the study area, showing initial ratios for lithologic units relative to the depleted mantle evolution curve of DePaolo (1981). Symbols are the same as figure 6. Error bars represent estimated 2-sigma analytical uncertainties of individual analyses. Dash-dot line indicates a model isotopic evolution path for crust represented by the *ca.* 1.32 Ga orthogranofels of the composite Ygg lithologic unit. Data for Mesoproterozoic basement rocks of the Shenandoah massif and other Blue Ridge crust are indicated as described above.

Compositional Analogs of Early Magmatic Suite Rocks

The geochemistry rocks of *ca.* 1180 to 1145 Ma age in the study area is similar to that of younger arc-related suites, including the (1) Neogene to Holocene volcanics of the Nevados de Payachata region of the Central Volcanic Zone in the Chilean Andes (Davidson and others, 1990), (2) Late Cretaceous to late Eocene Coastal Batholith of the Peruvian Andes (Bussell, 1983; Atherton and Sanderson, 1985; Boily and others, 1989), and (3) Late Cretaceous Tuolumne Intrusive Suite of the Sierra Nevada batholith in California (Bateman and Chappell, 1979; Bateman and others, 1984). Like the Mount Rogers rocks, each suite is dominated by high-K, magnesian compositions with calc-alkalic affinity (figs. 6E–6G). Moreover, these analog suites have low HFSE concentrations and marked decoupling of LILE and HFSE abundances, as are characteristic of arc-related magmatic systems (Pearce, 1983; Pearce and others, 1984), overlapping the data arrays defined by the Ybg and Ypg granites (figs. 7A, 7B and 8A).

Studies have demonstrated the importance of continental crust in modifying the compositions of primary mantle-derived magmas produced in subduction-related settings through processes including melting, assimilation, storage, and homogenization (MASH model) (Hildreth and Moorbath, 1988; Davidson and others, 1990). Increased involvement of continental crust in the magma-generation process typically leads to (1) high SiO_2, K_2O, Rb, Ba, and Th contents, (2) increased volume of silicic magmas, (3) calc-alkaline compositions with high LILE/HFSE, (4) elevated Ce/Yb, and (5) less radiogenic Nd isotopic compositions (Bateman and Dodge, 1970; Saunders and others, 1980; Hildreth and Moorbath, 1988; Ague and Brimhall, 1988; Davidson and others, 1990). The high-K, magnesian, granitic plutons of 1180 to 1145 Ma age in the study area share many characteristics of arc rocks developed in regions of thick continental crust such as the Chilean Andes (compare Hildreth and Moorbath, 1988; Fierstein and others, 1989; Davidson and others, 1990). Consequently, the available evidence indicates that magma generation at 1180 to 1145 Ma in the Mount Rogers area involved MASH-type processes similar to those of the Andean belt. As such, the magnesian plutons in the Mount Rogers area may represent remnants of a similar, subduction-related, continental-arc system that developed in association with relatively thick continental crust.

Geochronologic data indicate that the Ylbg pluton was emplaced in a late syn- to possibly post-orogenic setting following the main calc-alkaline magmatic pulse during waning stages of the *ca.* 1170 to 1140 Ma regional metamorphic episode (table 7), a tectonic environment that is typical of alkaline granitoids (White and Chappell, 1983; Sylvester, 1989; Eby, 1992). The ferroan and alkaline nature of Ylbg rocks distinguishes them from calc-alkaline predecessors (fig. 11A). Moreover, a differentiation relationship with the older granites, which would likely involve crystallization of plagioclase and an Fe-Mg silicate mineral such as orthopyroxene (Patiño-Douce, 1997), is precluded by overlapping Sr concentrations (fig. 11B left), higher FeO_t/MgO and Sc concentrations (fig. 11B right), and lack of negative Eu anomalies (fig. 11C) among Ylbg rocks.

Elevated HFSE concentrations in Ylbg rocks are comparable to post-orogenic A-type granitoids such as the Gabo and Mumbulla suites of the Lachlan Fold Belt in Australia (Collins and others, 1982) and late Neoproterozoic stratoid (sheet-like) syenites in Madagascar (Nédélec and others, 1995) (figs. 6E–G, 7A, and 11D–11F). Relatively high concentrations of Sr and Eu, and low Ga/Al in Ylbg rocks (figs. 11B left, 11C, and 11E left) are generally considered uncharacteristic of A-type granitoids (Whalen and others, 1987; Eby, 1990); however, these parameters are influenced by fractionation of plagioclase (Goodman, 1972; Weill and Drake, 1973; Drake, 1975). Consequently, Ylbg rocks likely represent A-type magmas that underwent minimal plagioclase differentiation (Collins and others, 1982).

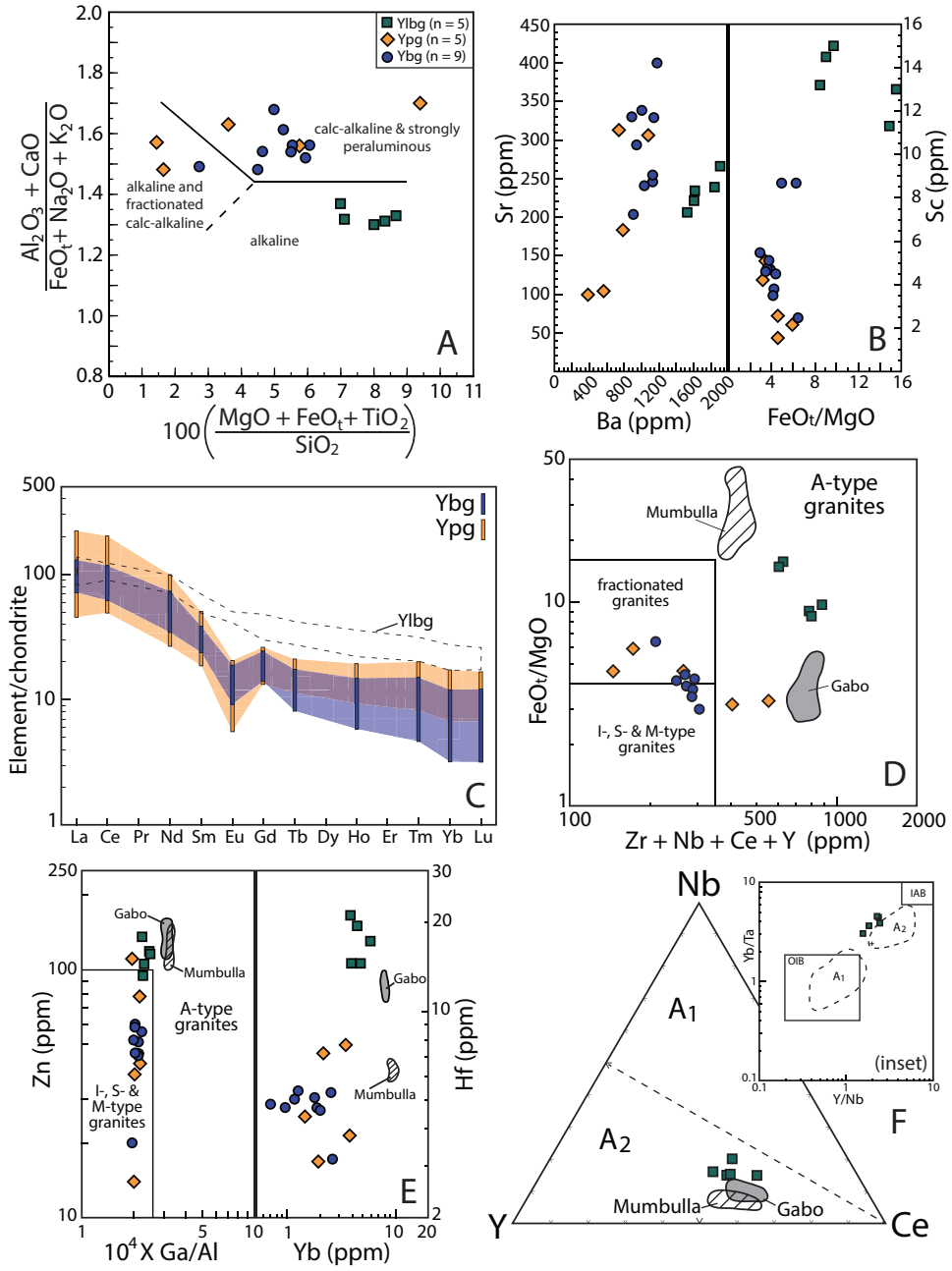

Fig. 11. (A) Plot of 100X((MgO + FeO_t + TiO_2)/SiO_2) vs ((Al_2O_3 + CaO)/(FeO_t + Na_2O + K_2O) for samples of the Ylbg, Ybg, and Ypg plutons. Diagram after Sylvester (1989). (B) Plot of Ba vs Sr (left) and FeO_t/MgO vs Sc (right) for samples of the Ylbg, Ybg, and Ypg plutons. (C) Plot showing the range in normalized REE concentrations for samples of the Ybg (n = 9) and Ypg (n = 5) plutons. Dashed field indicates range of data from the Ylbg pluton (n = 5). REE data are normalized to the chondritic values of Nakamura (1974) with additions from Haskin and others (1968) for Tb, Ho, and Tm. (D) Plot of Zr + Nb + Ce + Y concentrations vs FeO_t/MgO for samples of the Ylbg, Ybg, and Ypg plutons. Diagram after Whalen and others (1987). (E) Plot of 10^4 X Ga/Al vs Zn (left) and Yb vs Hf (right) for samples of the Ylbg, Ybg, and Ypg plutons. Diagram on left is after Whalen and others (1987). (F) Plot of Nb vs Y vs Ce for samples of the Ylbg pluton. Inset shows plot of Y/Nb vs Yb/Ta for samples of the Ylbg pluton. IAB = field of island-arc

The transition from magnesian to A-type granitoids in the Early Magmatic Suite is comparable to the change from Early Devonian orogenic I-types to Late Devonian late- to post-tectonic A-type granites in the Lachlan Fold Belt (Collins and others, 1982; Chappell and White, 1992; Gray and others, 1997). A similar transition is represented by the Madagascan syenites that were emplaced following Pan African orogenesis (Nédélec and others, 1995).

Compositional Analogs of Late Magmatic Suite Rocks

HFSE-enriched low-silica rocks of alkaline and ferroan affinity emplaced in late-syn to post-orogenic settings occur in many Precambrian orogens (Owens and Dymek, 1992) but, unlike the A-type foliated biotite meta-quartz monzodiroite (Yfbd) pluton, are typically associated with and petrologically related to penecontemporaneous anorthosite, a rock type that is absent in the southern Blue Ridge (table 1). The Klewno intrusion of the *ca.* 1.5 Ga, largely post-collisional Mazury Complex in the East European Craton of northeastern Poland (Duchesne and others, 2010) (fig. 6F), which is not directly related to anorthosite, is similarly ferroan and has comparable, high concentrations of HFSE and elevated Ga/Al (figs. 8D, 9A–9C), making it a close compositional analog for Yfbd pluton. Part of a compositionally variable granitic suite, the Klewno rocks are likewise considered to be derived from chemically fertile crustal sources remaining after orogeny (Skridlaite and others, 2003).

Granitic rocks of the Late Ordovician to Early Silurian Topsails igneous suite in central Newfoundland (Whalen and Currie, 1990), which have similar HFSE enrichments and elevated Ga/Al (figs. 9A–9C), constitute a close geological and compositional analog for the silicic porphyroclastic foliated meta-granite (Ypfg) bodies in the study area. Like Ypfg rocks, granitoids of the A-type Topsails suite are spatially associated with coeval mafic rocks and were emplaced during regional deformation and metamorphism, characteristics that distinguish both from most A-type suites, which are typically associated with post-orogenic or anorogenic settings (Collins and others, 1982; Eby, 1990). Ypfg granites were likely derived from crustal sources similar to those of the older magnesian suite as indicated by similar trace-element compositions (fig. 8C). Significantly, average normalized trace-element concentrations of Topsails granites either overlap or plot between values characteristic of the HNT and FHNT variants of the Ypfg lithologic unit (fig. 9E), suggesting that these anomalous, orogenic A-types were derived from comparable crustal sources. Among Mount Rogers area granitoids, Rb/Ta is lower in the *ca.* 1060 Ma Yfbd and Ypfg plutons than in older rocks (fig. 9F), and Th/Ta is low in Yfbd rocks but transitional in Ypfg rocks (fig. 9F inset). These data suggest that Late Magmatic Suite magmas likely involved contributions from both mantle-derived magmas and chemically depleted crustal sources, as suggested by Nd isotope characteristics (fig. 10).

Evolution of Grenville-age Rocks in the Northern French Broad Massif

Field relations, petrologic characteristics, and geochronologic data provide a timeline of geologic events and processes involved in the Grenville-age development of the northern French Broad massif. Collectively, this information forms the basis for detailed reconstruction of orogenesis and for correlations with comparable age events and processes that occurred in other Mesoproterozoic terranes of eastern North America. Use of nomenclature applied to orogenic episodes in the Canadian Grenville

Fig. 11 (continued). basalts; OIB = field of ocean-island basalts. A1 and A2 refer to subgroups of A-type granitoids defined by Eby (1992). Both diagrams in (F) are after Eby (1992). Data for the Gabo and Mumbulla suites (Australia, Collins and others, 1982) are shown for comparison in (D), (E), and (F). Symbols in A, B, and D-F are the same as in figure 4.

province (Rivers, 1997) is employed in order to emphasize temporal comparisons; however, this use is not intended to signify physical continuity of orogenic processes between the study area and other regions in eastern North America.

Earliest crust at ca. 1.3 Ga.—Multiple lines of evidence illustrate the formerly widespread distribution of *ca.* 1.3 Ga crust in the Mount Rogers area, and geochemical data, including the high-K and strongly magnesian composition of the meta-igneous granofels component of the Ygg unit (figs. 6E and 6F), suggest a collisional, arc-related origin. Other rock types that may be vestiges of comparable-age crust include the similarly high-K and magnesian (figs. 6E and 6F), but undated, amphibolites of the gray and white migmatitic amphibolite (Ygw; > *ca.* 1174 Ma) and layered amphibolite (Yla; > *ca.* 1145 Ma). Rocks of comparable age in eastern North America include lithologies produced by calc-alkaline, Andean-style magmatism documented during Geon 13 evolution of the New Jersey Highlands (Volkert and others, 2010), Green Mountain massif (Ratcliffe and others, 1991), Adirondacks (McLelland and Chiarenzelli, 1990), and Grenville province of Canada (Rivers, 1997).

Pre-Shawinigan-age exhumation, erosion, and sedimentary deposition.—Crosscutting field relations and the age of detrital zircons indicate that pre-Shawinigan age crust was exposed and locally covered by sedimentary deposits prior to emplacement of the *ca.* 1190 to 1130 Ma Early Magmatic Suite. Critical field relations include the observation that *ca.* 1166 ± 9 Ma meta-leucogranite intrudes fine- to medium-grained pelitic schist of the biotitic migmatite (Ybm) lithologic unit. U-Pb SHRIMP analyses of zircon indicate that both lithologies were metamorphosed at *ca.* 1060 to 1030 Ma (table 7). The crosscutting field relations indicate that the unmetamorphosed sedimentary protolith was intruded, probably at relatively shallow crustal levels (Tollo and others, 2012), and therefore likely formed part of a regional cover sequence. Similarly, the quartzitic sedimentary protolith of the granofels component of the migmatitic granofels (Ymg) xenolith was intruded by *ca.* 1140 Ma lineated biotite meta-granite (Ylbg). Both granite and xenolith were metamorphosed at *ca.* 1050 to 1020 Ma (table 7). Deposition 10 to 20 m.y. prior to Ylbg emplacement is indicated by detrital zircons as young as *ca.* 1150 Ma in the granofels. Circa 1.32 to 1.26 Ga detrital zircons in the granofels indicate that oldest crustal rocks in the Mount Rogers area were exposed and actively shed zircon into pre-Shawinigan-age deposits. Collectively, such field relations and geochronologic data indicate that clastic sedimentary deposits contain detritus from pre-existing crust, remnants of which are currently exposed in the study, and likely covered portions of the Mount Rogers area before intrusion of the Early Magmatic Suite.

Early magmatic suite: Shawinigan-age plutonism at 1190 to 1130 Ma.—The *ca.* 1190 to 1130 Ma Early Magmatic Suite was emplaced during an interval coeval with the Shawinigan orogeny in the Canadian Grenville province (Rivers, 1997, 2008). The petrogenesis of such high-K, calc-alkalic granites typically involves both crustal and mantle source inputs, and a thermal environment dominated by the effects of crustal thickening and/or upwelling mafic magma (Hildreth and Moorbath, 1988; Roberts and Clemens, 1993). For the Blue Ridge rocks, the dominant role of crustal sources is indicated by trace-element concentrations (figs. 7, 8A and 8B) and Nd isotope characteristics (fig. 10; table 9). In the southern Blue Ridge, such sources were likely related to earlier crustal-building events, including the *ca.* 1.33 to 1.26 Ga magmatic episode represented by Ygg orthogranofels and inherited zircon cores in Early Magmatic Suite plutons (table 7; fig. 12). Petrogenesis of such Shawinigan-age magmas may be modeled by experiments involving partial melting of arc-related source rocks (Carroll and Wyllie, 1990) that produced a series of potassic liquids which could, by differentiation, develop compositions similar to the magnesian, 1180 to 1145 Ma pink and gray meta-granite (Ypg) and biotite meta-granite (Ybg) plutons (fig. 6E). The

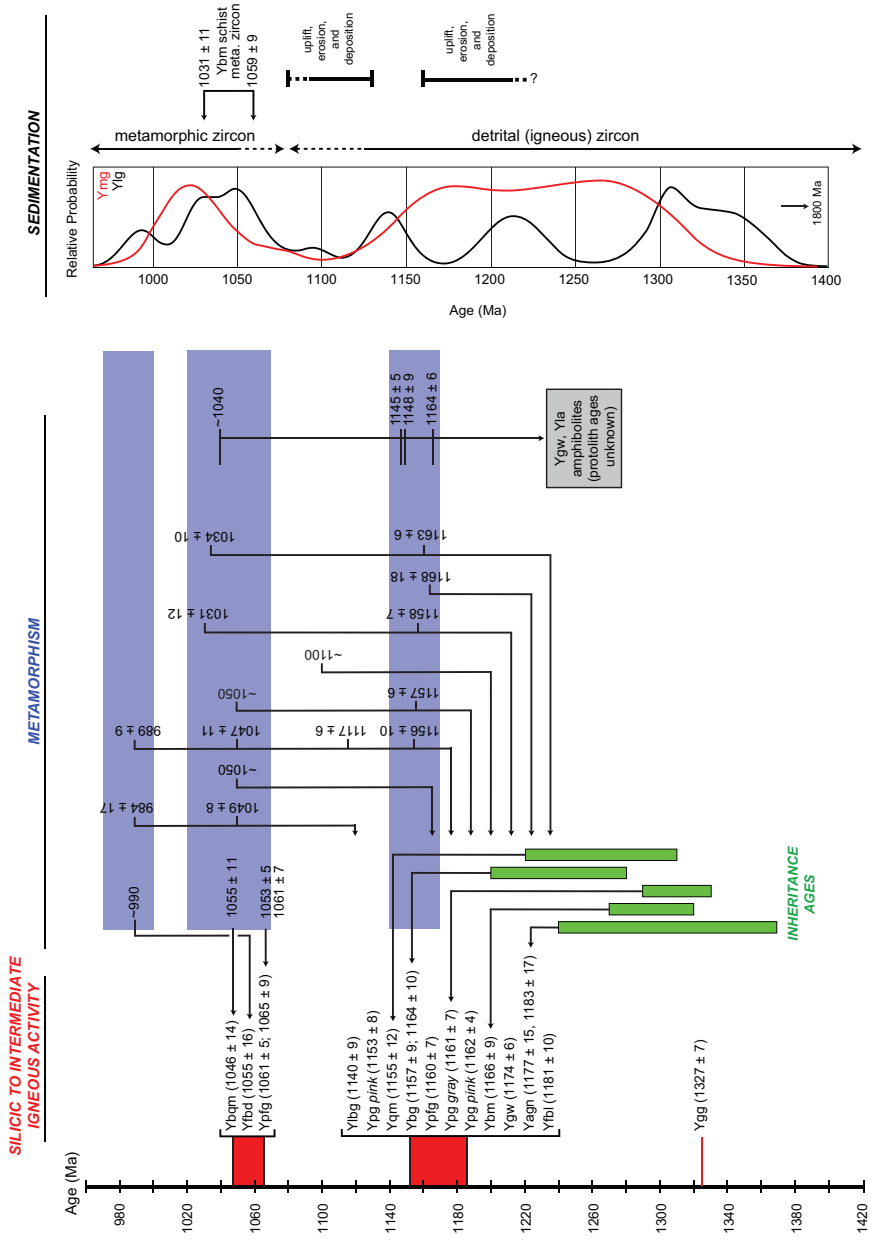

Fig. 12. Synoptic diagram summarizing U-Pb geochronology of zircon from Mesoproterozoic rocks of the Mount Rogers area. Color highlights distinguish igneous (red), metamorphic (blue), and inherited (green) age ranges. Age distribution curves of detrital and metamorphic zircon from the meta-sedimentary Ylg and Ymg lithologic units are indicated by the Relative Probability plot at right.

experiments further indicate melt generation at temperatures consistent with the high-grade conditions prevailing in lower parts of southern Blue Ridge crust at *ca.* 1150 Ma (Tollo and others, 2010).

A-type characteristics of the *ca.* 1140 Ma Ylbg pluton indicate a change in magma genesis near the end of the Early Magmatic Suite episode (figs. 7A-7B and 8D). However, Nd isotope data indicate that continental crust remained a dominant input (fig. 10). Studies indicate that A-type magmatism may be a consequence of (1) differentiation of mantle-derived basaltic melts (Turner and others, 1992; Vander Auwer and others, 2003) or (2) high-temperature melting of tonalitic to granodioritic crustal sources (Clemens and others, 1986; Creaser and others, 1991). Eby (1990, 1992) demonstrated that magmas produced through high-temperature melting are typically associated with late-syn- to post-collisional tectonic environments, which is consistent with the inferred geologic setting, geochronology, and enriched Nd-isotope composition of the Ylbg pluton. A crustal origin is further supported by experiments involving vapor-absent melting of granodiorite that produced liquids comparable to the Ylbg pluton (fig. 6E) (Skjerlie and Johnston, 1992). Collectively, the experimental, geochemical, and Nd isotope data suggest that sources of Early Magmatic Suite magmas changed through time but were consistently dominated by crustal inputs. Very high temperatures required for magma genesis suggest pronounced heating that may reflect enhanced thermal influx associated with mantle-derived magma emplaced following regional compression (Corrigan and Hanmer, 1997); however, there is no direct evidence of such products at the current level of erosion.

The compositional and temporal characteristics of magmatism during the *ca.* 1190 to 1130 Ma interval suggest that the region was the locus of Andean-style, continental-arc magmatism for *ca.* 40 m.y. Subsequent ferroan and more alkalic magmatic activity, represented by the Ylbg pluton, likely reflects the diminished influence of subduction-related processes (Corrigan and Hanmer, 1997). Comparable magmatic events have been recognized in southeastern Canada (Rivers, 1997), the Adirondacks (Heumann and others, 2006), and the Shenandoah massif of the Blue Ridge (Tollo and others, 2006). Contrasts between the geochemistry of nearly synchronous magmatism in the French Broad and Shenandoah massifs likely reflect different relative positions in the formerly contiguous Mesoproterozoic arc system of the southern Appalachians.

Shawinigan-age metamorphism: regional thermal effects at 1170 to 1140 Ma.—U-Pb SHRIMP geochronologic data indicate that metamorphic zircon formed at *ca.* 1170 to 1140 Ma in rocks of the Early Magmatic Suite and associated xenoliths (table 7; fig. 12). Metamorphic mineral assemblages consisting of plagioclase + hornblende + quartz ± clinopyroxene in temperature-sensitive mafic to intermediate compositions of the Yla, Ygg, and Ygw xenoliths (table 2) indicate that upper amphibolite- to lower granulite-facies conditions were attained (Spear, 1993, Harley and others, 2007). Moreover, igneous zircon crystallization ages for the leucogranitic components of the Ybm, Ygw, and Yagn migmatitic units, which range from *ca.* 1190 to *ca.* 1155 Ma (table 7), suggest that melt production occurred during this metamorphic episode. Accordingly, the overlapping periods of magmatism and regional metamorphism represent local effects of Shawinigan-age orogenesis in the Mount Rogers area.

Geochronological evidence indicative of similar-age regional metamorphism is uncommon in Mesoproterozoic rocks of the Shenandoah massif, which suggests that most Shenandoah rocks were either too anhydrous to promote zircon crystallization (Corfu and others, 2003), or that the Shenandoah region at *ca.* 1170 to 1140 Ma was located in an area of the orogen characterized by lower metamorphic grade. Similarly, geochronologic evidence of Shawinigan-age regional metamorphism is rare in the New Jersey Highlands, where geologic relations suggest closure of a back-arc basin and

termination of arc-related magmatism during this interval (Volkert and others, 2010). A different history is recorded in Mesoproterozoic rocks of the Adirondacks where local anatexis at *ca.* 1180 to 1160 Ma resulted from heating associated with Shawinigan orogenesis, possibly augmented by heat related to penecontemporaneous magmatism (Heumann and others, 2006; McLelland and others, 2010). Regionally, Mesoproterozoic terranes of the eastern United States preserve evidence of arc-related magmatism followed or accompanied by regional convergence and/or metamorphism and A-type magmatism. However, the timing and nature of events do not correlate along strike within the orogen or between the orogen sensu stricto and Appalachian outliers such as the Blue Ridge. This apparent lack of consistent tectonic setting likely reflects the complex spatial geometry of the regional arc system(s) as currently preserved in amalgamated components of the Grenville orogenic belt.

The high ratio of plutons to pre-existing country rocks in the study area (fig. 3) suggests that magmatic heat contributed to the thermal budget of metamorphism. Ti-in-zircon geothermometry data indicate that average metamorphic temperatures were likely within 100 °C of probable solidi for Early Magmatic Suite magmas (Carroll and Wyllie, 1990; Tollo and others, 2010). The large volume of magma likely helped to maintain crustal temperatures at near-solidus conditions, which fostered slow cooling and extended the duration required for magma solidification. The Archean Minto block in the Superior province of Quebec, where plutons intrude supracrustal rocks that constitute only about 5 to 15 percent of the total crustal volume, likely records a similar geologic history (Bédard, 2003).

Post-Shawinigan-age uplift, erosion, and sedimentary deposition.—Field relations and ages of detrital zircon in the layered granofels (Ylg) unit indicate that Mesoproterozoic crust was uplifted and subjected to erosion and sedimentary deposition following Shawinigan-age orogenic activity. The Ylg unit forms a small, isolated body surrounded by the *ca.* 1177 ± 7 Ma foliated biotite meta-leucogranite (Yfbl) pluton in the southwest part of the study area (fig. 3). Contacts between the units are not exposed; however, crosscutting meta-leucogranite dikes, which are otherwise abundant in the area, are absent within the Ylg body (Tollo and others, 2012). These field relations and the lack of fault-related ductile textures near the contact zones suggest that Ylg rocks (1) form a xenolith within Yfbl meta-leucogranite, or (2) are separated from the surrounding pluton by an unconformity. The youngest U-Pb SHRIMP ages of detrital zircon cores in Ylg cluster at *ca.* 1160 to 1130 Ma (fig. 5Id), contemporaneous with Shawinigan-age metamorphism and igneous activity, and requires that crust of this age was exposed and subject to erosion. Absence of younger detrital zircons indicates that such activity occurred prior to emplacement of the *ca.* 1075 to 1030 Ma Late Magmatic Suite (fig. 12). U-Pb ages of metamorphic rims developed on most Ylg zircons indicate an interval of crystallization commencing at *ca.* 1050 Ma. These rim ages are coeval with the *ca.* 1070 to 1020 Ma regional metamorphic episode recorded in many lithologies within the study area, including Yfbl meta-leucogranite metamorphosed at *ca.* 1060 Ma (table 7). These data indicate that sedimentary protoliths of the Ylg granofels were likely deposited at *ca.* 1130 to *ca.* 1070 Ma. Correspondingly, field relations indicate that the Ylg unit is separated from the Yfbl pluton by an erosional surface. As indicated by the common metamorphic ages, the near-vertical layering and foliation developed in the Ylg unit, and pervasive foliation and ductile features that characterize the Yfbl meta-leucogranite, likely developed penecontemporaneously during regional Ottawan-age orogenesis. These results, in combination with data indicating the presence of pre-Shawinigan-age sedimentary deposits, demonstrate that episodes of crustal uplift and erosion occurred both prior to and following Shawinigan-age orogenesis in the Mount Rogers region.

Late magmatic suite: Ottawan-age plutonism at 1075 to 1030 Ma.—Magmatism resumed following a nearly 60 m.y. hiatus with emplacement of a compositionally bimodal suite at *ca.* 1075 to 1030 Ma, a period coincident with regional metamorphism (table 7). Ypfg meta-granites are enriched in Ce and HFSE, including Zr, Nb, and Hf, and have elevated Ga/Al relative to *ca.* 1180 to 1145 Ma granites of the Early Magmatic Suite (figs. 8C and 9A–9C). The A-type characteristics, *ca.* 1060 Ma age, and compositional similarities to the subduction-related Topsails igneous suite in Newfoundland (fig. 9) suggest that Ypfg magmas could have been derived through melting of continental crust in a syn- to late syn-collisional tectonic environment involving sources that differed from those that produced the older rocks. Nd isotope characteristics and low Rb/Ta in Ypfg HNT-type rocks may suggest that mantle-derived mafic magma participated in the melting process (figs. 9F and 10B).

Mesoproterozoic granitic rocks with A-type characteristics were also generated in the Adirondack Highlands where the Hawkeye Granite suite represents a compositional analog to Ypfg rocks in the study area (figs. 7A, 9A, and 9B). The *ca.* 1160 Ma age (J.N. Aleinikoff, unpublished data) indicates that the Hawkeye suite and coeval silicic magmas were emplaced in the Adirondack Highlands during waning stages of Shawinigan orogenesis (McLelland and others, 2010), in a tectonic setting comparable to that in which Ypfg magmas were emplaced during Ottawan-age orogenesis in the study area. Chemical similarities among the Topsails, Hawkeye, and Ypfg rocks suggest that A-type compositions reflect the nature of magmatic sources and magma-producing processes, not tectonic environment. The data further suggest that each of these suites was derived from crustal sources affected by previous orogeny and that earlier magma genesis resulted in depleted compositional characteristics that were conducive to subsequent production of A-type magmas (Whalen and others, 1990; McLelland and others, 2001; Tollo and others, 2010).

HFSE-enriched mafic rocks of syn- to post-kinematic origin are recognized in other parts of the Grenville orogenic belt, including the Adirondacks where such rocks are accompanied by *ca.* 1150 Ma anorthosites and a variety of coeval granites (McLelland and others, 1994, 2004). However, the petrogenesis of the Adirondack ferrodioritic rocks is linked with plagioclase fractionation responsible for producing the anorthosites (McLelland and others, 2010). Such plagioclase-rich cumulates are not present in the French Broad massif. Moreover, a comagmatic origin for mafic and silicic constituents of the Late Magmatic Suite is unlikely because of the (1) lack of compositionally transitional lithologies (fig. 4), (2) HFSE concentrations in the Yfbd rocks that are similar to or significantly greater than abundances in the silicic Ypfg bodies (figs. 9A and 9B), (3) higher Ga/Al characteristic of Yfbd rocks (fig. 9C), and (4) markedly lower La/Yb of Nb-enriched Ypfg lithologies (fig. 9D). No experiments have reproduced HFSE-enriched, mafic compositions like those of the Yfbd pluton; however, partial melting of alkaline and calc-alkaline basalts yields liquids that could, upon differentiation, approach Yfbd compositions, especially where the mafic sources were unusually fertile (Roberts and Clemens, 1993). As a result, magmatic protoliths of the *ca.* 1075 to 1030 Ma bodies in the Mount Rogers area are interpreted as products of penecontemporaneous melting of distinct crustal sources, including derivation of Ypfg meta-granitoids from intermediate lower crust (Clemens and others, 1986) and possible derivation of the Yfbd meta-quartz monzodiorites from underplated mafic crust (Roberts and Clemens (1993) and references therein). The experimental results of Rapp and Watson (1995) indicate that compositional characteristics of the Yfbd rocks, including elevated TiO_2 content, could result from advanced partial melting at relatively high temperature of fertile basaltic sources (fig. 6A). Generation of these Late Magmatic Suite magmas likely postdated peak Ottawan-age deformation because high-temperature, ductile structures, which are commonly present in rocks of the Early

Magmatic Suite, are absent in these rocks (Tollo and others, 2012). Petrogenesis of the compositionally bimodal Late Magmatic Suite is thus interpreted to reflect the waning stages of local orogenesis and tectonic transition to a post-orogenic setting.

Ottawan-age metamorphism: regional thermal effects at ca. 1070 to 1020 Ma.—Isotopic and textural evidence of regional heating in the study area at *ca.* 1070 to 1020 Ma is preserved by zircon from the (1) *ca.* 1180 to 1145 Ma Ybg and Ypg plutons, (2) *ca.* 1175 Ma meta-leucogranite of the composite Ygw xenolith, (3) *ca.* 1065 Ma Ypfg bodies, and (4) biotite schist of the composite Ybm lithologic unit (table 7). U-Pb isotopic ages of *ca.* 1027 ± 35 and 1033 ± 11 Ma obtained from titanite from the *ca.* 1160 and 1046 Ma Ybg and Ybqm plutons, respectively, also indicate elevated temperatures during this interval. Temperature estimates from Ti-in-zircon geothermometry, obtained from *ca.* 1050 Ma-age zircon overgrowths in Ypfg meta-granite, suggest peak metamorphism at upper amphibolite-facies conditions (Tollo and others, 2010). Statistically indistinguishable ages of igneous crystallization and metamorphism recorded by zircon in the Ypfg and Ybqm plutons suggest that Late Magmatic Suite magmas crystallized in a crustal environment characterized by near-solidus conditions. These elevated temperatures, together with development of pervasive foliation, compositional layering, and local ductile structures in Late Magmatic Suite rocks, suggest that deformation accompanied metamorphism. Accordingly, we consider the contemporaneous plutonism, metamorphism, and compressional deformation to represent local effects of regional Ottawan-age orogenesis.

Geochronologic data indicate differences in timing and duration of Mesoproterozoic regional heating between the Shenandoah and French Broad massifs. In the Mount Rogers area, the two metamorphic periods are separated by a hiatus during which uplift and sedimentation ensued; in contrast, rocks of the northern Blue Ridge define a continuum of metamorphism (fig. 5Kb). Consequently, we suggest that the two massifs were originally located in separate parts of the Grenville-age orogenic system, and that each underwent a distinct geodynamic evolution until *ca.* 1070 Ma when their metamorphic histories became coincident. Isotopic data indicate similar, Ottawan-age metamorphism in Mesoproterozoic rocks of the New Jersey Highlands (Volkert and others, 2010), and in the Adirondacks, where metamorphism was likely restricted to a brief interval at *ca.* 1050 Ma following a more extended period of deformation (McLelland and others, 2013).

Post-Ottawan-age activity: extended regional Metamorphism during Geon 9.—U-Pb SHRIMP geochronologic data indicate that a third episode of regional metamorphism began at *ca.* 1000 Ma and continued for nearly 30 m.y. This period of Neoproterozoic metamorphism is temporally coincident with the Rigolet phase of the Grenvillian orogeny recognized in southeastern Canada (Rivers, 1997, 2008). A similar episode extending to *ca.* 970 Ma is preserved in Mesoproterozoic basement of the northern Shenandoah massif (Southworth and others, 2010) and New Jersey Highlands (Volkert and others, 2010). This extended interval indicates that tectonic processes associated with amalgamation of Rodinia persisted after arc development, uplift, Ottawan-age orogeny, and a probable additional episode of exhumation (Aleinikoff and others, 2013) into the early part of Geon 9.

SUMMARY AND CONCLUSIONS

Results from this study support the following interpretations regarding the geology of Mesoproterozoic basement in the Mount Rogers area.

1. Field relations and geochronologic data indicate that basement consists of multiple plutons, map- and outcrop-scale xenoliths of pre-existing crustal rocks, and meta-sedimentary lithologies that formerly constituted a supracrustal sequence.
2. U-Pb SHRIMP geochronologic data for zircon indicate magmatic activity at *ca.* 1190 to 1130 Ma (Early Magmatic Suite) and *ca.* 1075 to 1030 Ma (Late

Magmatic Suite). Additional data for zircon and titanite document regional metamorphism at *ca.* 1170 to 1140, 1070 to 1020, and 1000 to 970 Ma.

3. Mineral assemblages developed in amphibolites and granofels indicate metamorphism during the *ca.* 1170 to 1140 and 1070 to 1020 Ma episodes occurred at upper amphibolite- to lower granulite-facies conditions. Most rocks preserve evidence of Paleozoic-age middle to upper greenschist-facies retrograde metamorphism. Paleozoic deformation fostered local development of pervasive foliation and porphyroclastic to protomylonitic textures that obfuscate deduction of relative age based on field characteristics.
4. Most meta-igneous rocks have granitic protoliths that range from alkali feldspar granite to monzogranite. Major syn-orogenic plutons of the Early Magmatic Suite emplaced at *ca.* 1180 to 1145 Ma have high-K, variably magnesian and calc-alkalic compositions, and trace-element concentrations indicating continental-arc magmatic origin dominated by partial melting of thick continental crust. Circa 1190 to 1155 Ma leucogranites, which form both plutons and leucocratic components of migmatites and gneisses, are compositionally similar and indicate widespread magmatism during this episode. In contrast, *ca.* 1140 Ma amphibole-bearing quartz syenite displays A-type affinity, is distinctly ferroan, and exhibits marked HFSE enrichments. These features likely result from a change in magmatic source involving derivation from previously melted continental crust, reflecting transition to a late syn- to post-tectonic environment. Plutons of the compositionally bimodal Late Magmatic Suite include the silicic, *ca.* 1060 Ma porphyroclastic foliated meta-granite (Ypfg) pluton that displays hybrid compositions transitional between arc-type and A-type affinity. The coeval, mafic foliated biotite meta-quartz-monzodiorite (Yfbd) pluton displays A-type characteristics and was likely produced by partial melting of fertile basaltic sources. Collectively, these rocks mark the transition to a post-orogenic environment.
5. Nd isotopic model ages are significantly older than igneous crystallization ages, indicating that magma generation involved melting older continental crust. However, models of Nd isotopic evolution suggest that magma genesis also involved inputs derived from Nd-rich mantle differentiates.
6. Pre-Shawinigan-age crust was exhumed and became a source for clastic deposits that formed local sedimentary cover prior to emplacement of the Early Magmatic Suite. Remnants of these cover rocks occur only as xenoliths.
7. Emplacement of calc-alkalic plutons of the Early Magmatic Suite and coeval metamorphism overlapped a period of regional contraction (Shawinigan-age orogeny) that likely represents development of a magmatic arc and deformation of the cratonic margin.
8. Field relations and U-Pb geochronologic data indicate that Shawinigan-age crust was uplifted and became the locus of sedimentary deposition at *ca.* 1130 to 1070 Ma. Remnants of supracrustal rocks locally unconformably overlie plutonic rocks of Early Magmatic Suite age.
9. Late Magmatic Suite plutons indicate renewed magmatic activity following post-Shawinigan-age uplift. Silicic rocks of *ca.* 1060 Ma age were emplaced into hot crust heated to near-solidus temperatures that reflect peak conditions of the *ca.* 1070 to 1020 Ma metamorphic episode associated with regional Ottawan-age orogenesis. A-type mafic magma emplaced at *ca.* 1055 Ma involved contributions from multiple magmatic sources and transition to a late-orogenic tectonic setting.
10. A third pulse of regional metamorphism at 1000 to 970 Ma is contemporaneous with the Rigolet phase of the Grenvillian orogeny, indicating that re-

newed tectonic activity associated with amalgamation of Rodinia extended into the Neoproterozoic.

11. Detailed geochronologic and geochemical studies of zircon indicate that plutons comprising both magmatic suites likely underwent metamorphism immediately upon cooling to solidus conditions. Despite this extended continuum of igneous and metamorphic processes, geochemical data defining tight clusters or displaying trends that are similar to those exhibited by younger, unmetamorphosed igneous suites indicate that magmatic geochemical characteristics are preserved, suggesting that, in most instances, fluid activity in the high-temperature environment of magma emplacement was insufficient to induce significant mobilization.
12. Distinctions involving geochemical and mineralogical composition of plutonic rocks, sedimentary history, crustal uplift record, and timing of regional metamorphism illustrate differences between the Mesoproterozoic geology of the Shenandoah and French Broad massifs. Both regions record magmatism centered at *ca.* 1160 and 1050 Ma, and regional metamorphism at *ca.* 1070 to 1020 Ma; however, metamorphism at *ca.* 1170 to 1140 Ma is documented only in the French Broad massif, which suggests that the massifs were likely separated prior to *ca.* 1070 Ma when Ottawan-age tectonics began to affect both areas.
13. Similarities in the timing of igneous and metamorphic processes beginning at *ca.* 1070 Ma between the Blue Ridge massifs, other Grenville-age inliers located northward, and the Grenville province in southeastern Canada, including its southern extension forming the Adirondacks, suggest that these formerly distinct regions were amalgamated to form part of a common, regional orogen prior to onset of Ottawan-age orogenesis that affected them all (Rivers, 1997; Volkert and others, 2010; Mclelland and others, 2013; this study). Differences in geodynamic history between the Blue Ridge and other Grenvillian-age outliers likely reflect distinct geographic subsettings within an orogen that was probably comparable in lateral extent to modern systems at various stages in its tectonic evolution (Nance and others, 2014).

ACKNOWLEDGEMENTS

This study was supported by awards from the Educational Geologic Mapping Program administered by the U.S. Geological Survey (USGS) to George Washington University (GWU). The research also benefited from additional support provided by the USGS Appalachian Landscape Project. Any use of trade, firm, or product names is for descriptive purposes only and does not imply endorsement by the U.S. Government. Technical reviews by Robert Ayuso, Edward du Bray, Robert Wintsch, Robert Hatcher, Greg Dunning, and two anonymous sources are greatly appreciated. The prodigious and dedicated efforts of GWU students A. Kentner, R. Gesserman, C. Parendo, M. Logan, A. Rubin, J. Kief, L. Ziminski, L. Finkelstein, and S. Bauer are gratefully acknowledged. Spencer Tollo also provided conscientious and diligent assistance in both the field and laboratory. Our gratitude is extended to J.M. Rhodes, M. Vollinger, and P. Dawson of the Ronald B. Gilmore Analytical Geochemistry Facility at the University of Massachusetts at Amherst who provided valuable assistance with XRF analyses, and to J. Budahn Survey in Denver who provided INAA support. We thank Renee Pillers for help with mineral separations, and image acquisition and processing. Finally, we wish to express our sincere gratitude to Douglas W. Rankin who established the foundation for this study through his mapping of Precambrian rocks in the Mount Rogers area. Doug shared his results and perceptive insights in support of the early stages of this project; he remains a source of inspiration.

Appendix Table A

Shrimp U-Th-Pb data for zircon from Mesoproterozoic rocks, Mount Rogers area, Virginia

sample[1]	measured $^{204}Pb/^{206}Pb$	measured $^{207}Pb/^{206}Pb$	%	common ^{206}Pb	U (ppm)	Th/U	$^{206}Pb/^{238}U$ (Ma)[2]	err[3]	^{206}Pb (Ma)	$^{207}Pb/^{235}U$ (Ma)[2]	err[3]	$^{207}Pb/^{206}Pb$ (%)[4]	err[3]	$^{238}U/^{206}Pb$ (%)[4]	err[3]
MR-10-132 (Ybqm biotite meta-quartz monzonite): coarse-grained, porphyroclastic meta-quartz monzonite, Middle Fox Creek quardrangle; UTM: 475336 4054336[5]															
MR10-132-1.1	0.000157	0.0759	0.267	119	0.84	993	11	1033	44	1.69	2.5	0.167	1.2	0.481	
MR10-132-1.2	-0.000042	0.0759	-0.071	179	0.48	1048	15	1108	29	1.87	2.1	0.177	1.5	0.708	
MR10-132-2.1	-0.000041	0.0723	-0.070	74	0.76	1048	20	1011	49	1.77	3.1	0.176	2.0	0.630	
MR10-132-3.1	-0.000066	0.0774	-0.112	24	0.83	997	18	1155	164	1.82	8.4	0.168	1.7	0.201	
MR10-132-4.1	0.000063	0.0752	0.107	100	1.85	991	12	1049	43	1.71	2.5	0.167	1.3	0.518	
MR10-132-5.1	0.000080	0.0738	0.137	320	0.52	1073	14	1006	26	1.81	1.8	0.181	1.3	0.728	
MR10-132-6.1	0.000260	0.0743	0.447	83	0.77	1002	19	945	63	1.63	3.7	0.168	2.0	0.547	
MR10-132-6.2	0.000108	0.0742	0.185	183	0.47	1060	16	1006	36	1.79	2.3	0.178	1.5	0.660	
MR10-132-7.1	-0.000175	0.0739	-0.296	50	1.00	1093	26	1106	66	1.95	4.1	0.185	2.4	0.593	
MR10-132-8.1	-0.000120	0.0713	-0.205	30	1.06	1107	32	1015	88	1.88	5.3	0.187	3.0	0.568	
MR10-132-9.1	0.000071	0.0725	0.122	120	0.93	1060	18	970	42	1.75	2.7	0.178	1.8	0.647	
MR10-132-10.1	0.000114	0.0744	0.194	48	0.80	1002	24	1009	70	1.69	4.3	0.168	2.5	0.580	
MR10-132-11.1	0.000059	0.0732	0.101	67	1.17	1116	70	997	26	1.88	6.6	0.188	6.5	0.980	
MR10-132-11.2	-0.000046	0.0752	-0.077	281	0.35	1034	14	1092	26	1.82	1.9	0.174	1.4	0.728	
MR10-132-12.1	-0.000092	0.0751	-0.155	61	0.72	1039	22	1106	58	1.85	3.7	0.175	2.2	0.603	
MR10-132-13.1	0.000121	0.0747	0.207	224	0.70	1066	15	1013	31	1.80	2.1	0.179	1.5	0.685	
MR10-132-14.1	0.000144	0.0768	0.244	26	0.87	1050	56	1061	95	1.82	7.3	0.177	5.6	0.762	
MR10-132-14.2	0.000084	0.0759	0.143	353	0.40	1069	14	1060	25	1.86	1.8	0.180	1.3	0.731	
MR10-132-15.1	0.000194	0.0761	0.331	106	0.74	1062	19	1022	46	1.81	2.9	0.179	1.8	0.629	
MR10-132-16.1	0.000155	0.0751	0.264	107	0.87	1051	19	1010	48	1.78	3.0	0.177	1.8	0.613	
MR10-132-16.2	0.000040	0.0739	0.068	278	0.54	1060	14	1023	28	1.80	1.9	0.178	1.4	0.712	
MR10-132-17.1	-0.000019	0.0694	-0.033	84	1.11	1014	31	919	50	1.63	4.0	0.170	3.1	0.789	
MR10-132-18.1	0.000031	0.0711	0.053	80	0.95	1023	21	947	62	1.67	3.7	0.172	2.1	0.568	
MR10-132-18.2	-0.000009	0.0745	-0.016	188	0.48	1060	16	1060	31	1.84	2.2	0.179	1.5	0.703	
MR10-132-19.1	0.000269	0.0728	0.465	45	1.27	1067	27	896	160	1.70	8.2	0.179	2.6	0.314	
MR10-132-19.2	-0.000047	0.0758	-0.079	182	0.70	1031	15	1107	31	1.83	2.2	0.174	1.5	0.701	
MR10-132-20.1	0.000131	0.0797	0.220	85	0.74	1062	20	1143	50	1.93	3.2	0.180	2.0	0.617	
MR-09-117 (Yfbd foliated biotite meta-monzodiorite): medium- to coarse-grained, foliated biotite meta-monzodiorite, Grassy Creek quadrangle; UTM: 460965 4041485															
MR117-1.1	0.000249	0.0774	0.424	39	1.10	1013	26	1039	84	1.74	4.9	0.170	2.6	0.534	
MR117-2.1	0.002063	0.0796	3.807	27	0.89	1014	31	162	487	1.12	21.1	0.165	3.4	0.161	
MR117-3.1	0.000418	0.0804	0.710	25	0.92	1042	33	1053	131	1.80	7.3	0.175	3.3	0.453	
MR117-4.1	0.000307	0.0739	0.528	108	1.29	1130	21	914	68	1.82	3.8	0.190	1.9	0.499	
MR117-6.1	0.000552	0.0790	0.946	53	0.71	1044	24	959	113	1.72	6.1	0.175	2.4	0.404	
MR117-6.2	0.001167	0.0861	2.011	24	0.81	976	34	911	401	1.56	19.8	0.163	3.4	0.174	
MR117-7.1	0.000140	0.0753	0.239	152	0.93	1053	17	1023	42	1.79	2.6	0.177	1.6	0.622	
MR117-8.1	0.000407	0.0763	0.699	70	0.78	1099	23	941	92	1.79	5.0	0.185	2.2	0.441	

Appendix Table A

(continued)

sample[1]	measured $^{204}Pb/^{206}Pb$	measured $^{207}Pb/^{206}Pb$	% common ^{206}Pb	U (ppm)	Th/U	$^{206}Pb/^{238}U$ (Ma)[2]	err[3]	^{206}Pb (Ma)	$^{207}Pb/^{235}U$ (Ma)[2]	err[3]	$^{207}Pb/^{206}Pb$ (%)[4]	err[3]	$^{238}U/^{206}Pb$ (%)[4]	err[3]
MR-09-117 (Yfbd foliated biotite meta-monzodiorite): medium- to coarse-grained, foliated biotite meta-monzodiorite, Grassy Creek quadrangle; UTM: 460965 4041485														
MR117-9.1	0.000684	0.0857	1.155	23	1.15	1111	36	1096	163	1.97	8.8	0.188	3.4	0.384
MR117-10.1	0.000210	0.0746	0.359	114	1.02	1070	19	975	53	1.78	3.2	0.180	1.8	0.573
MR117-11.1	-0.000096	0.0767	-0.162	113	0.79	1031	18	1149	37	1.88	2.6	0.174	1.8	0.702
MR117-11.2	0.000000	0.0812	0.000	26	0.76	1005	30	1225	54	1.91	4.2	0.170	3.1	0.748
MR117-12.1	-0.000106	0.0737	-0.180	59	1.20	1079	25	1073	58	1.89	3.7	0.182	2.4	0.641
MR117-13.2	0.003417	0.1068	6.125	31	1.11	968	30	495	509	1.25	23.3	0.159	3.5	0.151
MR117-14.1	0.000172	0.0748	0.293	112	0.71	1087	20	997	51	1.83	3.2	0.183	1.9	0.607
MR117-15.1	0.001755	0.0813	3.161	20	0.95	997	36	441	446	1.26	20.4	0.164	3.9	0.193
MR117-15.2	0.000219	0.0751	0.375	282	0.53	1115	17	985	41	1.86	2.6	0.188	1.6	0.609
MR117-16.1	0.000238	0.0788	0.403	104	0.69	1041	20	1080	56	1.83	3.4	0.176	2.0	0.578
MR117-16.2	0.000103	0.0739	0.176	180	0.63	988	15	997	36	1.65	2.4	0.166	1.6	0.672
MR117-3.2	0.000209	0.0748	0.357	177	0.63	994	13	980	32	1.65	2.1	0.167	1.3	0.647
MR117-7.2	0.000132	0.0678	0.230	165	0.57	1072	19	802	312	1.62	15.0	0.179	1.5	0.097
MR117-8.2	0.000095	0.0768	0.161	35	0.71	1051	18	1081	54	1.84	3.2	0.177	1.8	0.556
MR-08-76 (Ypfg porphyroclastic foliated meta-granite HNT): coarse-grained, porphyroclastic meta-syenogranite, Grassy Creek quadrangle; UTM: 466425 4050699														
MR76-1.1	0.000052	0.0759	0.089	290	1.80	1077	16	1074	13	1.89	1.7	0.182	1.5	0.921
MR76-1.2	0.000003	0.0747	0.004	610	0.11	1103	16	1060	8	1.92	1.5	0.186	1.5	0.965
MR76-2.1	0.000250	0.0757	0.427	54	1.78	1080	21	990	44	1.81	2.9	0.182	2.0	0.681
MR76-3.1	0.000168	0.0762	0.286	45	1.29	1062	22	1037	42	1.82	3.0	0.179	2.1	0.715
MR76-3.2	0.000040	0.0754	0.068	814	0.12	1089	15	1063	8	1.90	1.5	0.184	1.5	0.966
MR76-4.1	-0.000029	0.0748	-0.049	55	1.13	1092	22	1073	29	1.91	2.5	0.184	2.0	0.814
MR76-5.1	0.000092	0.0761	0.157	84	2.37	1090	19	1062	27	1.90	2.3	0.184	1.8	0.806
MR76-6.1	0.000111	0.0759	0.188	85	2.27	1051	18	1050	26	1.81	2.2	0.177	1.8	0.813
MR76-6.2	0.000030	0.0741	0.051	354	0.34	1048	15	1032	11	1.79	1.6	0.176	1.5	0.938
MR76-7.1	0.000136	0.0769	0.231	148	2.53	1112	18	1069	23	1.94	2.0	0.188	1.7	0.828
MR76-8.1	0.000020	0.0737	0.035	257	0.42	1075	16	1025	17	1.83	1.8	0.181	1.6	0.882
MR76-8.2	0.000026	0.0748	0.043	438	0.17	1077	16	1052	10	1.86	1.6	0.182	1.5	0.946
MR76-9.1	0.000709	0.0841	1.206	62	1.14	1059	20	1042	60	1.82	3.5	0.178	2.0	0.554
MR76-9.2	0.000052	0.0756	0.089	807	0.13	1055	15	1065	8	1.84	1.5	0.178	1.5	0.965
MR76-10.1	0.000065	0.0741	0.111	50	1.40	1092	22	1019	35	1.86	2.7	0.184	2.1	0.767
MR76-10.2	0.000149	0.0763	0.254	269	0.30	1122	17	1045	18	1.94	1.8	0.190	1.6	0.873
MR76-11.1	0.000071	0.0754	0.120	95	2.20	1094	19	1052	25	1.89	2.2	0.185	1.8	0.823
MR76-11.2	0.000123	0.0758	0.208	347	0.36	1050	16	1042	15	1.81	1.7	0.177	1.5	0.904
MR76-12.1	0.000053	0.0751	0.091	81	1.05	1074	19	1051	24	1.86	2.2	0.181	1.8	0.835
MR76-12.2	0.000008	0.0751	0.014	547	0.52	1080	15	1069	9	1.88	1.5	0.182	1.5	0.960
MR76-13.1	0.000081	0.0766	0.138	79	1.11	1074	19	1081	27	1.89	2.3	0.181	1.9	0.809

Appendix Table A

(continued)

sample[1]	measured $^{204}Pb/^{206}Pb$	measured $^{207}Pb/^{206}Pb$	%	common ^{206}Pb	U (ppm)	Th/U	$^{206}Pb/^{238}U$ (Ma)[2]	err[3]	$^{207}Pb/^{206}Pb$ (Ma)[2]	err[3]	$^{207}Pb/^{235}U$ (%)[4]	err[3]	$^{206}Pb/^{238}U$ (%)[4]	err[3]
MR-08-76 (Ypfg porphyroclastic foliated meta-granite HNT): coarse-grained, porphyroclastic meta-syenogranite, Grassy Creek quadrangle; UTM: 466425 4050699														
MR76-13.2	0.000016	0.0756	0.026	691	0.12	1092	16	1079	8	1.92	1.5	0.184	1.5	0.967
MR76-14.1	0.000507	0.0817	0.861	70	1.29	1098	21	1054	50	1.90	3.2	0.185	2.0	0.617
MR76-15.1	0.000000	0.0752	0.000	263	0.48	1051	16	1075	12	1.84	1.7	0.177	1.6	0.930
MR76-15.2	0.000015	0.0751	0.025	691	0.11	1113	16	1066	8	1.94	1.5	0.188	1.5	0.969
MR76-16.1	0.000158	0.0727	0.271	49	1.48	1068	21	940	43	1.74	2.9	0.179	2.1	0.706
MR76-17.1	0.000193	0.0762	0.329	56	0.97	1071	21	1027	40	1.83	2.8	0.180	2.0	0.719
MR76-17.2	0.000018	0.0747	0.030	381	0.31	1058	16	1054	11	1.83	1.6	0.178	1.5	0.938
MR76-18.1	0.000000	0.0748	0.000	187	0.79	1075	44	1064	16	1.87	4.3	0.181	4.2	0.984
MR76-18.2	0.000009	0.0758	0.016	332	0.75	1059	16	1087	11	1.86	1.6	0.179	1.5	0.939
MR76-19.1	0.000023	0.0749	0.038	476	0.15	1072	15	1058	10	1.86	1.6	0.181	1.5	0.953
MR76-20.1	0.000058	0.0762	0.099	110	1.39	1082	18	1079	22	1.90	2.1	0.183	1.8	0.848
MR-11-167 (Ylbg lineated biotite meta-granite): medium- to coarse-grained, lineated, porphyroclastic biotite-hornblende meta-granite, Mouth of Wilson quadrangle; UTM: 471989 4048570														
MR11-167-1.1	0.000117	0.0769	0.213	126	0.29	1074	22	1074	26	1.88	2.5	0.181	2.1	0.848
MR11-167-1.2	0.000049	0.0772	0.090	338	0.16	1078	13	1108	13	1.92	1.4	0.182	1.3	0.886
MR11-167-2.1	0.000022	0.0769	0.039	447	0.19	1162	43	1110	23	2.08	4.0	0.197	3.8	0.956
MR11-167-3.1	-0.000008	0.0779	-0.014	246	0.21	1160	19	1147	13	2.12	1.8	0.197	1.7	0.931
MR11-167-3.2	0.000043	0.0730	0.079	330	0.04	1011	16	995	15	1.69	1.8	0.170	1.6	0.909
MR11-167-4.1	0.000000	0.0785	0.000	213	0.28	1113	14	1159	14	2.04	1.5	0.189	1.3	0.882
MR11-167-5.1	0.000000	0.0778	0.000	454	0.21	1180	17	1142	9	2.15	1.6	0.200	1.5	0.954
MR11-167-5.2	-0.000009	0.0741	-0.016	1088	0.04	1054	14	1047	7	1.82	1.4	0.178	1.3	0.971
MR11-167-5.3	0.000099	0.0733	0.181	133	0.55	1063	22	984	26	1.77	2.5	0.179	2.1	0.854
MR11-167-6.1	0.000000	0.0717	0.000	324	0.12	992	15	978	13	1.64	1.7	0.166	1.6	0.932
MR11-167-7.1	0.000086	0.0760	0.157	209	0.45	1038	26	1061	19	1.80	2.7	0.175	2.6	0.941
MR11-167-7.2	0.000007	0.0714	0.013	287	0.27	1011	16	965	39	1.67	2.5	0.169	1.6	0.645
MR11-167-8.1	0.000006	0.0772	0.010	676	0.62	1113	15	1125	8	2.01	1.5	0.189	1.4	0.962
MR11-167-8.2	0.000342	0.0698	0.627	61	1.56	1034	17	770	110	1.54	5.5	0.172	1.7	0.303
MR11-167-9.1	0.000082	0.0771	0.150	171	0.35	1142	21	1092	28	2.02	2.4	0.193	1.9	0.803
MR11-167-9.2	0.000000	0.0728	0.000	106	0.78	1103	27	1008	29	1.86	2.9	0.186	2.5	0.874
MR11-167-10.1	0.000051	0.0778	0.094	287	0.51	1151	27	1123	14	2.07	2.5	0.195	2.4	0.962
MR11-167-10.2	0.000399	0.0740	0.729	80	0.94	1315	42	876	78	2.08	5.0	0.221	3.3	0.658
MR11-167-11.1	0.000039	0.0779	0.071	288	0.43	1144	14	1130	13	2.07	1.5	0.194	1.3	0.889
MR11-167-12.1	0.000027	0.0781	0.049	264	0.22	1136	18	1140	13	2.07	1.8	0.193	1.6	0.927
MR11-167-13.1	0.000016	0.0778	0.030	354	0.42	1146	18	1135	11	2.08	1.7	0.194	1.6	0.940
MR11-167-14.1	-0.000012	0.0776	-0.022	295	0.46	1108	17	1141	12	2.01	1.7	0.188	1.6	0.937
MR11-167-15.1	-0.000016	0.0777	-0.028	215	0.30	1110	19	1145	14	2.02	1.9	0.188	1.7	0.931
MR11-167-15.2	0.000006	0.0744	0.012	688	0.14	1059	15	1050	13	1.83	1.6	0.178	1.4	0.905

Appendix Table A

(continued)

sample[1]	measured $^{204}Pb/^{206}Pb$	measured $^{207}Pb/^{206}Pb$	%	common ^{206}Pb	U (ppm)	Th/U	$^{206}Pb/^{238}U$ (Ma)[2]	err[3]	$^{207}Pb/^{206}Pb$ (Ma)[2]	err[3]	$^{207}Pb/^{235}U$ (%)[4]	err[3]	$^{206}Pb/^{238}U$ (%)[4]	err[3]
MR-11-167 (Ylbg lineated biotite meta-granite): medium- to coarse-grained, lineated, porphyroclastic biotite-hornblende meta-granite, Mouth of Wilson quadrangle; UTM: 471989 4048570														
MR11-167-16.1	0.000000	0.0763	0.000	257	0.24	1084	18	1104	13	1.93	1.8	0.183	1.7	0.930
MR11-167-16.2	0.000011	0.0745	0.019	1184	0.04	1039	13	1050	7	1.79	1.4	0.175	1.3	0.971
MR11-167-17.1	0.000003	0.0779	0.005	717	0.50	1136	15	1143	8	2.07	1.5	0.193	1.4	0.965
MR11-167-18.1	0.000021	0.0758	0.039	1126	0.41	1119	62	1081	62	1.97	6.5	0.189	5.7	0.879
MR11-167-19.1	-0.000003	0.0786	-0.006	583	0.37	1163	26	1164	8	2.14	2.3	0.198	2.3	0.984
MR11-167-20.1	0.000018	0.0781	0.033	346	0.23	1173	18	1143	12	2.14	1.7	0.199	1.6	0.933
MR11-167-21.1	0.000007	0.0769	0.013	508	0.37	1151	26	1116	15	2.07	2.5	0.195	2.3	0.950
MR11-167-22.1	0.000009	0.0774	0.016	663	0.25	1164	14	1127	8	2.10	1.3	0.198	1.3	0.951
MR11-167-23.1	0.000005	0.0777	0.008	373	0.51	1184	18	1137	10	2.15	1.6	0.201	1.5	0.950
MR11-167-24.1	0.000018	0.0774	0.032	106	0.51	1150	16	1125	21	2.07	1.8	0.195	1.5	0.812
MR11-167-25.1	0.000021	0.0769	0.038	513	0.55	1145	16	1112	9	2.05	1.5	0.194	1.5	0.952
MR11-167-25.2	0.000000	0.0783	0.000	89	0.56	1170	27	1156	22	2.15	2.6	0.199	2.3	0.904
MR11-167-26.1	-0.000054	0.0791	-0.100	34	0.74	1147	37	1194	66	2.15	4.7	0.195	3.3	0.700
MR11-167-27.1	0.000024	0.0782	0.044	412	1.10	1089	16	1142	11	1.98	1.6	0.184	1.5	0.937
MR11-167-28.1	0.000000	0.0783	0.000	280	0.77	1159	18	1155	14	2.13	1.8	0.197	1.6	0.921
MR11-167-29.1	0.004020	0.0789	7.356	75	0.44	1011	33			0.38	55.0	0.159	3.6	0.065
MR11-167-14.2	0.001257	0.0788	2.301	371	0.86	1647	50	622	162	2.30	8.1	0.276	3.1	0.382
MR11-167-30.1	0.002137	0.0790	3.911	115	0.82	1388	27	72.0	383	1.49	16.2	0.228	2.1	0.128
MR11-167-30.2	0.001048	0.0758	1.918	135	0.53	1087	27	625	112	1.51	5.8	0.180	2.6	0.452
MR11-167-30.3	0.000020	0.0781	0.037	357	0.66	1160	17	1143	11	2.11	1.6	0.197	1.5	0.940
MR-11-193 (Ylbg lineated biotite meta-granite): coarse-grained, lineated biotite-hornblende meta-granite, Mouth of Wilson quadrangle; UTM: 472624 4048678														
MR11-193-1.1	0.000075	0.0783	0.137	131	0.22	1146	23	1128	22	2.07	2.4	0.194	2.1	0.885
MR11-193-1.2	0.000010	0.0721	0.019	189	0.25	1048	18	986	16	1.75	2.0	0.176	1.8	0.916
MR11-193-2.1	0.000075	0.0770	0.137	76	0.11	1134	17	1094	29	2.01	2.1	0.192	1.5	0.730
MR11-193-3.1	-0.000047	0.0777	-0.086	39	0.36	1265	38	1156	60	2.33	4.3	0.216	3.1	0.714
MR11-193-3.2	0.000037	0.0742	0.068	419	0.12	1063	16	1031	13	1.82	1.6	0.179	1.5	0.923
MR11-193-4.1	-0.000014	0.0774	-0.025	132	0.48	1133	22	1136	18	2.06	2.2	0.192	2.0	0.911
MR11-193-4.2	-0.000015	0.0724	-0.027	144	0.39	1055	33	1002	20	1.77	3.4	0.177	3.2	0.958
MR11-193-5.1	0.000052	0.0781	0.095	213	0.34	1180	34	1130	28	2.14	3.3	0.200	3.0	0.905
MR11-193-6.1	0.000000	0.0787	0.000	146	0.37	1106	15	1164	17	2.04	1.6	0.188	1.4	0.854
MR11-193-6.2	0.000024	0.0730	0.043	177	0.77	1068	19	1004	18	1.80	2.1	0.180	1.8	0.900
MR11-193-7.1	0.000029	0.0785	0.054	116	0.34	1125	40	1149	19	2.05	3.8	0.191	3.7	0.967
MR11-193-7.2	0.000020	0.0747	0.036	543	0.08	1032	12	1053	10	1.78	1.3	0.174	1.2	0.927
MR11-193-8.1	-0.000020	0.0777	-0.037	96	0.44	1146	26	1147	22	2.09	2.6	0.195	2.3	0.898
MR11-193-8.2	0.000080	0.0727	0.147	208	0.48	1031	18	974	20	1.71	2.0	0.173	1.8	0.879
MR11-193-9.1	0.000088	0.0771	0.160	101	0.37	1171	81	1090	59	2.07	7.7	0.198	7.1	0.924

Appendix Table A

(continued)

sample[1]	measured $^{204}Pb/^{206}Pb$	measured $^{207}Pb/^{206}Pb$	%	common ^{206}Pb	U (ppm)	Th/U	$^{206}Pb/^{238}U$ (Ma)[2]	err[3] (Ma)	$^{207}Pb/^{206}Pb$ (Ma)[2]	err[3] ^{235}U	$^{207}Pb/^{235}U$ (%)[4]	err[3] ^{238}U	$^{206}Pb/^{238}U$ (%)[4]	err[3]
MR-11-193 (Ylbg lineated biotite meta-granite): coarse-grained, lineated biotite-hornblende meta-granite, Mouth of Wilson quadrangle; UTM: 472624 4048678														
MR11-193-9.2	0.000092	0.0782	0.168	115	0.53	1135	23	1119	23	2.04	2.4	0.192	2.1	0.873
MR11-193-10.1	0.000299	0.0771	0.548	32	0.39	1080	35	1010	86	1.83	5.4	0.182	3.4	0.624
MR11-193-10.2	0.000000	0.0748	0.000	787	0.06	1046	24	1063	8	1.82	2.4	0.176	2.4	0.987
MR11-193-11.1	0.000019	0.0790	0.035	283	0.34	1157	18	1165	12	2.13	1.8	0.197	1.6	0.935
MR11-193-12.1	-0.000039	0.0786	-0.072	91	0.36	1222	40	1175	23	2.27	3.5	0.208	3.3	0.946
MR11-193-12.2	0.000052	0.0733	0.096	239	0.49	1060	18	1003	17	1.78	1.9	0.178	1.7	0.901
MR11-193-13.1	0.000000	0.0772	0.000	314	0.51	1127	18	1126	12	2.03	1.7	0.191	1.6	0.937
MR11-193-13.2	0.000064	0.0735	0.118	409	0.13	1048	16	1002	15	1.76	1.8	0.176	1.6	0.906
MR11-193-14.1	0.000000	0.0766	0.000	135	0.52	1136	16	1110	21	2.03	1.8	0.192	1.4	0.812
MR11-193-15.1	-0.000148	0.0692	-0.270	22	0.28	970	22	967	98	1.60	5.3	0.162	2.3	0.430
MR11-193-15.2	0.000084	0.0738	0.154	346	0.20	1054	16	1002	15	1.77	1.7	0.177	1.6	0.909
MR11-193-16.1	0.000054	0.0782	0.099	129	0.53	1113	15	1132	51	2.01	2.9	0.189	1.4	0.470
MR11-193-19.1	-0.000030	0.0778	-0.054	246	0.45	1201	20	1151	14	2.20	1.8	0.204	1.7	0.925
MR11-193-20.1	0.000025	0.0775	0.046	230	0.47	1207	20	1125	14	2.18	1.8	0.205	1.7	0.925
MR11-193-21.1	-0.000009	0.0746	-0.016	230	0.45	1042	17	1060	15	1.81	1.9	0.176	1.7	0.920
MR-06-19 (Ypg pink and gray meta-granite): medium- to coarse-grained, porphyritic biotite meta-syenogranite, Park quadrangle; UTM: 446200 4047320														
MR19-1.1	0.000438	0.0825	0.740	1182	0.42	1000	20	1102	12	1.77	2.1	0.169	2.0	0.958
MR19-2.1	0.000018	0.0791	0.031	449	0.56	1165	12	1167	9	2.15	1.2	0.198	1.1	0.919
MR19-3.1	0.004041	0.1291	6.922	1413	0.49	748	8	968	39	1.22	2.2	0.124	1.1	0.483
MR19-4.1	0.001056	0.0850	1.816	1667	0.35	786	8	925	17	1.26	1.3	0.130	1.0	0.775
MR19-4.2	0.002364	0.0945	4.194	2685	0.34	549	5	610	30	0.74	1.7	0.089	1.0	0.600
MR19-5.1	0.001287	0.0971	2.157	825	0.25	1089	12	1170	68	2.01	3.6	0.185	1.1	0.297
MR19-6.1	0.000373	0.0824	0.628	556	0.26	1134	12	1125	17	2.05	1.4	0.192	1.1	0.795
MR19-7.1	0.003301	0.1195	5.636	1938	0.24	804	21	998	225	1.34	11.4	0.134	2.7	0.238
MR19-8.1	0.000498	0.0849	0.838	1189	0.41	1068	11	1143	11	1.94	1.2	0.181	1.0	0.877
MR19-9.1	0.001120	0.0968	1.867	121	0.64	1117	15	1222	54	2.12	3.1	0.190	1.4	0.461
MR19-10.1	0.001320	0.0939	2.236	654	0.34	900	23	1072	61	1.56	4.0	0.151	2.6	0.647
MR19-10.2	0.003928	0.1183	6.938	2472	0.64	502	8	655	455	0.69	21.3	0.081	1.4	0.064
MR19-11.1	0.000451	0.0844	0.759	280	0.62	1123	13	1148	23	2.05	1.7	0.190	1.2	0.705
MR19-11.2	0.008078	0.1848	13.935	2425	0.53	541	8	900	259	0.84	12.6	0.089	1.1	0.084
MR19-12.1	0.000796	0.0877	1.343	993	0.52	944	10	1106	51	1.67	2.8	0.159	1.1	0.387
MR19-13.1	0.000916	0.0880	1.553	756	0.36	889	9	1067	23	1.54	1.6	0.149	1.1	0.687
MR19-14.1	0.002575	0.1144	4.331	898	0.45	824	9	1144	33	1.48	2.0	0.138	1.1	0.542
MR19-15.1	0.000050	0.0790	0.084	1754	0.56	1144	12	1154	6	2.10	1.1	0.194	1.0	0.965
MR19-15.2	0.000317	0.0808	0.535	3195	0.05	1033	19	1103	33	1.83	2.5	0.174	1.9	0.765
MR19-16.1	0.000041	0.0794	0.068	548	0.27	1121	12	1168	10	2.07	1.2	0.190	1.1	0.915

Appendix Table A

(continued)

sample[1]	measured $^{204}Pb/^{206}Pb$	measured $^{207}Pb/^{206}Pb$	%	common ^{206}Pb	U (ppm)	Th/U	$^{206}Pb/^{238}U$ (Ma)[2]	err[3]	$^{207}Pb/^{206}Pb$ (Ma)[2]	err[3]	$^{207}Pb/^{235}U$ (Ma)[4]	err[3]	$^{206}Pb/^{238}U$ (Ma)[4]	err[3]
MR-06-19 (Ypg pink and gray meta-granite): medium- to coarse-grained, porphyritic biotite meta-syenogranite, Park quadrangle; UTM: 446200 4047320														
MR19-17.1	0.000203	0.0802	0.341	971	0.41	1053	11	1129	10	1.90	1.2	0.178	1.1	0.897
MR19-18.1	0.000111	0.0789	0.186	253	0.59	1126	13	1128	16	2.03	1.4	0.191	1.2	0.827
MR19-19.1	0.000096	0.0794	0.161	328	0.32	1124	12	1148	14	2.05	1.3	0.191	1.2	0.857
MR19-20.1	0.000298	0.0793	0.505	991	0.44	973	10	1071	12	1.69	1.2	0.164	1.1	0.870
MR19-21.1	0.004715	0.1246	8.488	3806	0.32	440	5	447	219	0.54	9.9	0.071	1.2	0.120
MR19-21.2	0.002970	0.1109	5.133	1885	0.48	682	9	878	422	1.06	20.5	0.112	1.8	0.088
MR19-22.1	0.000050	0.0795	0.083	414	0.69	1151	13	1166	11	2.12	1.3	0.196	1.1	0.893
MR19-23.1	0.000830	0.0887	1.400	815	0.48	1041	11	1120	80	1.87	4.2	0.176	1.1	0.271
MR19-24.1	0.000228	0.0797	0.384	1039	0.56	997	10	1107	10	1.77	1.2	0.168	1.1	0.900
MR19-25.1	0.002256	0.0973	3.942	2153	0.26	641	12	768	72	0.94	3.9	0.105	1.9	0.497
MR19-26.1	0.000168	0.0794	0.283	634	0.39	1014	11	1122	13	1.82	1.3	0.171	1.1	0.856
MR19-27.1	0.000226	0.0811	0.379	1042	0.46	1098	11	1144	12	2.00	1.2	0.186	1.1	0.882
MR19-28.1	0.000186	0.0803	0.312	285	0.38	1136	13	1140	18	2.06	1.5	0.193	1.2	0.790
MR19-29.1	0.000140	0.0806	0.234	390	0.63	1197	13	1162	13	2.21	1.3	0.204	1.1	0.859
MR-08-79 (Ypfg porphyroclastic foliated meta-syenogranite LNT): coarse-grained, foliated porphyroclastic biotite meta-granite, Grassy Creek quadrangle; UTM: 460449 4046050														
MR-08-79-1.1	0.000084	0.0790	0.140	136	0.39	1172	18	1142	23	2.14	2.0	0.199	1.6	0.807
MR-08-79-1.2	0.000004	0.0742	0.006	791	0.14	1055	10	1044	10	1.82	1.1	0.178	1.0	0.886
MR-08-79-2.1	0.000024	0.0780	0.040	325	0.42	1173	11	1137	13	2.13	1.2	0.199	1.0	0.836
MR-08-79-2.2	0.000035	0.0744	0.060	722	0.14	1053	10	1039	12	1.81	1.2	0.177	1.0	0.847
MR-08-79-3.1	-0.000013	0.0794	-0.021	246	0.38	1121	12	1186	18	2.09	1.5	0.190	1.1	0.769
MR-08-79-4.1	0.000350	0.0778	0.597	681	0.12	1050	10	1010	19	1.77	1.4	0.177	1.0	0.716
MR-08-79-5.1	0.000017	0.0801	0.028	278	0.37	1118	14	1194	15	2.09	1.5	0.190	1.3	0.850
MR-08-79-6.1	0.000013	0.0793	0.022	170	0.40	1159	16	1174	19	2.15	1.7	0.197	1.4	0.830
MR-08-79-7.1	0.000011	0.0786	0.018	203	0.38	1170	12	1159	17	2.15	1.4	0.199	1.1	0.786
MR-08-79-8.1	0.000015	0.0793	0.026	143	0.36	1171	13	1174	21	2.17	1.6	0.199	1.2	0.746
MR-08-79-9.1	-0.000011	0.0786	-0.018	203	0.38	1156	12	1165	17	2.13	1.4	0.196	1.1	0.785
MR-08-79-10.1	0.000078	0.0788	0.131	177	0.42	1137	16	1139	22	2.07	1.8	0.193	1.5	0.799
MR-08-79-11.1	-0.000021	0.0790	-0.035	313	0.39	1146	11	1181	14	2.13	1.3	0.195	1.0	0.823
MR-08-79-12.1	0.000020	0.0793	0.034	109	0.37	1161	19	1172	24	2.15	2.1	0.197	1.7	0.813
MR-08-79-13.1	-0.000007	0.0788	-0.012	312	0.41	1170	12	1170	14	2.16	1.3	0.199	1.0	0.829
MR-08-88 (Yqm meta-quartz monzonite): medium-grained, amphibole-bearing meta-quartz monzonite, Grassy Creek quadrangle; UTM: 461358 4043748														
MR88-1.1	0.000076	0.0776	0.128	751	0.69	1170	12	1109	8	2.09	1.2	0.198	1.1	0.931
MR88-2.1	0.000458	0.0799	0.779	136	1.35	918	13	1025	42	1.56	2.5	0.154	1.4	0.572
MR88-3.1	0.000036	0.0785	0.061	1079	0.02	1134	12	1147	7	2.07	1.2	0.192	1.1	0.950
MR88-4.1	0.000083	0.0848	0.138	855	0.87	1293	13	1285	10	2.56	1.2	0.222	1.1	0.906

Appendix Table A

(continued)

sample[1]	measured $^{204}Pb/^{206}Pb$	measured $^{207}Pb/^{206}Pb$	%	common ^{206}Pb	U (ppm)	Th/U	$^{206}Pb/^{238}U$ (Ma)[2]	err[3] (Ma)	$^{207}Pb/^{206}Pb$ (Ma)[2]	err[3] ^{235}U	$^{207}Pb/^{206}Pb$ (%)[4]	err[3] ^{238}U	$^{206}Pb/^{238}U$ (%)[4]	err[3]
MR-08-88 (Yqm meta-quartz monzonite): medium-grained, amphibole-bearing meta-quartz monzonite, Grassy Creek quadrangle; UTM: 461358 4043748														
MR88-5.1	0.000030	0.0793	0.050	377	0.67	1133	60	1168	54	2.09	6.1	0.193	5.5	0.897
MR88-6.1	0.000062	0.0827	0.103	781	0.28	1204	13	1242	8	2.32	1.2	0.206	1.1	0.929
MR88-7.1	0.000506	0.0778	0.869	77	2.39	1047	16	946	55	1.71	3.1	0.176	1.6	0.522
MR88-8.1	0.000058	0.0790	0.098	705	0.23	1139	12	1151	9	2.08	1.2	0.193	1.1	0.918
MR88-9.1	0.001032	0.0970	1.715	607	0.78	1241	13	1256	21	2.42	1.5	0.212	1.1	0.717
MR88-10.1	0.000176	0.0819	0.295	759	0.20	1201	13	1183	11	2.24	1.2	0.205	1.1	0.892
MR88-11.1	0.000060	0.0790	0.100	458	0.31	1157	13	1151	11	2.12	1.3	0.197	1.1	0.894
MR88-12.1	0.000079	0.0802	0.132	484	0.18	1137	13	1174	87	2.11	4.6	0.193	1.1	0.247
MR88-13.1	0.000104	0.0796	0.174	489	0.54	1179	13	1151	12	2.16	1.3	0.200	1.1	0.877
MR88-14.1	0.000060	0.0652	0.106	385	0.15	767	9	751	19	1.12	1.5	0.126	1.2	0.790
MR88-15.1	0.000299	0.0753	0.513	155	2.48	1064	14	957	32	1.75	2.1	0.179	1.4	0.658
MR88-16.1	0.000170	0.0845	0.283	597	0.32	1309	14	1248	89	2.54	4.7	0.224	1.2	0.253
MR88-17.1	0.000056	0.0827	0.092	706	0.30	1285	13	1243	8	2.49	1.2	0.220	1.1	0.931
MR88-18.1	0.001388	0.1039	2.294	478	0.75	1318	14	1301	29	2.64	1.9	0.227	1.1	0.606
MR88-19.1	0.000045	0.0797	0.076	709	0.03	1168	12	1173	8	2.17	1.2	0.199	1.1	0.930
MR88-20.1	0.000232	0.0867	0.385	688	0.46	1301	14	1280	52	2.57	2.9	0.223	1.1	0.387
MR88-21.1	0.000089	0.0784	0.150	366	0.52	1172	14	1124	59	2.12	3.2	0.199	1.2	0.365
MR88-22.1	0.000775	0.0899	1.299	1053	0.92	1172	12	1172	15	2.17	1.3	0.199	1.1	0.807
MR88-23.1	0.002134	0.0998	3.678	86	3.02	945	58	906	123	1.50	8.8	0.158	6.4	0.733
MR88-24.1	0.000484	0.0810	0.822	140	0.65	1040	15	1044	43	1.79	2.6	0.175	1.5	0.570
MR88-25.1	0.000067	0.0820	0.111	966	0.87	1218	13	1223	9	2.32	1.2	0.208	1.1	0.929
MR88-25.2	0.000047	0.0779	0.079	822	0.04	1140	12	1128	10	2.06	1.2	0.193	1.1	0.915
MR88-26.1	0.000150	0.0776	0.254	1327	0.11	1062	11	1082	12	1.87	1.3	0.179	1.1	0.885
MR88-27.1	0.000090	0.0753	0.153	430	0.32	1085	12	1041	16	1.87	1.4	0.183	1.2	0.837
MR88-28.1	0.000105	0.0863	0.173	1763	0.46	1337	14	1311	6	2.69	1.1	0.230	1.1	0.953
MR-08-66 (Ybg biotite meta-granite, medium-coarse facies): medium-grained, biotite meta-monzogranite, Grassy Creek quadrangle; UTM: 462483 4052445														
MR66-1.1	0.000011	0.0790	0.018	288	0.62	1148	17	1168	12	2.12	1.7	0.195	1.6	0.936
MR66-2.1	-0.000005	0.0742	-0.008	763	0.06	1027	15	1048	8	1.77	1.5	0.173	1.5	0.968
MR66-3.1	0.000116	0.0806	0.194	452	0.42	1126	16	1172	12	2.08	1.6	0.191	1.5	0.928
MR66-4.1	0.000083	0.0792	0.140	854	0.55	1050	24	1146	9	1.91	2.4	0.178	2.4	0.984
MR66-5.1	0.000010	0.0746	0.016	1033	0.07	1024	14	1054	8	1.77	1.5	0.172	1.5	0.964
MR66-6.1	-0.000006	0.0787	-0.010	808	0.42	1174	17	1167	7	2.17	1.5	0.200	1.5	0.973
MR66-7.1	0.000063	0.0793	0.105	312	0.33	1160	17	1158	12	2.13	1.6	0.197	1.5	0.931
MR66-8.1	0.000077	0.0782	0.130	1235	0.24	1126	16	1124	6	2.03	1.5	0.191	1.5	0.977
MR66-9.1	0.000036	0.0788	0.060	254	0.32	1157	17	1154	12	2.12	1.7	0.197	1.6	0.933
MR66-10.1	0.000076	0.0805	0.127	250	0.20	1156	18	1182	14	2.15	1.7	0.197	1.6	0.914

Appendix Table A

(continued)

sample[1]	measured $^{204}Pb/^{206}Pb$	measured $^{207}Pb/^{206}Pb$	%	common ^{206}Pb	U (ppm)	Th/U	$^{206}Pb/^{238}U$ (Ma)[2]	err[3] ^{206}Pb (Ma)	^{207}Pb (Ma)[2]	err[3] ^{235}U	^{207}Pb (%)[4]	err[3] ^{238}U	^{206}Pb (%)[4]	err[3]
MR-08-88 (Yqm meta-quartz monzonite): medium-grained, amphibole-bearing meta-quartz monzonite, Grassy Creek quadrangle; UTM: 461358 4043748														
MR66-11.1	0.000059	0.0705	0.101	2072	0.09	789	11	919	6	1.26	1.5	0.131	1.4	0.981
MR66-12.1	0.000203	0.0662	0.356	3068	0.94	652	18	718	8	0.93	2.8	0.107	2.8	0.990
MR66-13.1	0.000082	0.0801	0.138	396	0.13	1137	17	1170	11	2.10	1.6	0.193	1.5	0.936
MR66-14.1	0.000024	0.0727	0.041	1057	0.04	958	13	996	7	1.60	1.5	0.160	1.5	0.973
MR66-15.1	0.000017	0.0780	0.029	426	0.26	1118	30	1141	11	2.03	2.8	0.190	2.8	0.982
MR66-15.2	0.000059	0.0710	0.102	1526	0.71	738	19	932	24	1.18	2.8	0.122	2.6	0.913
MR66-16.1	0.000015	0.0793	0.025	296	0.22	1131	17	1174	11	2.10	1.7	0.192	1.6	0.938
MR66-16.2	0.000381	0.0692	0.668	3037	0.34	633	16	732	49	0.91	3.4	0.104	2.6	0.743
MR66-17.1	0.000181	0.0783	0.306	486	0.63	857	12	1089	15	1.50	1.7	0.144	1.5	0.897
MR66-18.1	0.000085	0.0782	0.143	656	0.12	1093	16	1121	9	1.96	1.5	0.185	1.5	0.954
MR66-19.1	0.000181	0.0784	0.306	1482	0.26	985	14	1089	8	1.73	1.5	0.166	1.4	0.965
MR66-20.1	0.000044	0.0839	0.072	568	0.18	1198	17	1276	9	2.36	1.6	0.205	1.5	0.951
MR66-21.1	0.000025	0.0793	0.042	547	0.74	1153	17	1170	8	2.13	1.5	0.196	1.5	0.964
MR66-22.1	0.000022	0.0806	0.036	318	0.20	1183	17	1204	10	2.23	1.6	0.202	1.5	0.946
MR66-23.1	0.000104	0.0802	0.174	56	0.93	1138	22	1165	32	2.10	2.6	0.193	2.0	0.784
MR66-24.1	0.000033	0.0785	0.055	190	0.39	1140	18	1149	15	2.08	1.8	0.194	1.6	0.905
MR66-25.1	0.000023	0.0778	0.039	221	0.40	1118	17	1133	14	2.02	1.8	0.189	1.6	0.911
MR66-26.1	-0.000021	0.0783	-0.035	143	0.48	1125	18	1161	16	2.07	1.9	0.191	1.7	0.898
MR66-27.1	0.000151	0.0801	0.253	110	0.36	1146	20	1146	26	2.09	2.2	0.195	1.8	0.808
MR66-28.1	-0.000007	0.0806	-0.011	220	0.47	1167	18	1214	15	2.21	1.8	0.199	1.6	0.900
MR-08-71 (Ybg biotite meta-granite, porphyritic facies): medium- to coarse-grained, feldspar porphyritic biotite meta-monzogranite, Grassy Creek quadrangle; UTM: 464813 4052509														
MR71-1.1	0.000017	0.0790	0.028	240	0.89	1148	17	1166	12	2.12	1.7	0.195	1.6	0.935
MR71-1.2	0.000010	0.0793	0.017	479	0.11	1066	17	1175	11	1.97	1.7	0.181	1.6	0.944
MR71-2.1	0.000399	0.0830	0.671	147	0.51	1137	19	1131	34	2.06	2.4	0.193	1.7	0.713
MR71-3.1	0.000018	0.0791	0.030	342	0.40	1142	17	1168	11	2.11	1.6	0.194	1.5	0.943
MR71-4.1	0.000218	0.0802	0.366	73	0.61	1019	19	1124	35	1.83	2.6	0.172	1.9	0.737
MR71-5.1	0.000000	0.0801	0.000	199	1.11	1142	18	1200	13	2.15	1.7	0.194	1.6	0.928
MR71-5.2	0.002546	0.1211	4.197	1275	0.23	869	13	1323	76	1.73	4.2	0.147	1.5	0.347
MR71-6.1	0.000155	0.0814	0.260	105	0.34	1148	19	1178	24	2.13	2.1	0.195	1.7	0.824
MR71-7.1	0.000268	0.0800	0.453	60	0.45	1142	21	1099	38	2.03	2.7	0.193	1.9	0.719
MR71-8.1	0.000037	0.0798	0.062	226	0.33	1137	17	1179	13	2.11	1.7	0.193	1.6	0.922
MR71-9.1	0.000053	0.0806	0.089	288	0.51	1151	17	1194	12	2.16	1.7	0.196	1.5	0.931
MR71-9.2	0.000287	0.0773	0.489	1243	0.15	891	19	1019	39	1.50	2.9	0.149	2.2	0.758
MR71-10.1	0.000009	0.0783	0.015	161	0.62	1146	18	1150	15	2.10	1.8	0.195	1.6	0.912
MR71-11.1	0.000174	0.0804	0.293	150	0.82	1134	20	1144	30	2.07	2.4	0.193	1.8	0.764
MR71-12.1	0.000125	0.0800	0.210	118	1.01	1182	20	1152	24	2.17	2.1	0.201	1.8	0.826

Appendix Table A

(continued)

sample[1]	measured $^{204}Pb/^{206}Pb$	measured $^{207}Pb/^{206}Pb$	%	common ^{206}Pb	U (ppm)	Th/U	$^{206}Pb/^{238}U$ (Ma)[2]	err[3]	$^{207}Pb/^{206}Pb$ (Ma)[2]	err[3]	$^{207}Pb/^{235}U$ (%)[4]	err[3]	$^{206}Pb/^{238}U$ (%)[4]	err[3]
MR-08-71 (Ybg biotite meta-granite, porphyritic facies): medium- to coarse-grained, feldspar porphyritic biotite meta-monzogranite, Grassy Creek quadrangle; UTM: 464813 4052509														
MR71-13.1	0.000099	0.0793	0.166	153	0.71	1183	20	1145	23	2.16	2.1	0.201	1.7	0.834
MR71-14.1	0.000062	0.0785	0.105	176	0.68	1169	19	1138	20	2.13	2.0	0.199	1.7	0.861
MR71-15.1	0.000018	0.0783	0.031	241	0.68	1165	18	1148	16	2.13	1.8	0.198	1.6	0.901
MR71-16.1	0.000016	0.0796	0.028	455	1.04	1177	17	1182	10	2.19	1.6	0.200	1.5	0.948
MR71-17.1	0.000047	0.0791	0.079	139	0.51	1165	20	1159	21	2.14	2.1	0.198	1.8	0.853
MR71-18.1	0.000000	0.0799	0.000	198	0.88	1164	18	1194	14	2.18	1.8	0.198	1.6	0.915
MR71-19.1	-0.000027	0.0784	-0.045	61	0.38	1131	22	1167	27	2.09	2.4	0.192	2.0	0.829
MR-09-100 (Yfbl foliated biotite meta-leucogranite): medium- to coarse-grained, foliated biotite meta-leucogranite, Park quadrangle; UTM: 452051 4040285														
MR100-1.1	0.000276	0.0804	0.466	109	0.82	1115	21	1106	55	1.99	3.4	0.189	1.9	0.570
MR100-2.1	0.000034	0.0793	0.057	697	0.59	1158	13	1167	14	2.14	1.4	0.197	1.2	0.859
MR100-1.2	0.000016	0.0786	0.027	1426	0.05	1071	11	1156	8	1.96	1.2	0.182	1.1	0.933
MR100-3.1	0.000015	0.0785	0.025	1385	0.11	1080	11	1155	8	1.98	1.2	0.183	1.1	0.937
MR100-4.1	0.000079	0.0808	0.133	183	1.15	1175	17	1188	26	2.20	2.0	0.200	1.5	0.762
MR100-5.1	0.000036	0.0738	0.062	1035	0.09	937	10	1023	12	1.59	1.3	0.157	1.1	0.888
MR100-5.2	0.000118	0.0792	0.199	395	0.91	1162	15	1134	22	2.11	1.7	0.197	1.3	0.759
MR100-5.3	0.000046	0.0745	0.079	2631	0.27	1030	10	1037	6	1.77	1.1	0.173	1.1	0.957
MR100-6.1	0.000102	0.0768	0.172	1877	1.26	1045	11	1077	10	1.83	1.2	0.176	1.1	0.915
MR100-6.2	0.000100	0.0812	0.166	746	1.19	1090	12	1193	13	2.04	1.3	0.185	1.1	0.871
MR100-7.1	0.000124	0.0795	0.208	151	1.32	1180	18	1141	32	2.15	2.2	0.201	1.6	0.704
MR100-8.1	0.000042	0.0818	0.070	122	0.99	1147	20	1226	29	2.19	2.3	0.196	1.8	0.769
MR100-9.1	0.000017	0.0794	0.029	276	0.52	1156	15	1175	17	2.14	1.6	0.197	1.4	0.844
MR100-10.1	0.000033	0.0774	0.055	2709	0.35	1077	11	1119	6	1.93	1.1	0.182	1.1	0.960
MR100-10.2	0.000154	0.0820	0.258	110	0.93	1103	20	1193	42	2.06	2.9	0.187	1.9	0.658
MR100-11.1	0.000065	0.0794	0.109	1679	0.21	1135	12	1160	9	2.09	1.2	0.193	1.1	0.920
MR100-11.2	0.000102	0.0809	0.171	187	0.95	1202	19	1183	31	2.24	2.3	0.205	1.6	0.723
MR100-12.1	0.000092	0.0802	0.154	334	0.75	1148	15	1171	21	2.12	1.7	0.195	1.4	0.793
MR100-13.1	0.000030	0.0742	0.051	1583	0.19	1067	12	1035	10	1.83	1.2	0.180	1.1	0.911
MR100-14.1	0.000000	0.0810	0.000	161	0.96	1181	19	1221	22	2.25	2.0	0.202	1.7	0.826
MR100-15.1	0.000135	0.0809	0.227	280	0.64	1196	16	1172	25	2.22	1.9	0.204	1.4	0.745
MR100-16.1	0.000015	0.0806	0.025	345	0.64	1179	15	1207	16	2.23	1.6	0.201	1.3	0.856
MR100-19.1	-0.000002	0.0789	-0.003	2306	0.18	1178	12	1171	6	2.18	1.1	0.201	1.1	0.967
MR100-19.2	0.000434	0.0798	0.738	110	1.06	1245	103	1032	61	2.14	9.1	0.211	8.6	0.943
MR100-20.1	0.000175	0.0814	0.293	133	0.43	1205	20	1171	37	2.23	2.5	0.205	1.7	0.677
MR100-16.2	0.000070	0.0798	0.118	852	0.13	1180	12	1168	9	2.18	1.1	0.201	1.0	0.916
MR100-17.1	0.000028	0.0788	0.048	993	0.14	1181	12	1156	9	2.17	1.1	0.201	1.1	0.921

Appendix Table A

(continued)

sample[1]	measured $^{204}Pb/^{206}Pb$	measured $^{207}Pb/^{206}Pb$	%	common ^{206}Pb	U (ppm)	Th/U	$^{206}Pb/^{238}U$ (Ma)[2]	err[3]	$^{207}Pb/^{206}Pb$ (Ma)[2]	err[3]	$^{207}Pb/^{235}U$ (Ma)[4]	err[3]	$^{206}Pb/^{238}U$ (%)[4]	err[3]
MR-09-100 (Yfbl foliated biotite meta-leucogranite): medium- to coarse-grained, foliated biotite meta-leucogranite, Park quadrangle; UTM: 452051 4040285														
MR100-17.2	0.000015	0.0790	0.025	184	0.43	1195	14	1168	16	2.21	1.5	0.203	1.2	0.825
MR100-21.1	0.000018	0.0801	0.031	111	0.32	1225	15	1194	18	2.30	1.6	0.209	1.3	0.810
MR100-22.1	0.000103	0.0823	0.172	80	0.67	1183	16	1218	31	2.25	2.1	0.202	1.4	0.667
MR100-23.1	0.000381	0.0819	0.642	110	1.14	1219	15	1107	42	2.18	2.5	0.207	1.3	0.526
MR100-24.1	0.000013	0.0795	0.022	408	0.69	1251	13	1180	10	2.33	1.2	0.214	1.1	0.900
MR100-25.1	0.000078	0.0810	0.130	178	0.57	1201	14	1194	74	2.25	3.9	0.205	1.2	0.299
MR-08-84 (Ybm biotitic migmatite): medium- to coarse-grained, biotite meta-alkali feldspar granite (leucosome), Grassy Creek quadrangle; UTM: 465933 4042152														
MR84-1.1	0.000038	0.0812	0.064	1156	0.17	1236	13	1212	30	2.35	1.8	0.211	1.0	0.569
MR84-2.1	0.000094	0.0803	0.157	347	0.60	1191	13	1171	12	2.21	1.3	0.203	1.2	0.879
MR84-3.1	0.000022	0.0791	0.036	323	0.71	1152	13	1168	13	2.13	1.4	0.196	1.2	0.875
MR84-4.1	0.000005	0.0799	0.008	405	0.87	1187	13	1193	11	2.23	1.3	0.202	1.2	0.899
MR84-5.1	0.000054	0.0797	0.091	370	0.66	1183	14	1170	14	2.19	1.4	0.201	1.2	0.873
MR84-6.1	0.000137	0.0856	0.226	331	0.26	1359	16	1286	14	2.70	1.4	0.234	1.2	0.865
MR84-7.1	0.000106	0.0782	0.178	504	0.29	1207	13	1113	15	2.17	1.4	0.205	1.1	0.844
MR84-7.2	0.000084	0.0769	0.143	798	0.10	1180	13	1088	10	2.09	1.2	0.200	1.1	0.905
MR84-8.1	0.000151	0.0804	0.254	280	0.91	1141	14	1153	19	2.09	1.6	0.194	1.3	0.791
MR84-9.1	0.000161	0.0803	0.271	279	1.27	1205	14	1148	18	2.21	1.5	0.205	1.2	0.807
MR84-9.2	0.000669	0.0848	1.134	1740	0.09	1109	11	1075	13	1.94	1.2	0.187	1.0	0.844
MR84-10.1	0.000117	0.0811	0.196	332	1.64	1207	14	1182	87	2.25	4.6	0.206	1.2	0.273
MR84-11.1	0.000036	0.0836	0.059	567	0.43	1260	35	1272	10	2.48	2.9	0.216	2.9	0.985
MR84-12.1	0.000033	0.0844	0.054	551	0.44	1369	15	1290	10	2.73	1.2	0.236	1.1	0.904
MR84-13.1	0.000040	0.0851	0.066	834	0.40	1379	14	1304	7	2.77	1.1	0.238	1.1	0.947
MR84-14.1	0.000044	0.0781	0.074	779	0.08	1150	12	1133	42	2.08	2.4	0.195	1.1	0.464
MR84-15.1	0.000273	0.0878	0.452	1006	0.23	1342	14	1291	40	2.67	2.3	0.231	1.1	0.470
MR84-15.2	0.000062	0.0795	0.103	842	0.04	1207	36	1162	9	2.23	3.1	0.205	3.1	0.990
MR84-16.1	0.000046	0.0773	0.078	1006	0.22	1192	12	1111	8	2.14	1.1	0.202	1.1	0.939
MR84-17.1	0.000158	0.0815	0.264	305	0.59	1227	14	1180	16	2.29	1.4	0.209	1.2	0.830
MR84-18.1	0.000142	0.0763	0.241	816	0.04	1196	14	1050	17	2.07	1.5	0.202	1.2	0.815
MR84-19.1	0.000072	0.0861	0.119	856	0.55	1380	14	1317	8	2.79	1.2	0.238	1.1	0.933
MR84-20.1	0.000065	0.0835	0.108	832	0.31	1231	13	1259	8	2.40	1.2	0.211	1.1	0.934
MR84-21.1	0.000192	0.0854	0.319	826	0.41	1280	13	1262	10	2.50	1.2	0.219	1.1	0.905
MR84-22.1	0.000037	0.0790	0.061	1172	0.18	1232	13	1160	7	2.27	1.1	0.210	1.1	0.946
MR84-23.1	0.000051	0.0845	0.085	599	0.36	1326	14	1287	10	2.63	1.2	0.228	1.1	0.916
MR84-23.2	0.000011	0.0795	0.018	1324	0.19	1231	13	1182	7	2.30	1.1	0.210	1.1	0.955
MR84-24.1	0.000017	0.0781	0.029	1197	0.62	1144	12	1142	7	2.08	1.1	0.194	1.1	0.948

Appendix Table A

(continued)

sample[1]	measured $\frac{^{204}Pb}{^{206}Pb}$	measured $\frac{^{207}Pb}{^{206}Pb}$	%	common ^{206}Pb	U (ppm)	Th/U (Ma)	$\frac{^{206}Pb}{^{238}U}$[2] (Ma)	err[3] ^{206}Pb (Ma)	$\frac{^{207}Pb}{^{235}U}$[2] (Ma)	err[3]	$\frac{^{207}Pb}{^{238}U}$[4] (%)	err[3]	$\frac{^{206}Pb}{^{238}U}$[4] (%)	err[3]
MR-08-84 (Ybm biotitic migmatite): medium- to coarse-grained, biotite meta-alkali feldspar granite (leucosome), Grassy Creek quadrangle; UTM: 465933 4042152														
MR84-25.1	0.000176	0.0815	0.295	250	1.08	1183	14	1171	18	2.19	1.5	0.201	1.2	0.800
MR84-26.1	0.000142	0.0867	0.234	996	0.25	1332	14	1308	10	2.68	1.2	0.229	1.1	0.902
MR-10-124 (Yagn foliated amphibole gneiss): medium-grained, massive, amphibole meta-leucogranite (leucosome), Middle Fox Creek quadrangle; UTM: 471184 4053763														
MR10-124-1.1	0.000014	0.0801	0.024	536	0.62	1168	20	1195	18	2.19	2.0	0.199	1.8	0.887
MR10-124-1.2	0.000009	0.0797	0.015	423	0.55	1148	15	1187	20	2.14	1.7	0.195	1.4	0.797
MR10-124-2.1	-0.000016	0.0791	-0.027	242	0.77	1189	18	1180	27	2.21	2.1	0.202	1.6	0.746
MR10-124-3.1	0.000103	0.0805	0.173	137	1.18	1116	20	1174	38	2.07	2.7	0.189	1.9	0.704
MR10-124-4.1	0.000134	0.0753	0.228	147	0.88	1087	13	1024	40	1.85	2.3	0.183	1.2	0.517
MR10-124-4.2	0.000204	0.0785	0.345	733	0.20	1015	12	1086	26	1.79	1.8	0.171	1.2	0.680
MR10-124-5.1	0.000072	0.0805	0.120	105	0.90	1211	24	1184	42	2.26	2.9	0.206	2.0	0.683
MR10-124-6.1	0.000023	0.0753	0.039	174	1.28	1136	14	1069	35	1.99	2.2	0.192	1.3	0.598
MR10-124-6.2	0.000358	0.0792	0.609	1410	0.13	995	11	1045	26	1.71	1.7	0.167	1.1	0.664
MR10-124-7.1	0.000020	0.0797	0.033	385	0.37	1150	15	1183	22	2.14	1.8	0.196	1.4	0.780
MR10-124-8.1	-0.000073	0.0780	-0.123	207	1.19	1179	18	1173	31	2.19	2.2	0.201	1.6	0.723
MR10-124-9.1	0.000194	0.0805	0.326	243	0.95	976	15	1140	35	1.76	2.4	0.165	1.6	0.657
MR10-124-9.2	0.000000	0.0746	0.000	1270	0.22	1040	11	1058	13	1.80	1.3	0.175	1.1	0.871
MR10-124-10.1	0.000035	0.0797	0.059	229	1.31	1173	18	1178	30	2.18	2.2	0.200	1.6	0.716
MR10-124-11.1	0.000011	0.0801	0.018	196	1.20	1124	13	1195	31	2.11	2.0	0.191	1.2	0.610
MR-10-123 (Yagn foliated amphibole gneiss): medium-grained, amphibole-bearing granitic gneiss (melanosome), Middle Fox Creek quadrangle; UTM: 471181 4053763														
MR10-123-1.1	0.000123	0.0785	0.208	255	1.06	1127	15	1114	28	2.02	2.0	0.191	1.4	0.712
MR10-123-1.2	0.000365	0.0834	0.613	563	0.08	1224	15	1153	57	2.25	3.1	0.208	1.3	0.405
MR10-123-2.1	0.000023	0.0798	0.038	278	1.13	1155	15	1184	24	2.15	1.8	0.196	1.4	0.759
MR10-123-3.1	0.000032	0.0782	0.054	329	1.35	1225	16	1142	22	2.24	1.7	0.208	1.3	0.775
MR10-123-4.1	0.000002	0.0875	0.003	156	1.37	1440	22	1370	27	3.01	2.1	0.249	1.6	0.748
MR10-123-4.2	0.000071	0.0803	0.119	1671	0.12	1131	12	1179	11	2.10	1.2	0.192	1.1	0.885
MR10-123-5.1	-0.000035	0.0814	-0.059	308	1.44	1148	15	1243	21	2.21	1.7	0.196	1.4	0.780
MR10-123-6.1	0.000070	0.0806	0.118	239	1.34	1180	17	1186	56	2.20	3.2	0.201	1.4	0.452
MR10-123-7.1	-0.000011	0.0787	-0.019	564	1.77	1146	12	1170	16	2.12	1.3	0.195	1.1	0.785
MR10-123-8.1	0.000034	0.0823	0.057	409	0.56	1328	16	1241	18	2.57	1.6	0.228	1.3	0.808
MR10-123-8.2	0.000003	0.0784	0.005	1038	0.09	1190	13	1156	12	2.19	1.3	0.202	1.1	0.878
MR10-123-9.1	0.000031	0.0794	0.051	240	0.97	1153	16	1173	25	2.14	1.9	0.196	1.4	0.751
MR10-123-9.2	0.000026	0.0773	0.043	983	0.14	1158	13	1119	26	2.08	1.7	0.196	1.1	0.660
MR10-123-10.1	0.000024	0.0851	0.039	461	0.93	1260	23	1311	30	2.53	2.5	0.216	1.9	0.769
MR10-123-10.2	0.000002	0.0793	0.003	1012	0.02	1192	13	1180	12	2.22	1.3	0.203	1.1	0.880
MR10-123-11.1	0.000234	0.0870	0.388	497	0.61	1291	15	1287	25	2.56	1.8	0.222	1.2	0.700
MR10-123-12.1	0.000151	0.0812	0.254	474	1.62	1171	14	1174	25	2.17	1.8	0.199	1.3	0.699

Appendix Table A
(continued)

sample[1]	measured $^{204}Pb/^{206}Pb$	measured $^{207}Pb/^{206}Pb$	%	common ^{206}Pb	U (ppm)	Th/U	$^{206}Pb/^{238}U$ (Ma)[2]	err[3] ^{206}Pb (Ma)	^{207}Pb (Ma)[2]	err[3] ^{235}U	^{207}Pb (%)[4]	err[3] ^{238}U	^{206}Pb (%)[4]	err[3]
MR-10-123 (Yagn foliated amphibole gneiss): medium-grained, amphibole-bearing granitic gneiss (melanosome), Middle Fox Creek quadrangle; UTM: 471181 4053763														
MR10-123-13.1	0.000042	0.0849	0.069	278	0.87	1303	18	1301	22	2.60	1.8	0.224	1.4	0.777
MR10-123-14.1	0.000013	0.0801	0.022	511	1.50	1195	14	1196	18	2.25	1.5	0.204	1.2	0.812
MR10-123-16.1	-0.000026	0.0804	-0.044	251	1.06	1201	17	1216	25	2.28	1.9	0.205	1.4	0.749
MR10-123-17.1	-0.000020	0.0784	-0.034	233	1.20	1179	17	1163	26	2.17	1.9	0.200	1.5	0.744
MR10-123-18.1	0.000007	0.0788	0.012	1125	0.06	1164	19	1166	22	2.15	2.0	0.198	1.7	0.839
MR10-123-19.1	-0.000013	0.0851	-0.022	304	0.49	1298	17	1322	20	2.63	1.7	0.223	1.4	0.805
MR10-123-19.2	0.000012	0.0762	0.021	2547	0.12	947	11	1096	9	1.67	1.3	0.159	1.3	0.938
MR10-123-23.1	0.000060	0.0860	0.099	428	0.62	1281	16	1319	17	2.59	1.6	0.220	1.3	0.816
MR10-123-25.1	0.000020	0.0839	0.034	611	0.73	1305	15	1284	14	2.58	1.4	0.224	1.2	0.852
MR10-123-25.2	0.000050	0.0776	0.084	823	0.10	1149	13	1119	15	2.07	1.4	0.195	1.2	0.842
MR-08-70 (Yla layered amphibolite): fine-grained, lineated amphibolite (melanosome), Grassy Creek quadrangle; UTM: 464857 4052862														
MR70-1.1	0.000009	0.0792	0.015	969	1.26	1137	12	1175	8	2.11	1.1	0.193	1.1	0.940
MR70-2.1	0.000455	0.0747	0.787	2455	1.01	790	8	872	12	1.23	1.2	0.131	1.0	0.867
MR70-3.1	0.000224	0.0713	0.388	1597	0.47	802	8	870	11	1.25	1.2	0.133	1.1	0.894
MR70-4.1	0.000054	0.0776	0.090	1355	1.45	1090	12	1116	7	1.95	1.1	0.184	1.1	0.954
MR70-5.1	0.000439	0.0755	0.756	1814	0.25	767	8	906	15	1.21	1.3	0.127	1.0	0.828
MR70-6.1	0.000129	0.0789	0.218	182	0.29	1165	15	1122	21	2.10	1.7	0.198	1.3	0.780
MR70-6.2	0.000200	0.0811	0.335	681	1.16	1118	12	1155	13	2.05	1.3	0.190	1.1	0.854
MR70-6.3	0.000284	0.0714	0.493	2071	0.81	745	8	848	12	1.14	1.2	0.123	1.0	0.882
MR70-7.1	0.000253	0.0796	0.427	583	0.68	801	9	1095	19	1.40	1.5	0.134	1.1	0.759
MR70-8.1	0.000183	0.0800	0.308	157	0.70	1075	14	1133	24	1.94	1.8	0.182	1.4	0.741
MR70-8.2	0.000020	0.0778	0.033	1133	0.50	1128	12	1134	7	2.04	1.1	0.191	1.1	0.946
MR70-9.1	0.000079	0.0794	0.133	361	0.95	1083	12	1155	13	1.98	1.4	0.183	1.2	0.869
MR70-10.1	0.000041	0.0686	0.070	2345	5.40	1011	10	869	5	1.58	1.1	0.169	1.0	0.977
MR70-11.1	0.000035	0.0782	0.059	839	1.33	1165	12	1139	8	2.12	1.2	0.198	1.1	0.932
MR70-12.1	0.000048	0.0791	0.080	310	0.28	1119	13	1157	14	2.05	1.4	0.190	1.2	0.860
MR70-13.1	0.000164	0.0760	0.280	812	0.58	915	10	1031	13	1.56	1.3	0.153	1.1	0.863
MR70-14.1	0.000086	0.0795	0.144	221	0.10	1165	14	1155	18	2.14	1.6	0.198	1.3	0.815
MR70-15.1	0.000055	0.0781	0.093	1052	0.92	1146	12	1129	8	2.07	1.2	0.194	1.1	0.934
MR70-16.1	0.000108	0.0790	0.182	479	1.12	1121	12	1134	13	2.03	1.3	0.190	1.1	0.868
MR70-17.1	0.000042	0.0792	0.070	725	1.06	1183	13	1162	9	2.18	1.2	0.201	1.1	0.918
MR70-18.1	0.000192	0.0775	0.326	354	0.16	1031	41	1063	19	1.79	4.2	0.174	4.1	0.975
MR70-19.1	0.000104	0.0769	0.176	364	0.41	1098	13	1080	19	1.93	1.5	0.186	1.2	0.779
MR70-20.1	0.000106	0.0791	0.178	209	0.66	1150	15	1136	20	2.09	1.7	0.195	1.4	0.801
MR70-21.1	0.000052	0.0790	0.088	729	1.23	1193	12	1153	8	2.19	1.1	0.203	1.1	0.937
MR70-22.1	0.000997	0.0921	1.676	728	0.89	1116	11	1145	21	2.03	1.5	0.189	1.1	0.714

Appendix Table A

(continued)

sample[1]	measured $^{204}Pb/^{206}Pb$	measured $^{207}Pb/^{206}Pb$	%	common ^{206}Pb	U (ppm)	Th/U	$^{206}Pb/^{238}U$ (Ma)[2]	err[3]	$^{207}Pb/^{206}Pb$ (Ma)[2]	err[3]	$^{207}Pb/^{235}U$ (Ma)[4]	err[3]	$^{206}Pb/^{238}U$ (Ma)[4]	err[3]
MR-08-70 (Yla layered amphibolite): fine-grained, lineated amphibolite (melanosome), Grassy Creek quadrangle; UTM: 464857 4052862														
MR70-23.1	0.000043	0.0767	0.073	881	0.72	1040	11	1098	7	1.84	1.1	0.176	1.1	0.948
MR70-23.2	0.000123	0.0802	0.207	335	1.02	1123	12	1159	13	2.06	1.3	0.191	1.1	0.863
MR70-24.1	0.000041	0.0788	0.068	800	0.12	1116	11	1152	7	2.04	1.1	0.189	1.1	0.942
MR70-25.1	0.000082	0.0769	0.139	970	0.80	1036	10	1087	8	1.82	1.1	0.175	1.0	0.936
MR70-26.1	0.000088	0.0783	0.148	947	0.95	1112	11	1122	26	2.00	1.7	0.188	1.1	0.633
MR70-27.1	0.000126	0.0796	0.212	743	1.10	1102	12	1142	10	2.00	1.2	0.187	1.1	0.916
MR70-27.2	0.000277	0.0732	0.477	1209	0.69	818	8	907	37	1.30	2.1	0.136	1.0	0.506
MR70-28.1	0.000150	0.0764	0.254	1006	0.83	962	17	1050	9	1.65	1.9	0.161	1.9	0.972
MR70-29.1	0.001400	0.0921	2.393	1976	0.92	917	24	988	73	1.52	4.5	0.153	2.8	0.610
MR-12-233 (Ymg migmatitic granofels): fine-grained, equigranular micaceous granofels, Mouth of Wilson quadrangle; UTM: 472528 4048620														
MR12-233A-1.1	0.000137	0.0757	0.234	1009	0.07	1016	14	1035	22	1.74	1.8	0.171	1.4	0.787
MR12-233A-2.1	0.000146	0.0757	0.248	1127	0.02	1015	14	1032	21	1.73	1.8	0.171	1.4	0.807
MR12-233A-3.1	0.000145	0.0773	0.246	1202	0.01	1048	14	1074	23	1.83	1.8	0.177	1.4	0.780
MR12-233A-4.1	0.000137	0.0756	0.233	753	0.08	1004	14	1033	29	1.71	2.1	0.169	1.5	0.711
MR12-233A-5.1	0.000080	0.0752	0.136	1224	0.01	1031	14	1042	15	1.77	1.6	0.174	1.4	0.880
MR12-233A-6.1	0.000054	0.0754	0.092	1209	0.01	1039	14	1057	11	1.80	1.5	0.175	1.4	0.929
MR12-233A-7.1	0.000231	0.0769	0.394	1159	0.03	1024	14	1030	42	1.75	2.5	0.172	1.4	0.567
MR12-233A-8.1	0.000171	0.0771	0.290	1150	0.05	1014	14	1058	20	1.76	1.7	0.171	1.4	0.819
MR12-233A-9.1	0.000170	0.0752	0.289	1332	0.02	1026	14	1008	30	1.73	2.1	0.172	1.4	0.698
MR12-233A-10.1	0.000096	0.0758	0.162	1596	0.01	1031	14	1052	8	1.78	1.5	0.174	1.4	0.962
MR12-233A-11.1	0.000321	0.0776	0.547	1033	0.05	1032	14	1014	40	1.75	2.4	0.174	1.5	0.595
MR12-233A-12.1	0.000191	0.0811	0.321	1771	0.00	1077	13	1157	31	1.97	2.0	0.182	1.3	0.625
MR12-233A-13.1	0.000179	0.0767	0.304	1077	0.05	1011	14	1047	41	1.74	2.5	0.170	1.5	0.583
MR12-233A-14.1	0.000209	0.0787	0.354	1158	0.01	1066	15	1088	43	1.88	2.6	0.180	1.4	0.559
MR12-233A-15.1	0.000259	0.0784	0.439	1071	0.02	1026	14	1062	54	1.78	3.1	0.173	1.5	0.475
MR12-233A-100.1	0.000311	0.0888	0.515	438	0.92	1240	19	1301	65	2.47	3.7	0.213	1.6	0.421
MR12-233A-101.1	0.000156	0.0844	0.259	754	0.39	1155	16	1251	22	2.24	1.9	0.197	1.5	0.791
MR12-233A-102.1	0.000307	0.0887	0.508	288	0.49	1215	27	1300	73	2.42	4.4	0.208	2.3	0.524
MR12-233A-103.1	0.000695	0.0935	1.150	230	0.70	1216	20	1286	101	2.41	5.5	0.208	1.7	0.315
MR12-233A-104.1	0.000813	0.0888	1.370	274	0.80	960	13	1129	109	1.72	5.7	0.162	1.5	0.259
MR12-233A-106.1	0.000717	0.0953	1.182	141	0.52	1300	22	1320	78	2.63	4.4	0.224	1.7	0.393
MR12-233A-107.1	0.000842	0.0965	1.390	88	0.50	1177	20	1309	52	2.35	3.2	0.202	1.8	0.557
MR12-233A-108.1	0.000675	0.0891	1.130	218	1.31	1151	25	1186	35	2.15	2.9	0.196	2.3	0.791
MR12-233A-109.1	0.000347	0.0848	0.581	361	0.52	1235	33	1195	37	2.32	3.3	0.211	2.8	0.831
MR12-233A-110.1	0.000501	0.0898	0.831	235	0.73	1255	21	1264	42	2.45	2.8	0.215	1.7	0.625
MR12-233A-110.1	0.000501	0.0898	0.831	235	0.73	1255	21	1264	42	2.45	2.8	0.215	1.7	0.625

Appendix Table A
(continued)

sample[1]	measured $^{204}Pb/^{206}Pb$	measured $^{207}Pb/^{206}Pb$	%	common ^{206}Pb	U (ppm)	Th/U	$^{206}Pb/^{238}U$ (Ma)[2]	err[3] (Ma)	$^{207}Pb/^{206}Pb$ (Ma)[2]	err[3] ^{235}U	$^{207}Pb/^{206}Pb$ (%)[4]	err[3] ^{238}U	$^{206}Pb/^{238}U$ (%)[4]	err[3]
MR-12-233 (Ymg migmatitic granofels): fine-grained, equigranular micaceous granofels, Mouth of Wilson quadrangle; UTM: 472528 4048620														
MR12-233A-111.1	0.001128	0.0981	1.875	224	0.80	1287	22	1250	123	2.50	6.5	0.220	1.8	0.273
MR12-233A-112.1	0.000300	0.0825	0.503	684	0.34	1128	22	1152	22	2.07	2.3	0.192	2.0	0.880
MR12-233A-113.1	0.000506	0.0894	0.840	286	0.42	1260	21	1252	48	2.45	3.0	0.216	1.7	0.564
MR12-233A-114.1	0.000270	0.0892	0.445	478	0.59	1301	21	1324	15	2.64	1.9	0.224	1.7	0.912
MR12-233A-115.1	0.002341	0.1137	3.906	399	4.37	540	92	1214	463	1.00	29.3	0.090	17.4	0.593
MR12-233A-116.1	0.000587	0.0970	0.960	317	0.61	1300	27	1400	73	2.75	4.4	0.225	2.2	0.502
MR12-233A-117.1	0.000502	0.0868	0.840	292	0.54	1163	19	1190	88	2.18	4.8	0.198	1.7	0.359
MR12-233A-118.1	0.000166	0.1063	0.262	1064	0.77	1636	26	1696	10	4.16	1.7	0.290	1.6	0.952
MR12-233A-119.1	0.001203	0.1031	1.978	156	0.69	1276	28	1345	124	2.61	6.8	0.220	2.3	0.335
MR12-233A-120.1	0.000749	0.0946	1.239	149	0.52	1242	25	1294	135	2.47	7.3	0.213	2.1	0.290
MR12-233A-121.1	0.000337	0.0886	0.557	461	0.81	1267	20	1289	64	2.51	3.7	0.217	1.7	0.459
MR12-233A-122.1	0.000432	0.0899	0.715	233	0.49	1250	21	1289	84	2.48	4.7	0.214	1.7	0.370
MR12-233A-123.1	0.000444	0.0901	0.735	263	0.57	1254	21	1288	74	2.49	4.2	0.215	1.7	0.411
MR12-233A-124.1	0.000639	0.0936	1.055	238	0.64	1238	20	1306	72	2.48	4.1	0.212	1.7	0.423
MR12-233A-125.1	0.000145	0.0842	0.241	531	1.12	1173	19	1249	34	2.27	2.4	0.200	1.7	0.698
MR12-233A-126.1	0.000388	0.0821	0.655	118	3.04	1896	60	1111	95	3.44	5.7	0.326	3.2	0.555
MR12-233A-127.1	0.000284	0.0876	0.471	283	0.80	1273	30	1282	47	2.52	3.4	0.218	2.4	0.708
MR12-233A-128.1	0.001156	0.0987	1.920	116	0.61	1275	51	1255	80	2.48	5.8	0.219	4.2	0.712
MR12-233A-129.1	0.001870	0.1096	3.100	450	0.73	1210	19	1275	38	2.38	2.6	0.207	1.7	0.655
MR12-233A-130.1	0.000877	0.0914	1.471	246	0.39	1202	25	1170	132	2.23	7.0	0.205	2.2	0.307
MR12-233A-131.1	0.000284	0.0892	0.468	395	0.84	1279	21	1322	45	2.59	2.9	0.220	1.7	0.582
MR12-233A-132.1	0.000339	0.0884	0.561	484	1.15	1276	21	1285	51	2.53	3.1	0.219	1.7	0.533
MR12-233A-133.1	0.000712	0.0880	1.196	348	0.71	1284	64	1145	99	2.35	7.2	0.219	5.2	0.719
MR12-233A-134.1	0.000634	0.0909	1.054	276	0.63	1222	26	1244	111	2.36	6.1	0.209	2.2	0.364
MR12-233A-135.1	0.000537	0.0924	0.886	317	0.55	1295	21	1312	41	2.61	2.7	0.223	1.7	0.633
MR12-233A-136.1	0.000749	0.0883	1.261	203	0.52	1159	42	1138	80	2.11	5.5	0.197	3.8	0.685
MR12-233A-137.1	0.000809	0.0946	1.341	255	0.53	1204	26	1275	79	2.37	4.6	0.206	2.2	0.486
MR12-233A-138.1	0.000709	0.0949	1.170	278	0.71	1201	20	1314	68	2.41	3.9	0.206	1.7	0.436
MR12-233A-139.1	0.001330	0.0987	2.225	177	0.52	1170	30	1195	216	2.20	11.3	0.199	2.7	0.241
MR12-233A-140.1	0.001598	0.1036	2.663	149	0.46	1174	21	1224	274	2.24	14.1	0.200	2.1	0.149
MR12-233A-141.1	0.000702	0.0940	1.161	401	0.44	1272	21	1296	99	2.53	5.4	0.218	1.7	0.320
MR12-233A-142.1	0.001164	0.0966	1.945	308	0.44	1150	19	1200	104	2.16	5.6	0.196	1.8	0.317
MR12-233A-143.1	0.001181	0.0987	1.963	201	0.68	1179	21	1248	183	2.28	9.5	0.201	1.9	0.199
MR12-233A-144.1	0.000595	0.0949	0.978	236	0.71	1306	25	1350	107	2.69	5.9	0.225	2.0	0.341
MR12-233A-145.1	0.000989	0.0907	1.669	298	0.51	1198	28	1113	108	2.15	5.9	0.203	2.4	0.412
MR12-233A-146.1	0.000700	0.0938	1.158	248	0.63	1185	25	1291	116	2.35	6.3	0.203	2.2	0.348

Appendix Table A

(continued)

sample[1]	measured $^{204}Pb/^{206}Pb$	measured $^{207}Pb/^{206}Pb$	%	common ^{206}Pb	U (ppm)	Th/U	$^{206}Pb/^{238}U$ (Ma)[2]	err[3]	$^{207}Pb/^{206}Pb$ (Ma)[2]	err[3]	$^{207}Pb/^{235}U$ (Ma)[4]	err[3]	$^{206}Pb/^{238}U$ (Ma)[4]	err[3]
MR-12-233 (Ymg migmatitic granofels): fine-grained, equigranular micaceous granofels, Mouth of Wilson quadrangle; UTM: 472528 4048620														
MR12-233A-147.1	0.000615	0.0945	1.012	222	0.73	1292	22	1336	42	2.64	2.8	0.222	1.7	0.623
MR12-233A-148.1	0.000555	0.0870	0.929	258	0.50	1167	19	1176	127	2.17	6.6	0.199	1.8	0.267
MR12-233A-149.1	0.000565	0.0909	0.938	373	0.71	1236	20	1269	82	2.42	4.5	0.212	1.7	0.381
MR12-233A-150.1	0.000379	0.0858	0.632	490	0.55	1200	23	1208	37	2.27	2.7	0.205	2.0	0.722
MR12-233A-151.1	0.000718	0.0946	1.187	264	0.76	1213	26	1304	103	2.42	5.8	0.208	2.2	0.383
MR12-233A-152.1	0.001618	0.1080	2.668	271	0.72	1293	22	1321	145	2.61	7.7	0.222	1.8	0.233
MR12-233A-153.1	0.000932	0.0939	1.554	239	0.53	1267	41	1216	72	2.41	5.0	0.217	3.3	0.672
MR12-233A-154.1	0.000640	0.0891	1.069	420	0.55	1167	19	1199	78	2.19	4.3	0.199	1.7	0.397
MR-09-104 (Ylg layered granofels): medium-grained, foliated amphibole + biotite granofels, Park quadrangle; UTM: 451392 4040775														
MR09-104-1.1	0.000045	0.1067	0.541	445	0.21	1660.4	13.1	1733	9	4.32	1.0	0.295	0.8	0.848
MR09-104-2.1	0.000150	0.1058	2.239	333	0.65	1353.9	11.3	1692	13	3.41	1.1	0.238	0.9	0.776
MR09-104-3.1	0.000022	0.0746	0.120	745	0.26	1029.3	7.8	1048	11	1.77	1.0	0.173	0.8	0.812
MR09-104-4.1	0.000039	0.0748	0.163	255	0.40	1024.9	8.8	1047	23	1.76	1.4	0.172	0.9	0.621
MR09-104-5.1	-0.000040	0.0747	0.043	236	0.42	1049.3	9.1	1075	23	1.84	1.5	0.177	0.9	0.621
MR09-104-6.1	0.000122	0.1093	0.458	305	0.61	1719.0	14.1	1759	12	4.55	1.1	0.306	0.8	0.798
MR09-104-7.1	0.000060	0.0811	0.391	178	0.09	1141.7	10.3	1203	24	2.15	1.5	0.194	0.9	0.613
MR09-104-8.1	0.000205	0.0853	0.848	891	0.53	1151.6	8.7	1256	17	2.23	1.2	0.197	0.8	0.668
MR09-104-9.1	0.000063	0.0749	0.079	172	0.43	1048.7	9.7	1042	25	1.80	1.6	0.177	1.0	0.608
MR09-104-10.1	0.000506	0.0837	0.391	63	0.44	1207.1	15.7	1109	82	2.16	4.3	0.205	1.4	0.323
MR09-104-11.1	0.000035	0.0818	0.490	377	0.37	1139.2	9.0	1229	15	2.18	1.1	0.194	0.8	0.740
MR09-104-12.1	0.000160	0.0790	0.507	148	0.31	1062.5	9.8	1115	35	1.90	2.0	0.180	1.0	0.480
MR09-104-13.1	0.000108	0.0859	0.122	354	0.42	1311.5	10.5	1301	16	2.62	1.2	0.225	0.8	0.702
MR09-104-14.1	0.000277	0.0905	1.573	546	0.73	1128.7	22.0	1353	75	2.31	4.4	0.193	2.0	0.452
MR09-104-15.1	0.000012	0.1065	-0.084	342	0.74	1753.1	14.2	1738	9	4.58	1.0	0.312	0.8	0.866
MR09-104-16.1	0.000041	0.0781	0.237	869	0.03	1098.2	8.4	1135	10	1.99	0.9	0.186	0.8	0.841
MR09-104-17.1	0.000230	0.0813	0.419	94	0.39	1141.7	12.1	1148	62	2.09	3.3	0.194	1.1	0.340
MR09-104-18.1	0.000158	0.1055	0.597	166	0.75	1630.3	14.8	1685	18	4.11	1.4	0.289	0.9	0.690
MR09-104-19.1	0.000478	0.0804	0.963	59	0.36	995.4	12.0	1030	131	1.70	6.6	0.167	1.4	0.207
MR09-104-20.1	0.000364	0.0865	1.197	1244	0.51	1105.7	9.9	1229	35	2.11	2.0	0.188	0.9	0.462
MR09-104-21.1	0.000071	0.0855	0.491	507	0.58	1229.4	9.5	1304	13	2.46	1.0	0.211	0.8	0.765
MR09-104-22.1	0.000088	0.0859	0.042	278	0.91	1326.9	11.0	1307	19	2.66	1.3	0.228	0.9	0.662
MR09-104-23.1	0.000016	0.0849	0.250	1238	0.65	1263.2	9.3	1307	7	2.53	0.8	0.217	0.8	0.915
MR09-104-24.1	0.000063	0.0857	0.432	515	0.68	1245.5	9.6	1310	13	2.50	1.0	0.214	0.8	0.772
MR09-104-25.1	0.000794	0.0960	1.446	448	0.75	1285.3	10.4	1311	59	2.58	3.2	0.221	0.8	0.265
MR09-104-26.1	0.000062	0.0867	0.319	462	0.96	1292.0	10.0	1334	12	2.63	1.0	0.222	0.8	0.792
MR09-104-27.1	0.000080	0.0866	0.317	330	0.54	1289.5	10.4	1325	16	2.61	1.2	0.222	0.8	0.720

Appendix Table A
(continued)

sample[1]	measured $^{204}Pb/^{206}Pb$	measured $^{207}Pb/^{206}Pb$	%	common ^{206}Pb	U (ppm)	Th/U	$^{206}Pb/^{238}U$ (Ma)[2]	err[3] ^{206}Pb (Ma)	^{207}Pb (Ma)[2]	err[3] ^{235}U	^{207}Pb (%)[4]	err[3] ^{238}U	^{206}Pb (%)[4]	err[3]
MR-09-104 (Ylg layered granofels): medium-grained, foliated amphibole + biotite granofels, Park quadrangle; UTM: 451392 4040775														
MR09-104-28.1	0.000012	0.0817	0.521	333	0.62	1128.8	15.2	1234	14	2.16	1.6	0.192	1.4	0.895
MR09-104-29.1	0.000077	0.0848	0.018	203	0.89	1308.0	11.4	1286	27	2.59	1.7	0.225	0.9	0.544
MR09-104-30.1	0.000074	0.0761	0.283	304	0.69	1035.3	8.6	1071	19	1.81	1.3	0.174	0.9	0.671
MR09-104-31.1	0.000812	0.0844	0.402	21	0.86	1222.2	38.3	1010	217	2.08	11.2	0.207	3.4	0.302
MR09-104-33.1	0.000085	0.0980	0.239	89	0.69	1546.7	17.6	1564	26	3.62	1.8	0.271	1.2	0.649
MR09-104-34.1	0.000006	0.0869	0.300	359	0.64	1299.7	10.8	1356	13	2.68	1.1	0.224	0.9	0.791
MR09-104-35.1	0.000034	0.0859	0.288	153	0.34	1279.4	12.6	1325	21	2.59	1.5	0.220	1.0	0.687
MR09-104-36.1	-0.000020	0.0758	0.171	404	0.34	1051.1	8.7	1097	16	1.86	1.2	0.177	0.9	0.738
MR09-104-37.1	0.000158	0.0995	1.707	312	0.46	1314.2	11.4	1573	20	3.08	1.4	0.229	0.9	0.642
MR09-104-38.1	0.000069	0.0870	0.188	409	0.83	1323.9	11.3	1338	16	2.71	1.2	0.228	0.9	0.726
MR09-104-39.1	0.000254	0.0844	0.450	137	0.37	1211.6	12.3	1217	42	2.30	2.4	0.207	1.1	0.450
MR09-104-40.1	0.000202	0.0855	0.100	157	0.70	1307.0	14.1	1261	33	2.55	2.0	0.224	1.1	0.554
MR09-104-41.1	0.000017	0.0867	0.185	270	0.74	1318.6	11.6	1349	16	2.71	1.2	0.227	0.9	0.745
MR09-104-42.1	0.000010	0.0863	0.102	203	0.39	1324.7	13.3	1341	18	2.71	1.4	0.228	1.0	0.749
MR09-104-43.1	0.000078	0.0880	0.361	688	0.63	1314.1	10.5	1359	13	2.72	1.1	0.227	0.8	0.781
MR09-104-44.1	0.000346	0.0834	0.263	121	0.97	1224.7	14.3	1159	53	2.26	2.9	0.209	1.2	0.416
MR09-104-45.1	-0.000035	0.1007	-0.092	129	0.27	1651.9	17.0	1646	18	4.07	1.4	0.292	1.1	0.728
MR09-104-46.1	0.000035	0.0842	0.414	519	0.15	1215.3	10.0	1287	15	2.40	1.2	0.208	0.9	0.742
MR09-104-47.1	0.000056	0.0827	0.302	288	0.95	1201.2	10.4	1244	21	2.32	1.4	0.205	0.9	0.639
MR09-104-48.1	0.000105	0.1043	0.493	213	0.62	1625.1	14.8	1677	16	4.08	1.3	0.288	0.9	0.726
MR09-104-49.1	0.000026	0.1064	0.702	214	0.89	1630.8	14.8	1733	13	4.24	1.2	0.290	0.9	0.790
MR09-104-50.1	0.000076	0.0834	0.648	226	0.50	1145.9	11.1	1254	22	2.22	1.5	0.196	1.0	0.672
MR09-104-53.1	0.000036	0.0742	-0.054	212	0.41	1059.6	9.9	1033	23	1.81	1.5	0.178	1.0	0.644
MR09-104-54.1	0.000064	0.0747	0.281	222	0.29	997.1	9.7	1037	27	1.71	1.7	0.168	1.0	0.600
MR09-104-55.1	0.000301	0.0732	-0.267	161	0.27	1079.5	10.7	894	56	1.72	2.9	0.181	1.0	0.358
MR09-104-56.1	0.000061	0.0764	0.242	183	0.36	1052.0	10.9	1083	26	1.85	1.7	0.178	1.1	0.638
MR09-104-57.1	0.000061	0.0764	0.314	253	0.50	1034.2	13.5	1082	24	1.82	1.8	0.174	1.3	0.747
MR09-104-58.1	0.000000	0.0748	0.311	156	0.14	992.2	9.9	1064	24	1.72	1.6	0.167	1.0	0.657
MR09-104-58.2	0.000295	0.0763	0.342	185	0.40	1026.5	9.9	989	44	1.71	2.4	0.172	1.0	0.427
MR-08-83B (Ybm biotite schist): fine-grained biotite schist, Grassy Creek quadrangle; UTM: 465933 4042152														
MR08-083B-1.1	0.000471	0.0922	1.643	517	0.61	1156.7	9.3	1330	19	2.34	1.3	0.198	0.8	0.652
MR08-083B-2.1	0.000015	0.0744	0.083	1508	0.19	1033.1	7.5	1046	8	1.78	0.8	0.174	0.8	0.894
MR08-083B-3.1	0.000040	0.0747	0.229	1166	0.20	1008.2	7.5	1045	11	1.73	0.9	0.170	0.8	0.818
MR08-083B-4.1	0.000417	0.0738	-0.022	121	0.95	1040.5	11.1	862	60	1.63	3.1	0.174	1.1	0.364
MR08-083B-5.1	0.000015	0.0723	-0.152	80	0.84	1029.7	11.5	988	31	1.72	1.9	0.173	1.1	0.605
MR08-083B-6.1	0.000144	0.0743	0.064	211	0.86	1035.4	9.1	993	42	1.73	2.2	0.174	0.9	0.412

Appendix Table A

(continued)

sample[1]	measured $^{204}Pb/^{206}Pb$	measured $^{207}Pb/^{206}Pb$	%	common ^{206}Pb	U (ppm)	Th/U (Ma)	$^{206}Pb/^{238}U$ (Ma)[2]	err[3] ^{206}Pb (Ma)	^{207}Pb[2] (Ma)	err[3] ^{235}U	^{207}Pb[4] (%)	err[3] ^{238}U	^{206}Pb[4] (%)	err[3]
MR-08-83B (Ybm biotite schist): fine-grained biotite schist, Grassy Creek quadrangle; UTM: 465933 4042152														
MR08-083B-8.1	0.000427	0.0754	0.284	157	1.50	1014.1	10.5	907	71	1.62	3.6	0.170	1.1	0.308
MR08-083B-106.1	0.000017	0.0753	0.238	2480	0.12	1022.2	7.3	1070	6	1.78	0.8	0.172	0.7	0.917
MR08-083B-105.1	0.000009	0.0750	0.147	2456	0.12	1035.5	7.5	1065	6	1.80	0.8	0.174	0.8	0.935
MR08-083B-104.1	0.000019	0.0798	0.407	1558	0.05	1105.5	8.1	1186	7	2.06	0.8	0.188	0.8	0.911
MR08-083B-103.1	0.000002	0.0749	0.033	3102	0.11	1058.1	7.6	1065	5	1.84	0.8	0.178	0.7	0.946
MR08-083B-102.1	0.000016	0.0749	0.122	903	0.26	1037.9	8.0	1060	11	1.80	1.0	0.175	0.8	0.822
MR08-083B-101.1	0.000060	0.0744	0.296	866	0.36	983.0	7.4	1028	12	1.67	1.0	0.165	0.8	0.789
MR08-083B-13.1	0.000088	0.0752	0.202	180	1.38	1028.8	10.3	1041	36	1.77	2.1	0.173	1.0	0.504
MR08-083B-9.1	0.000309	0.0540	0.140	530	0.44	325.1	2.8	171	78	0.35	3.5	0.051	0.9	0.258
MR08-083B-109.1	0.000007	0.0742	0.092	2559	0.12	1025.7	7.4	1044	6	1.76	0.8	0.173	0.8	0.933
MR08-083B-110.1	0.000004	0.0755	0.141	2289	0.12	1048.9	7.6	1079	7	1.84	0.8	0.177	0.8	0.908
MR08-083B-108.1	0.000004	0.0745	0.245	1915	0.14	999.6	7.3	1054	6	1.73	0.8	0.168	0.8	0.921
MR08-083B-18.1	0.000327	0.0747	0.141	131	0.92	1029.6	10.4	930	52	1.67	2.7	0.172	1.1	0.390
MR08-083B-19.1	0.000141	0.0742	0.166	175	1.08	1008.4	9.4	991	39	1.68	2.2	0.169	1.0	0.453
MR08-083B-21.1	0.000124	0.0757	0.192	212	1.64	1044.9	9.3	1041	26	1.79	1.6	0.176	0.9	0.578
MR08-083B-22.1	0.000216	0.0754	0.132	144	1.16	1048.4	10.2	994	49	1.76	2.6	0.176	1.0	0.392

[1] Prefix "m" for monazite, analyzed on SHRIMP II, Research School of Earth Sciences, Australian National University. All zircon samples analyzed on USGS/Stanford SHRIMP-RG, Stanford University.

[2] 206Pb/238U and 207Pb/206Pb ages corrected for common Pb using the 204Pb-correction method. Decay constants from Steiger and Jäger (1977).

[3] 1-sigma errors.

[4] Radiogenic ratios, corrected for common Pb using the 204Pb-correction method, based on the Stacey and Kramers (1975) model.

[5] All coordinates refer to UTM Grid Zone 17, NAD27.

Appendix Table B

Shrimp U-Th-Pb data for titanite from Mesoproterozoic rocks, Mount Rogers area, Virginia

sample[1]	measured $\frac{^{204}Pb}{^{206}Pb}$	measured $\frac{^{207}Pb}{^{206}Pb}$	% common ^{206}Pb	U (ppm)	$\frac{Th}{U}$	$\frac{^{206}Pb}{^{238}U}$[1] (Ma)	err[2] (Ma)	$\frac{^{238}U}{^{206}Pb}$[3]	err[2] (%)	$\frac{^{207}Pb}{^{206}Pb}$[3]	err[2] (%)
MR-08-66 (Ybg biotite meta-granite, medium-coarse facies): medium-grained, biotite meta-monzogranite, Grassy Creek quadrangle; UTM: 462483 4052445											
MR66-1.1	0.000380	0.0778	0.76	315	0.61	973	22	6.09	2.4	0.0778	0.5
MR66-1.2	0.000484	0.0813	1.08	137	2.69	993	24	5.94	2.6	0.0813	0.6
MR66-2.1	0.001438	0.0928	2.28	63	3.63	1032	31	5.63	3.1	0.0928	1.1
MR66-2.2	0.001897	0.0974	3.14	146	1.41	963	24	6.01	2.6	0.0974	0.7
MR66-3.1	0.001095	0.0893	2.17	84	2.19	963	26	6.07	2.8	0.0893	2.1
MR66-4.1	0.002663	0.0982	3.09	48	1.57	995	32	5.81	3.3	0.0982	1.2
MR66-5.1	0.000808	0.0859	1.39	118	3.63	1046	32	5.60	3.2	0.0859	1.0
MR66-6.1	0.001174	0.0883	1.91	133	2.14	995	31	5.88	3.3	0.0883	2.6
MR66-6.2	0.000934	0.0881	2.02	104	4.04	964	33	6.08	3.5	0.0881	1.2
MR66-7.1	0.001071	0.0942	2.09	76	5.81	1110	38	5.21	3.6	0.0942	1.1
MR66-7.2	0.001247	0.0940	2.50	111	2.88	1017	34	5.71	3.4	0.0940	2.0
MR66-8.1	0.000376	0.0796	0.63	335	0.62	1049	26	5.62	2.5	0.0796	0.6
MR66-8.2	0.002638	0.1137	4.50	356	2.07	1094	27	5.17	2.6	0.1137	1.5
MR66-9.1	0.000333	0.0791	0.68	243	2.21	1023	26	5.78	2.7	0.0791	0.7
MR66-9.2	0.001413	0.0940	1.40	325	1.81	1248	32	4.62	2.7	0.0940	1.3
MR66-9.3	0.001906	0.1024	3.29	97	1.79	1064	36	5.39	3.5	0.1024	1.1
MR66-10.1	0.000661	0.0879	1.65	160	1.37	1043	30	5.60	3.0	0.0879	0.9
MR66-10.2	0.001451	0.0956	2.90	97	2.37	969	34	5.98	3.7	0.0956	1.2
MR66-10.3	0.001441	0.1016	3.37	163	2.24	1024	30	5.61	3.1	0.1016	0.9
MR-08-70 (Yla layered amphibolite): fine-grained, lineated amphibolite (melanosome), Grassy Creek quadrangle; UTM: 464857 4052862											
MR70-1.1	0.001250	0.0899	2.06	79	2.16	1004	30	5.81	3.1	0.0899	1.2
MR70-2.1	0.001779	0.1120	4.55	31	6.43	1037	39	5.47	3.9	0.1120	3.1
MR70-3.1	0.002259	0.1019	3.26	45	5.40	1058	51	5.43	5.0	0.1019	1.7
MR70-3.2	0.000720	0.0889	2.14	92	2.65	959	34	6.10	3.6	0.0889	1.2
MR70-4.1	0.001854	0.1037	3.91	52	5.01	961	38	5.98	4.1	0.1037	3.7
MR70-5.1	0.000729	0.0880	1.87	144	2.22	998	29	5.86	3.0	0.0880	3.1
MR70-5.2	0.003728	0.1289	6.32	36	1.44	1091	58	5.08	5.4	0.1289	8.3
MR70-6.1	0.002473	0.1074	4.40	46	2.64	951	44	6.01	4.7	0.1074	4.7
MR70-7.1	0.002165	0.0982	3.13	63	2.65	987	39	5.85	4.0	0.0982	6.1
MR70-8.1	0.002447	0.1087	4.13	52	1.99	1043	44	5.46	4.3	0.1087	1.7
MR70-9.1	0.000699	0.0878	1.88	86	5.55	990	37	5.91	3.9	0.0878	1.6
MR70-9.2	0.001816	0.1060	3.64	43	4.30	1079	46	5.29	4.4	0.1060	2.8
MR70-10.1	0.010015	0.2204	18.81	7	1.39	777	80	6.34	10.2	0.2204	9.2
MR70-10.2	0.002797	0.1153	5.29	28	1.65	961	51	5.89	5.5	0.1153	2.1
MR70-11.1	0.002038	0.1023	3.40	52	5.65	1037	43	5.53	4.3	0.1023	1.5
MR70-11.2	0.000913	0.0864	1.70	118	2.30	992	32	5.91	3.3	0.0864	2.3
MR-10-132 (Ybqm biotite meta-quartz monzonite): coarse-grained, porphyroclastic meta-quartz monzonite, Middle Fox Creek quardrangle; UTM: 475336 4054336[5]											
MR-10-132-1.1	0.002236	0.1197	3.66	55	10.01	1031	21	5.46	2.1	0.1197	1.3
MR-10-132-2.1	0.002776	0.1113	4.75	66	0.98	924	18	6.17	2.1	0.1113	1.4
MR-10-132-3.1	0.001470	0.1043	2.43	89	6.23	1048	19	5.46	1.9	0.1043	1.9
MR-10-132-4.1	0.002940	0.1385	4.70	40	4.63	1029	24	5.36	2.4	0.1385	1.5
MR-10-132-5.1	0.002483	0.1329	3.96	43	3.14	1016	22	5.46	2.3	0.1329	1.4
MR-10-132-6.1	0.003944	0.1445	6.44	39	5.04	1015	24	5.38	2.4	0.1445	1.5
MR-10-132-7.1	0.002071	0.1106	3.45	81	1.81	1009	19	5.64	1.9	0.1106	1.2
MR-10-132-8.1	0.005923	0.1644	9.88	36	4.27	999	27	5.32	2.5	0.1644	5.3
MR-10-132-9.1	0.002996	0.1290	4.92	49	4.42	1019	22	5.46	2.2	0.1290	1.4
MR-10-132-10.1	0.003453	0.1329	5.71	42	4.26	985	22	5.63	2.3	0.1329	1.5
MR-10-132-11.1	0.002566	0.1251	4.19	60	2.66	1061	21	5.26	2.1	0.1251	1.3
MR-10-132-12.1	0.004377	0.1716	6.78	27	3.60	951	26	5.60	2.8	0.1716	1.7
MR-10-132-13.1	0.001033	0.0887	1.76	255	2.14	980	15	5.97	1.6	0.0887	0.8
MR-10-132-14.1	0.002330	0.1157	3.87	113	7.77	1023	26	5.53	2.6	0.1157	1.2
MR-10-132-15.1	0.005041	0.1646	8.12	34	15.49	1069	28	4.98	2.7	0.1646	1.6
MR-10-132-16.1	0.009923	0.2348	15.87	14	2.44	997	34	4.89	3.5	0.2348	1.9
MR-10-132-17.1	0.006550	0.2035	10.09	17	3.74	1059	35	4.81	3.4	0.2035	1.9
MR-10-132-18.1	0.008444	0.2001	14.09	15	4.49	969	31	5.24	3.2	0.2001	1.8
MR-10-132-19.1	0.008754	0.2246	13.78	5	3.76	1147	61	4.30	5.5	0.2246	2.6
MR-10-132-20.1	0.004544	0.1859	6.86	7	2.60	1082	46	4.82	4.4	0.1859	2.3
MR-10-132-21.1	0.003238	0.1410	5.20	12	2.64	1137	37	4.81	3.4	0.1410	2.0

Appendix Table B

(continued)

sample[1]	measured $^{204}Pb/^{206}Pb$	measured $^{207}Pb/^{206}Pb$	% common ^{206}Pb	U (ppm)	Th/U	$^{206}Pb/^{238}U$ (Ma)[1]	err[2] (Ma)	$^{238}U/^{206}Pb$[3]	err[2] (%)	$^{207}Pb/^{206}Pb$[3]	err[2] (%)
MR-10-123 (Yagn foliated amphibole gneiss): medium-grained, amphibole-bearing granitic gneiss (melanosome), Middle Fox Creek quadrangle; UTM: 471181 4053763											
MR-10-123-1.1	0.000111	0.0747	0.19	423	1.91	975	31	6.10	3.3	0.0747	1.0
MR-10-123-2.1	0.000185	0.0739	0.32	390	0.83	977	17	6.10	1.8	0.0739	0.7
MR-10-123-3.1	0.000070	0.0744	0.12	363	1.70	965	14	6.17	1.5	0.0744	0.7
MR-10-123-4.1	0.000072	0.0751	0.12	616	0.93	962	27	6.18	2.9	0.0751	0.9
MR-10-123-5.1	0.000075	0.0739	0.13	482	1.52	973	17	6.12	1.8	0.0739	0.6
MR-10-123-6.1	0.000105	0.0757	0.18	525	0.88	965	16	6.16	1.8	0.0757	0.6
MR-10-123-7.1	0.000060	0.0750	0.10	634	1.78	972	19	6.12	2.1	0.0750	0.5
MR-10-123-8.1	0.000317	0.0786	0.54	260	2.49	980	14	6.04	1.5	0.0786	0.8
MR-10-123-9.1	0.000131	0.0755	0.22	518	1.29	932	23	6.39	2.5	0.0755	1.0
MR-10-123-10.1	0.000240	0.0761	0.41	367	1.93	981	21	6.05	2.2	0.0761	0.7
MR-10-123-11.1	0.000084	0.0736	0.14	665	0.88	971	19	6.14	2.0	0.0736	0.6
MR-10-123-12.1	0.000125	0.0736	0.21	495	1.14	966	17	6.17	1.8	0.0736	0.6
MR-10-123-13.1	0.000152	0.0768	0.26	371	2.41	971	18	6.11	2.0	0.0768	0.6
MR-10-123-14.1	0.000089	0.0747	0.15	425	1.65	951	15	6.26	1.7	0.0747	0.6
MR-10-123-15.1	0.000116	0.0739	0.20	421	1.01	944	20	6.32	2.2	0.0739	0.6
MR-10-123-16.1	0.000114	0.0742	0.19	578	0.95	978	14	6.08	1.5	0.0742	0.6
MR-10-123-17.1	0.000061	0.0731	0.10	561	1.16	964	13	6.18	1.4	0.0731	0.6
MR-10-123-18.1	0.000203	0.0756	0.35	493	1.15	956	19	6.22	2.1	0.0756	1.5

[1] 206Pb/238U ages corrected for common Pb using the 207Pb-correction method. Decay constants from Steiger and Jäger (1977).
[2] 1-sigma errors.
[4] Total ratios, uncorrected for common Pb, used to calculate 3-dimensional linear regression.
[5] All coordinates refer to UTM Grid Zone 17, NAD27.

REFERENCES

Ague, J. J., and Brimhall, G. H., 1988, Regional variations in bulk chemistry, mineralogy, and the compositions of mafic and accessory minerals in the batholiths of California: Geological Society of America Bulletin, v. 100, n. 6, p. 891–911, https://doi.org/10.1130/0016-7606(1988)100<0891:RVIBCM>2.3.CO;2

Aleinikoff, J. N., Wintsch, R. P., Tollo, R. P., Unruh, D. M., Fanning, C. M., and Schmitz, M. D., 2007, Ages and origin of rocks of the Killingworth dome, south-central Connecticut: Implications for the tectonic evolution of southern New England: American Journal of Science, v. 307, n. 1, p. 63–118, https://doi.org/10.2475/01.2007.04

Aleinikoff, J. N., Ratcliffe, N. M., and Walsh, G. J., 2011, Provisional zircon and monazite uranium-lead geochronology for selected rocks from Vermont: U.S. Geological Survey Open-File Report 2011–1309, 46 p., available only online at https://pubs.usgs.gov/of/2011/1309/

Aleinikoff, J. N., Southworth, S., and Merschat, A. J., 2013, Implications for late Grenvillian (Rigolet phase) construction of Rodinia using new U-Pb data from the Mars Hill terrane, Tennessee and North Carolina, United States: Geology, v. 41, n. 10, p. 1087–1090, https://doi.org/10.1130/G34779.1

Atherton, M. P., and Sanderson, L. M., 1985, The chemical variation and evolution of the super-units of the segmented Coastal Batholith, *in* Pitcher, W. S., Atherton, M. P., Cobbing, E. J., and Beckinsale, R. D., editors, Magmatism at a Plate Edge: The Peruvian Andes: London, England, Blackie & Son Limited, p. 208–227.

Bailey, C. M., and Simpson, C., 1993, Extensional and contractional deformation in the Blue Ridge Province, Virginia: Geological Society of America Bulletin, v. 105, n. 4, p. 411–422, https://doi.org/10.1130/0016-7606(1993)105<0411:EACDIT>2.3.CO;2

Bartholomew, M. J., and Lewis, S. E., 1984, Evolution of Grenville massifs in the Blue Ridge geologic province, southern and central Appalachians, *in* Bartholomew, M. J., Force, E. R., Sinha, A. K., and Herz, N., editors, The Grenville Event in the Appalachians and Related Topics: Boulder, Colorado, Geological Society of America Special Paper 194, p. 229–254, https://doi.org/10.1130/SPE194-p229

Bateman, P. C., and Chappell, B. W., 1979, Crystallization, fractionation, and solidification of the Tuolumne Intrusive Series, Yosemite National Park, California: Geological Society of America Bulletin, v. 90, n. 5, p. 465–482, https://doi.org/10.1130/0016-7606(1979)90<465:CFASOT>2.0.CO;2

Bateman, P. C., and Dodge, F. C. W., 1970, Variations of major chemical constituents across the Central Sierra Nevada Batholith: Geological Society of America Bulletin, v. 81, n. 2, p. 409–420, https://doi.org/10.1130/0016-7606(1970)81[409:VOMCCA]2.0.CO;2

Bateman, P. C., Dodge, F. C. W., and Bruggman, P. E., 1984, Major oxide analyses, CPIW norms, modes, and bulk specific gravities of plutonic rocks from the Mariposa 1° x 2° sheet, central Sierra Nevada, California: U.S. Geological Survey Open-File Report 84–162, 49 p.

Bea, F., 2010, Crystallization dynamics of granitic magma chambers in the absence of regional stress: Multiphysics modeling with natural examples: Journal of Petrology, v. 51, n. 7, p. 1541–1569, https://doi.org/10.1093/petrology/egq028

Bédard, J., 2003, Evidence for regional-scale, pluton-driven, high-grade metamorphism in the Archean Minto Block, northern Superior Province, Canada: Journal of Geology, v. 111, n. 2, p. 183–205, https://doi.org/10.1086/345842

Berquist, P. J., Fisher, C. M., Miller, C. F., Wooden, J. L., Fullagar, P. D., and Loewy, S. L., 2005, Geochemistry and U-Pb zircon geochronology of Blue Ridge basement, western North Carolina and eastern Tennessee: Implications for tectonic assembly, *in* Hatcher, R. D., Jr., and Merschat, A. J., editors, Blue Ridge Geology Geotraverse East of the Great Smoky Mountains National Park, Western North Carolina: Carolina Geological Society Annual Field Trip, p. 33–56.

Black, L. P., Kamo, S. L., Allen, C. M., Davis, D. W., Aleinikoff, J. N., Valley, J. W., Mundil, R., Campbell, I. H., Korsuch, R. J., Williams, I. S., and Foudoulis, C., 2004, Improved $^{206}Pb/^{238}U$ microprobe geochronology by the monitoring of a trace-element-related matrix effect; SHRIMP, ID–TIMS, ELA–ICP–MS and oxygen isotope documentation for a series of zircon standards: Chemical Geology, v. 205, n. 1–2, p. 115–140, https://doi.org/10.1016/j.chemgeo.2004.01.003

Boily, M., Brooks, C., Ludden, J. N., and James, D. E., 1989, Chemical and isotopic evolution of the Coastal Batholith of southern Peru: Journal of Geophysical Research-Solid Earth, v. 94, n. B9, p. 12483–12498, https://doi.org/10.1029/JB094iB09p12483

Bryant, B. H., and Reed, J. C., Jr., 1970, Geology of the Grandfather Mountain window and vicinity, North Carolina and Tennessee: U.S. Geological Survey Professional Paper 615, 190 p.

Budahn, J. R., and Wandless, G. A., 2002, Instrumental neutron activation by long count: U.S. Geological Survey Open-File Report 2002-0223-X, p. X-1 to X-13.

Bussell, M. A., 1983, Crystallization history of granophyric intrusives from the Peruvian Coastal Batholith: Lithos, v. 16, n. 3, p. 169–184, https://doi.org/10.1016/0024-4937(83)90022-1

Carrigan, C. W., Miller, C. F., Fullagar, P. D., Bream, B. R., Hatcher, R. D., Jr., and Coath, C. D., 2003, Ion microprobe age and geochemistry of southern Appalachian basement, with implications for Proterozoic and Paleozoic reconstructions: Precambrian Research, v. 120, n. 1–2, p. 1–36, https://doi.org/10.1016/S0301-9268(02)00113-4

Carroll, M. R., and Wyllie, P. J., 1990, The system tonalite-H_2O at 15 kbar and the genesis of calc-alkaline magmas: American Mineralogist, v. 75, n. 34, p. 345–357.

Carter, M. W., Aleinikoff, J. N., and Southworth, S., 2012, Mesoproterozoic to late Paleozoic geology along the Blue Ridge Parkway from James River to Bearwallow Gap, central Virginia: Geological Society of America Abstracts with Programs, v. 44, n. 7, p. 612.

Chappell, B. W., and White, A. J. R., 1992, I- and S-type granites in the Lachlan Fold Belt: Earth and

Environmental Science Transactions of the Royal Society of Edinburgh, v. 83, n. 1–2, p. 1–26, https://doi.org/10.1017/S0263593300007720
Clemens, J. D., Holloway, J. R., and White, A. J. R., 1986, Origin of an A-type granite: Experimental constraints: American Mineralogist, v. 71, n. 3–4, p. 317–324.
Collins, W. J., Beams, S. D., White, A. J. R., and Chappell, B. W., 1982, Nature and origin of A-type granites with particular reference to southeastern Australia: Contributions to Mineralogy and Petrology, v. 80, n. 2, p. 189–200, https://doi.org/10.1007/BF00374895
Corfu, F., Hanchar, J. M., Hoskin, P. W. O., and Kinny, P., 2003, Atlas of zircon textures, *in* Hanchar, J. M., and Hoskin, P. W. O., editors, Zircon: Reviews in Mineralogy and Geochemistry, v. 53, p. 469–500, https://doi.org/10.2113/0530469
Corrigan, D., and Hanmer, S., 1997, Anorthosites and related granitoids in the Grenville orogen: A product of convective thinning of the lithosphere?: Geology, v. 25, n. 1, p. 61–64, https://doi.org/10.1130/0091-7613(1997)025<0061:AARGIT>2.3.CO;2
Coulon, C., and Thorpe, R. S., 1981, Role of continental crust in petrogenesis of orogenic volcanic associations: Tectonophysics, v. 77, n. 1–2, p. 79–93, https://doi.org/10.1016/0040-1951(81)90162-1
Creaser, R. A., Price, R. C., and Wormald, R. J., 1991, A-type granites revisited: Assessment of a residual-source model: Geology, v. 19, n. 2, p. 163–166, https://doi.org/10.1130/0091-7613(1991)019<0163:ATGRAO>2.3.CO;2
Davidson, J. P., McMillan, N. J., Moorbath, S., Wörner, G., Harmon, R. S., and Lopez-Escobar, L., 1990, The Nevados de Payachata region (18° S/69° W, N. Chile) II. Evidence for widespread crustal involvement in Andean magmatism: Contributions to Mineralogy and Petrology, v. 105, n. 4, p. 412–432, https://doi.org/10.1007/BF00286829
Davis, G. L., Tilton, G. R., and Wetherill, G. W., 1962, Mineral ages from the Appalachian province in North Carolina and Tennessee: Journal of Geophysical Research, v. 67, n. 5, p. 1987–1996, https://doi.org/10.1029/JZ067i005p01987
DePaolo, D. J., 1981, Trace element and isotopic effects of combined wallrock assimilation and fractional crystallization: Earth and Planetary Science Letters, v. 53, n. 2, p. 189–202, https://doi.org/10.1016/0012-821X(81)90153-9
Drake, M. J., 1975, Partition of Sr, Ba, Ca, Y, Eu^{2+}, Eu^{3+}, and other REE between plagioclase feldspar and magmatic liquid: An experimental study: Geochimica et Cosmochimica Acta, v. 39, n. 5, p. 689–712, https://doi.org/10.1016/0016-7037(75)90011-3
Duchesnse, J-C., Martin. H., Bagínski, B., Wiszniewska, J., and Vander Auwera, J., 2010, The origin of ferroan-potassic A-type granitoids: The case of the hornblende-biotite granite suite of the Mesoproterozoic Mazury Complex, northeasterm Poland: The Canadian Mineralogist, v. 48, n. 4, p. 947–968, https://doi.org/10.3749/canmin.48.4.947
Eby, G. N., 1990, The A-type granitoids: A review of their occurrence and chemical characteristics and speculations on their petrogenesis: Lithos, v. 26, n. 1–2, p. 115–134, https://doi.org/10.1016/0024-4937(90)90043-Z
——— 1992, Chemical subdivision of the A-type granitoids: Petrogenetic and tectonic implications: Geology, v. 20, n. 7, p. 641–644, https://doi.org/10.1130/0091-7613(1992)020<0641:CSOTAT>2.3.CO;2
Ferry, J. M., and Watson, E. B., 2007, New thermodynamic models and revised calibrations for the Ti-in-zircon and Zr-in-rutile thermometers: Contributions to Mineralogy and Petrology, v. 154, n. 4, p. 429–437, https://doi.org/10.1007/s00410-007-0201-0
Fettes, D., and Desmons, J., 2007, Metamorphic Rocks: A Classification and Glossary of Terms - Recommendations of the International Union of Geological Sciences Subcommission on the Systematics of Metamorphic Rocks: Cambridge, England, Cambridge University Press, 244 p.
Fierstein, J., Bruggman, P. E., Bartel, A. J., Stewart, K. C., Taggart, J. E., Drake, R. E., and Hildreth, W., 1989, Chemical analyses of rocks and sediments from central Chile: U.S. Geological Survey Open-File Report 89–78, 13 p.
Fisher, C. M., Loewy, S. L., Miller, C. F., Berquist, P., Van Schmus, W. R., Hatcher, R. D., Jr., Wooden, J. L., and Fullagar, P. D., 2010, Whole-rock Pb and Sm-Nd isotopic constraints on the growth of southeastern Laurentia during Grenvillian orogenesis: Geological Society of America Bulletin, v. 122, n. 9–10, p. 1646–1659, https://doi.org/10.1130/B30116.1
Förster, H.-J., Tischendorf, G., and Trumbull, R. B., 1997, An evaluation of the Rb vs. (Y + Nb) discrimination diagram to infer tectonic setting of silicic igneous rocks: Lithos, v. 40, n. 2–4, p. 261–293, https://doi.org/10.1016/S0024-4937(97)00032-7
Frost, B. R., Frost, C. D., Hulsebosch, T. P., and Swapp, S. M., 2000, Origin of the charnockites of the Louis Lake batholith, Wind River Range, Wyoming: Journal of Petrology, v. 41, n. 12, p. 1759–1776, https://doi.org/10.1093/petrology/41.12.1759
Frost, B. R., Barnes, C. G., Collins, W. J., Arculus, R. J., Ellis, D. J., and Frost, C. D., 2001, A geochemical classification for granitic rocks: Journal of Petrology, v. 42, n. 11, p. 2033–2048, https://doi.org/10.1093/petrology/42.11.2033
Gathright, T. M., III, 1976, Geology of the Shenandoah National Park, Virginia: Charlottesville, Virginia, Virginia Division of Mineral Resources Bulletin 86, 93 p.
Gill, J. B., 1981, Orogenic Andesites and Plate Tectonics: Berlin, Germany Springer, 390 p
Goodman, R. J., 1972, The distribution of Ga and Rb in coexisting groundmass and phenocryst phases of some basic volcanic rocks: Geochimica et Cosmochimica Acta, v. 36, n. 3, p. 303–317, https://doi.org/10.1016/0016-7037(72)90025-7
Gray, D. R., Foster, D. A, and Bucher, M., 1997, Recognition and defintion of orogenic events in the Lachlan Fold Belt: Australian Journal of Earth Sciences, v. 44, n. 4, p. 489–501, https://doi.org/10.1080/08120099708728328

Harley, S. L., Kelly, N. M., and Moller, A., 2007, Zircon behavior and the thermal histories of mountain chains: Elements, v. 3, n. 1, p. 25–30, https://doi.org/10.2113/gselements.3.1.25

Haskin, L. A., Haskin, M. A., Frey, F. A., and Wildman, T. R., 1968, Relative and absolute terrestrial abundances of the rare earths, *in* Ahrens, L. H., editor, Origin and distribution of the elements, volume 1: Oxford, England, Pergamon, International Series of Monographs in Earth Sciences, p. 889–911, https://doi.org/10.1016/B978-0-08-012835-1.50074-X

Hatcher, R. D., Jr., 2010, The Appalachian orogen: A brief summary, *in* Tollo, R. P., Bartholomew, M. J., Hibbard, J. P., and Karabinos, P. M., editors, From Rodinia to Pangea: The Lithotectonic Record of the Appalachian Region: Geological Society of America Memoir 206, p. 1–19, https://doi.org/10.1130/2010.1206(01)

Hatcher, R. D., Jr., Merschat, A. J., and Thigpen, J. R., 2005, Blue Ridge Primer, *in* Hatcher, R. D., Jr., and Merschat, A. J., editors, Blue Ridge Geology Geotraverse East of the Great Smoky Mountains National Park, Western North Carolina: Carolina Geological Society Annual Field Trip, p. 1–24.

Herz, N., and Force, E. R., 1984, Rock suites of the Grenvillian terrane of the Roseland district, Virginia Part 1. Lithologic relations, *in* Bartholomew, M. J., editor, The Grenville Event in the Appalachians and Related Topics: Geological Society of America Special Paper 194, p. 187–214, https://doi.org/10.1130/SPE194-p187

Heumann, M. J., Bickford, M. E., Hill, B. M., McLelland, J. M., Selleck, B. W., and Jercinovic, M. J., 2006, Timing of anatexis in metapelites from the Adirondack lowlands and southern highlands: A manifestation of the Shawinigan orogeny and subsequent anorthosite-mangerite-charnockite-granite magmatism: Geological Society of America Bulletin, v. 118, n. 11–12, p. 1283–1298, https://doi.org/10.1130/B25927.1

Hibbard, J. P., van Staal, C. R., Rankin, D. W., and Williams, H., 2006, Lithotectonic map of the Appalachian Orogen, Canada-United States of America: Geological Society of Canada, Map 2096A, scale 1:1,500,000.

Hildreth, W. E., and Moorbath, S., 1988, Crustal contributions to arc magmatism in the Andes of central Chile: Contributions to Mineralogy and Petrology, v. 98, n. 4, p. 455–499, https://doi.org/10.1007/BF00372365

Hoffman, P. H., 1989, Precambrian geology and tectonic history of North America, *in* Bally, A. W., and Palmer, A. R., editors, The Geology of North America - An overview: Boulder, Colorado, Geological Society of America, The Geology of North America, v. A, p. 447–512, https://doi.org/10.1130/DNAG-GNA-A.447

Hoskin, P. W. O., and Schaltegger, U., 2003, The composition of zircon and igneous and metamorphic petrogenesis, *in* Hanchar, J. M., and Hoskin, P. W. O., editors, Zircon: Reviews in Mineralogy and Geochemistry, v. 53, p. 27–62, https://doi.org/10.2113/0530027

Ireland, T. R., Wooden, J. L., Persing, H. M., and Ito, B., 1999, Geological applications and analytical development of the SHRIMP-RG: Eos, Transactions of the American Geophysical Union, v. 80, n. 46, Supplement, F1117.

Irvine, T. N., and Baragar, W. R. A., 1971, A guide to the chemical classification of the common volcanic rocks: Canadian Journal of Earth Sciences, v. 8, n. 5, p. 523–548, https://doi.org/10.1139/e71-055

Le Maitre, R. W., Streckiesen, A., Zanettin, B., Le Bas, M. J., Bonin, B., Bateman, P., Bellieni, G., Dudek, A., Efremova, S., Keller, J., Lameyre, J., Sabine, P. A., Schmid, R., Sorensen, H., and Wolley, A. R., 2002, Igneous Rocks: A Classification and Glossary of Terms - Recommendations of the International Union of Geological Sciences Subcommission on the Systematics of Igneous Rocks, 2nd edition: Cambridge, England, Cambridge University Press, 236 p.

Ludwig, K. R., 1980, Calculation of uncertainties of U-Pb isotope data: Earth and Planetary Science Letters, v. 46, n. 2, p. 212–220, https://doi.org/10.1016/0012-821X(80)90007-2

——— 2001, Squid, version 1.02, A user's manual: Berkeley, California, Berkeley Geochronology Center Special Publication, n. 2, 21 p.

——— 2003, Isoplot/Ex version 3.00, A geochronological toolkit for Mircosoft Excel: Berkeley, California, Berkeley Geochronology Center Special Publication, n. 4, 73 p.

——— 2009, Squid 2, version 2.50, A user's manual: Berkeley, California, Berkeley Geochronology Center, Special Publication, n. 5, 110 p.

McCulloch, M. T., and Gamble, J. A., 1991, Geochemical and geodynamical constraints on subduction zone magmatism: Earth and Planetary Science Letters, v. 102, n. 3–4, p. 358–374, https://doi.org/10.1016/0012-821X(91)90029-H

McLelland, J. M., and Chiarenzelli, J. R., 1990, Geochronological studies in the Adirondack Mountains and the implications of a Middle Proterozoic tonalite suite, *in* Gower, C. F., Rivers, T., and Ryan, A. B., editors, Mid-Proterozoic Laurentia-Baltica: St. John's, Newfoundland, Geological Association of Canada Special Paper 38, p. 175–194.

McLelland, J., Ashwall, L., and Moore, L., 1994, Composition and petrogenesis of oxide-, apatite-rich gabbronorites associated with Proterozoic anorthosite massifs: Examples from the Adirondack Mountains, New York: Contributions to Mineralogy and Petrology, v. 116, n. 1, p. 225–238, https://doi.org/10.1007/BF00310702

McLelland, J., Hamilton, M., Selleck, B., McLelland, J., Walker, D., and Orrell, S., 2001, Zircon U-Pb geochronology of the Ottawan Orogeny, Adirondack Highlands, New York: Regional and tectonic implications: Precambrian Research, v. 109, n. 1–2, p. 39–72, https://doi.org/10.1016/S0301-9268(01)00141-3

McLelland, J. M., Bickford, M. E., Hill, B. M., Clechenko, C. C., Valley, J. W., and Hamilton, M. A., 2004, Direct dating of Adirondack massif anorthosite by U-Pb SHRIMP analysis of igneous zircon: Implications for AMCG complexes: Geological Society of America Bulletin, v. 116, n. 11–12, p. 1299–1317, https://doi.org/10.1130/B25482.1

McLelland, J. M., Selleck, B. W., and Bickford, M. E., 2010, Review of the Proterozoic evolution of the

Grenville Province, its Adirondack outlier, and the Mesoproterozoic inliers of the Appalachians, *in* Tollo, R. P., Bartholomew, M. J., Hibbard, J. P., and Karabinos, P. M., editors, From Rodinia to Pangea: The Lithotectonic Record of the Appalachian region: Geological Society of America Memoirs, v. 206, p. 21–49, https://doi.org/10.1130/2010.1206(02)

McLelland, J. M., Selleck, B.W., and Bickford, M. E., 2013, Tectonic evolution of the Adirondack Mountains and Grenville orogen inliers within the USA: Geoscience Canada, v. 40, n. 3, p. 318–352, https://doi.org/10.12789/geocanj.2013.40.022

Nakamura, N., 1974, Determination of REE, Ba, Fe, Mg, Na, and K in carbonaceous and ordinary chondrites: Geochimica et Cosmochimica Acta, v. 38, n. 5, p. 757–775, https://doi.org/10.1016/0016-7037(74)90149-5

Nance, R. D., Murphy, J. B., and Santosh, M., 2014, The supercontinent cycle: A retrospective essay: Gondwana Research, v. 25, n. 1, p. 4–29, http://dx.doi.org/10.1016/j.gr.2012.12.026

Nédélec, A., Stephens, W. E., and Fallick, A. E., 1995, The Panafrican stratoid granites of Madagascar: Alkaline magmatism in a post-collisional extensional setting: Journal of Petrology, v. 36, n. 5, p. 1367–1391, https://doi.org/10.1093/petrology/36.5.1367

Owens, B. E., and Dymek, R. F., 1992, Fe-Ti-P-rich rocks and massif anorthosite: Problems of interpretation illustrated from the Labrieville and St.Urbain plutons, Quebec: The Canadian Mineralogist, v. 30, p. 163–190.

Ownby, S. E., Miller, C. F., Berquist, P. J., Carrigan, C. W., Wooden, J. L., and Fullagar, P. D., 2004, U-Pb geochronology and geochemistry of the Mars Hill terrane, North Carolina-Tennessee: Constraints of the origin, history, and tectonic assembly, *in* Tollo, R. P., Corriveau, L., McLelland, J., and Bartholomew, M. J., editors, Proterozoic Tectonic Evolution of the Grenville Orogen in North America: Geological Society of America Memoirs, v. 197, p. 609–632.

Patiño-Douce, A. E., 1997, Generation of metaluminous A-type granites by low-pressure melting of calc-alkaline granitoids: Geology, v. 25, n. 8, p. 743–746, https://doi.org/10.1130/0091-7613(1997)025<0743:GOMATG>2.3.CO;2

Pearce, J. A., 1983, Role of sub-continental lithosphere in magma genesis at active continental margins, *in* Hawkesworth, C. J., and Norry, M. J., editors, Continental basalts and mantle xenoliths: Cheshire, United Kingdom, Shiva Publishing Limited, p. 230–249.

Pearce, J. A., Harris, N. B. W., and Tindle, A. G., 1984, Trace element discrimination diagrams for the tectonic interpretation of granitic rocks: Journal of Petrology, v. 25, n. 4, p. 956–983, https://doi.org/10.1093/petrology/25.4.956

Peccerillo, A., and Taylor, S. R., 1976, Geochemistry of Eocene calc-alkaline volcanic rocks from the Kastamonu area, northern Turkey: Contributions to Mineralogy and Petrology, v. 58, n. 1, p. 63–81, https://doi.org/10.1007/BF00384745

Rankin, D. W., 1976, Appalachian salients and recesses: Late Precambrian continental breakup and the opening of the Iapetus ocean: Journal of Geophysical Research-Solid Earth and Planets, v. 81, p. 5605–5619, https://doi.org/10.1029/JB081i032p05605

——— 1993, The volcanogenic Mount Rogers Formation and the overlying glaciogenic Konnarock Formation – Two late Proterozoic units in southwestern Virginia: U.S. Geological Survey Bulletin 2029, 26 p.

Rankin, D. W., Espenshade, G. H., and Neuman, R. B., 1972, Geologic map of the west half of the Winston–Salem quadrangle, North Carolina, Virginia, and Tennessee: U.S. Geological Survey Miscellaneous Geologic Investigations Map I-709–A, 1:250,000 scale.

Rankin, D. W., Espanshade, G. H., and Shaw, K. W., 1973, Stratigraphy and structure of the metamorphic belt in northwestern North Carolina and southwestern Virginia: A study from the Blue Ridge across the Brevard fault zone to the Sauratown Mountains anticlinorium: American Journal of Science, v. 273–A, p. 1–40.

Rankin, D. W., Drake, A. A., Jr., Glover, L., III, Goldsmith, R., Hall, L. M., Murray, D. P., Ratcliffe, N. M., Read, J. F., Secor, D. T., Jr., and Stanley, R. S., 1989, Pre-orogenic terranes, *in* Hatcher, R. D., Jr., Thomas, W. A., and Viele, G. W., editors, The Appalachian-Ouachita Orogen in the United States: Geological Society of America, The Geology of North America, v. F-2, p. 7–100, https://doi.org/10.1130/DNAG-GNA-F2.7

Rapp, R. P., and Watson, E. B., 1995, Dehydration melting of metabasalt at 8–32 kbar: Implications for continental growth and crust-mantle recycling: Journal of Petrology, v. 36, n. 4, p. 891–931, https://doi.org/10.1093/petrology/36.4.891

Ratcliffe, N. M., Aleinikoff, J. N., Burton, W. C., and Karabinos, P., 1991, Trondhjemitic, 1.35–1.31 Ga gneisses of the Mount Holly Complex of Vermont: Evidence for an Elzevirian event in the Grenville Basement of the United States Appalachians: Canadian Journal of Earth Science, v. 28, n. 1, p. 77–93, https://doi.org/10.1139/e91-007

Rhodes, J. M., 1996, Geochemical stratigraphy of lava flows sampled by the Hawaii Scientific Drilling Project: Journal of Geophysical Research-Solid Earth, v. 101, n. B5, p. 11,729–11,746, https://doi.org/10.1029/95JB03704

Rhodes, J. M., and Vollinger, M. J., 2004, Composition of basaltic lavas sampled by phase-2 of the Hawaii Scientific Drilling Project: Geochemical stratigraphy and magma types: Geochemistry, Geophysics, Geosystems, v. 5, n. 3, p. 1–38, https://doi.org/10.1029/2002GC000434

Rivers, T., 1997, Lithotectonic elements of the Grenville province: Review and tectonic implications, Precambrian Research, v. 97, n. 3–4, p. 117–154, https://doi.org/10.1016/S0301-9268(97)00038-7

——— 2008, Assembly and preservation of lower, mid, and upper orogenic crust in the Grenville Province - Implications for the evolution of large hot long-duration orogens: Precambrian Research, v. 167, n. 3–4, p. 237–259, https://doi.org/10.1016/j.precamres.2008.08.005

Roberts, M. P., and Clemens, J. D., 1993, Origin of high-potassium, calc-alkaline, I-type granitoids: Geology, v. 21, n. 9, p. 825-828, https://doi.org/10.1130/0091-7613(1993)021<0825:OOHPTA>2.3.CO;2

Rubatto, D., 2002, Zircon trace element geochemistry: Partitioning with garnet and the link between U-Pb ages and metamorphism: Chemical Geology, v. 184, n. 1–2, p. 123–138, https://doi.org/10.1016/S0009-2541(01)00355-2

Saunders, A. D., Tarney, J., and Weaver, S. D., 1980, Transverse geochemical variations across the Antarctic Penninsula: Implications for the genesis of calc-alkaline magmas: Earth and Planetary Science Letters, v. 46, n. 3, p. 344–360, https://doi.org/10.1016/0012-821X(80)90050-3

Skjerlie, K. P., and Johnston, A. D., 1992, Vapor-absent melting at 10 bkar of a biotite- and amphibole-bearing tonalitic gneiss: Implications for the generation of A-type granites: Geology, v. 20, n. 3, p. 263–266, https://doi.org/10.1130/0091-7613(1992)020<0263:VAMAKO>2.3.CO;2

Skridlaite, G., Wiszniewska, J., and Duchesne, J.-C., 2003, Ferro-potassic A-type granites and related rocks in NE Poland and S. Lithuania: West of the east European Craton: Precambrian Research, v. 124, n. 2–4, p. 305–326, https://doi.org/10.1016/S0301-9268(03)00090-1

Slagstad, T., Culshaw, N. G., Jamieson, R. A., and Ketchum, J. W. F., 2004, Early Mesoproterozoic tectonic history of the southwestern Grenville Province, Ontario: Constraints from geochemistry and geochronology of high-grade gneisses, *in* Tollo, R. P., Corriveau, L., McLelland, J., and Bartholomew, M. J., editors, Proterozoic Tectonic Evolution of the Grenville Orogen in North America: Geological Society of America Memoirs, v. 197, p. 209–241, https://doi.org/10.1130/0-8137-1197-5.209

Southworth, S., Aleinikoff, J. N., Tollo, R. P., Bailey, C. M., Burton, W. C., Hackley, P. C., and Fanning, C. M., 2010, Mesoproterozoic magmatism and deformation in the northern Blue Ridge, Virginia and Maryland: Application of SHRIMP U-Pb geochronology and integrated field studies in the defintion of Grenvillian tectonic history, *in* Tollo, R. P., Bartholomew, M. J., Hibbard, J. P., and Karabinos, P. M., editors, From Rodinia to Pangea: The Lithotectonic Record of the Appalachian region: Geological Society of America Memoirs, v. 206, p. 795–836, https://doi.org/10.1130/2010.1206(31)

Spear, F. S., 1993, Metamorphic Phase Equilibria and Pressure-Temperature-Time Paths: Mineralogical Society of America Monograph, Washington, DC, 799 p.

Stacey, J. S., and Kramers, J. D., 1975, Approximation of terrestrial lead isotope composition by a two-stage model: Earth and Planetary Science Letters, v. 26, n. 2, p. 207–222, https://doi.org/10.1016/0012-821X(75)90088-6

Steiger, R. H., and Jäger, E., 1977, Subcommission on geochronology: Convention on the use of decay constants in geo- and cosmochronology: Earth and Planetary Science Letters, v 36, n. 3, p. 359–362, https://doi.org/10.1016/0012-821X(77)90060-7

Streckeisen, A. J., and Le Maitre, R. W., 1979. A chemical approximation to the modal QAPF classification of the igneous rocks: Neues Jahrbuch fuer Mineralogie, Abhandlungen, v. 136, p. 169–206.

Sylvester, P. J., 1989, Post-collisional alkaline granites: The Journal of Geology, v. 97, n. 1, p. 261–280, https://doi.org/10.1086/629302

Thompson, R. N., 1982, Magmatism of the British Tertiary volcanic province: Scottish Journal of Geology, v. 18, p. 49–107, https://doi.org/10.1144/sjg18010049

Tilton, G. R., Wetherill, G. W., David, G. L., and Bass, N. M., 1960, 1,000 million-year-old minerals from eastern United States and Canada: Journal of Geophysical Research, v. 65, n. 12, p. 4173–4179, https://doi.org/10.1029/JZ065i012p04173

Tollo, R. P., Aleinikoff, J. N., Borduas, E. A., Hackley, P. C., and Fanning, C. M., 2004a, Petrologic and geochronologic evolution of the Grenville orogen, northern Blue Ridge Province, Virginia, *in* Tollo, R. P., Corriveau, L., McLelland, J., and Bartholomew, M. J., editors, Proterozoic Tectonic Evolution of the Grenville Orogen in North America: Geological Society of America Memoirs, v. 197, p. 647–677, https://doi.org/10.1130/0-8137-1197-5.647

Tollo, R. P., Corriveau, L., McLelland, J., and Bartholomew, M. J., 2004b, Proterozoic tectonic evolution of the Grenville orogen in North America: An introduction, *in* Tollo, R. P., Corriveau, L., McLelland, J., and Bartholomew, M. J., editors, Proterozoic Tectonic Evolution of the Grenville Orogen in North America: Geological Society of America Memoirs, v. 197, p. 1–18, https://doi.org/10.1130/0-8137-1197-5.1

Tollo, R. P., Aleinikoff, J. N., Borduas, E. A. Dickin, A. P., McNutt, R. H., and Fanning, C. M., 2006, Grenvillian magmatism in the northern Virginia Blue Ridge: Petrologic implications of episodic granitic magma production and the significance of postorogenic A-type charnockite: Precambrian Research, v. 151, n. 3–4, p. 224–264, https://doi.org/10.1016/j.precamres.2006.08.010

Tollo, R. P., Aleinikoff, J. N., Wooden, J. L., Mazdab, F. K., Southworth, S., and Fanning, C. M., 2010, Thermomagmatic evolution of Mesoproterozoic crust in the Blue Ridge of SW Virginia and NW North Carolina: Evidence from U-Pb geochronology and zircon geothermometry, *in* Tollo, R. P., Bartholomew, M. J., Hibbard, J. P., and Karabinos, P. M., editors, From Rodinia to Pangea: The Lithotectonic Record of the Appalachian region: Geological Society of America Memoirs, v. 206, p. 859–896, https://doi.org/10.1130/2010.1206(33)

Tollo, R. P., Aleinikoff, J. N., Mundil, R., Southworth, C. S., Cosca, M. A., Rankin, D. W., Rubin, A. E., Kentner, A. E., Parendo, C. A., and Ray, M. S., 2012, Igneous activity, metamorphism, and deformation in the Mount Rogers area of SW Virginia and NW North Carolina: A geologic record of Precambrian tectonic evolution of the southern Blue Ridge Province, *in* Eppes, M. C., and Bartholomew, M. J., editors, From the Blue Ridge to the Coastal Plain: Field Excursions in the Southeastern United States: Geological Society of America Field Guides, v. 29, p. 1–66, https://doi.org/10.1130/2012.0029(01)

Trupe, C. H., Stewart, K. G., Adams, M. G., and Foudy, J. P., 2004, Deciphering the Grenville of the southern Appalachians through evaluation of the post-Grenville tectonic history in northwestern North Carolina, *in* Tollo, R. P., Corriveau, L., McLelland, J., and Bartholomew, M. J., editors, Proterozoic Tectonic Evolution of the Grenville Orogen in North America: Boulder, Colorado, Geological Society of America Memoirs, v. 197, p. 679–695, https://doi.org/10.1130/0-8137-1197-5.679

Turner, S. P., Foden, J. D., and Morrison, R. S., 1992, Derivation of some A-type magmas by fractionation of

basaltic magma: An example from the Padthaway Ridge, South Australia: Lithos, v. 28, n. 2, p. 151–179, https://doi.org/10.1016/0024-4937(92)90029-X

Vander Auwera, J., Bogaerts, M., Liégeois, J.-P., Demaiffe, D., Wilmart, E., Bolle, O., and Duchesne, J-C., 2003, Derivation of the 1.0-0.9 Ga ferro-potassic A-type granitoids of southern Norway by extreme differentiation from basic magmas: Precambrian Research, v. 124, n. 2–4, p. 107–148, https://doi.org/10.1016/S0301-9268(03)00084-6

Virginia Division of Mineral Resources, 1993, Geologic Map of Virginia: Charlottesville, Virginia Division of Mineral Resources, scale 1:500,000.

Volkert, R. A., Aleinikoff, J. N, and Fanning, C. M., 2010, Tectonic, magmatic, and metamorphic history of the New Jersey Highlands: New insights from SHRIMP U-Pb geochronology, *in* Tollo, R. P., Bartholomew, M. J., Hibbard, J. P., and Karabinos, P. M., editors, From Rodinia to Pangea: The Lithotectonic Record of the Appalachian region: Geological Society of America Memoirs, v. 206, p. 307–346, https://doi.org/10.1130/2010.1206(14)

Walsh, G. J., Aleinikoff, J. N., and Fanning, C. M., 2004, U-Pb geochronology and evolution of Mesoproterozoic basement rocks, western Connecticut, *in* Tollo, R. P., Corriveau, L., McLelland, J. M., and Bartholomew, M. J., editors, Proterozoic Tectonic Evolution of the Grenville Orogen in North America: Geological Society of America Memoirs, v. 197, p. 729–754, https://doi.org/10.1130/0-8137-1197-5.729

Watson, E. B., Wark, D. A., and Thomas, J. B., 2006, Crystallization thermometers for zircon and rutile: Contributions to Mineralogy and Petrology, v. 151, p. 413–433, https://doi.org/10.1007/s00410-006-0068-5

Weill, D. F., and Drake, M. J., 1973, Europium Anomaly in Plagioclase Feldspar: Experimental Results and Semiquantitative Model: Science, v. 180, n. 4090, p. 1059–1060, https://doi.org/10.1126/science.180.4090.1059

Whalen, J. B., and Currie, K. L., 1990, The Topsails igneous suite, western Newfoundland; Fractionation and magma mixing in an "orogenic" A-type granite suite, *in* Stein, H. J., and Hannah, J. L., editors, Ore-bearing granite systems; Petrogenesis and mineralizing processes: Geological Society of America Special Papers, v. 246, p. 287–299, https://doi.org/10.1130/SPE246-p287

Whalen, J. B., Currie, K. L., and Chappell, B. W., 1987, A-type granites: Geochemical characteristics, discrimination and petrogenesis: Contributions to Mineralogy and Petrology, v. 95, n. 4, p. 407–419, https://doi.org/10.1007/BF00402202

White, A. J. R., and Chappell, B. W., 1983, Granitoid types and their distribution in the Lachlan Fold Belt, southeastern Australia, *in* Roddick, J. A., editor, Circum-Pacific Plutonic terranes: Geological Society of America Memoirs, v. 159, p. 21–34, https://doi.org/10.1130/MEM159-p21

Whitney, D. L., and Evans, B. W., 2010, Abbreviations for names of rock-forming minerals: American Mineralogist, v. 95, n. 1, p. 185–187, https://doi.org/10.2138/am.2010.3371

Williams, I. S., 1998, U-Th-Pb geochronology by ion microprobe, *in* McKibben, M. A., Shanks, W. C., III, and Ridley, W. I., editors, Applications of microanalytical techniques to understanding mineralizing processes: Reviews in Economic Geology, v. 7, p. 1–35, https://doi.org/10.5382/Rev.07.01